Politecnico di Milano

SCHOOL OF INDUSTRIAL AND INFORMATION ENGINEERING
Master of Science – Nuclear Engineering

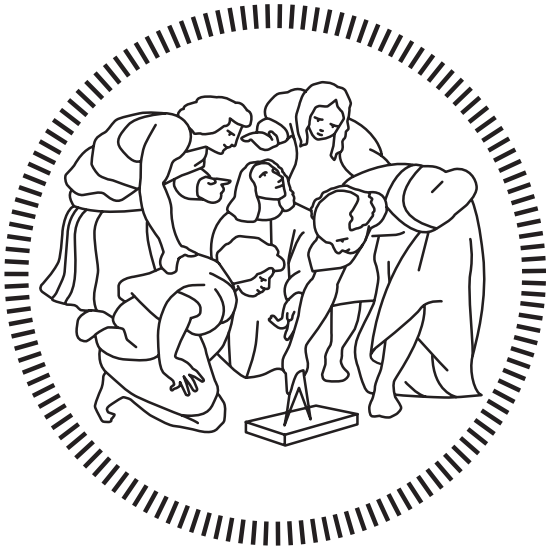

Multi-physics development and application of a reduced order model of fission gas diffusion in fuel performance codes

Supervisor
Lelio LUZZI

Co-Supervisor
Davide PIZZOCRI
Francesco Attilio Bruno SILVA

Candidate
Martina DI GENNARO – 916161

Academic Year 2020 – 2021

Bisogna saper attendere la propria sete e farla giungere al massimo
altrimenti non si scoprirà mai la propria sorgente,
che non può mai essere la stessa di un altro.

F. Nietzsche, Frammenti postumi

Acknowledgements

This research activity has received funding from the Euratom research and training programme 2017-2021 through the INSPYRE Project under grant agreement No.754329 and from the Euratom research and training programme 2020-2024 through the PATRICIA project under grant agreement No.945077. This research contributes to the Joint Programme on Nuclear Materials (JPNM) of the European Energy Research Alliance (EERA), in the specific framework of the COMBATFUEL Project.

Abstract

During the normal operation of a nuclear power plant, the irradiation of the fuel determines the production of gaseous fission products (xenon and krypton) whose behavior represent a life-limiting factor of the fuel itself. In particular, their low solubility determines their diffusion and their consequent release in the free volume of the fuel rod. The fission gases released into the fuel gap increase the internal pressure and temperature of the fuel by degrading the thermal conductivity of the filling gas. Consequently, understanding the fission product release process is essential for analyzing the thermal-mechanical behavior of the fuel rod. For this purpose, it is necessary to simulate the intra-granular behavior of fission gases through the fuel performance codes.

The numerical simulations on engineering-scale of the integral fuel rod requires high computational efforts, therefore the trade-off between the numerical solution accuracy and computational cost is essential in this context. For that reason, this thesis work aims to develop a reduced order model of the fission gases diffusion process, to be integrated with fuel performance codes. This was made possible by using: (i) the Proper Orthogonal Decomposition (POD) technique which has been employed to define the subspace of smaller dimension on which to project, through the Galerkin projection, the governing partial differential equation (PDE) (ii) the finite volume discretization technique necessary to carry out the high fidelity simulation and obtain the snapshots, i.e. the PDE solutions in correspondence of different time steps, necessary to build the eigenfunctions that populate the subspace and (iii) an Offline/Online procedure. In this way, the original PDE system is approximated by a system of ordinary differential equations (ODE).

The most adopted model to study the diffusional release of fission gases consists in assuming spherical grains in which the temperature is uniform along the grain. These are more than valid approximations in the case of light water reactors but cannot be adopted in the case of fast reactors in which the restructuring phenomenon, caused by the high temperature values, determines the formation of cylindrical grains in which the spatial dependence of the temperature it is no longer negligible. In addition, the diffusive behavior of the fission gases, which can be isotropic or anisotropic, depends on the particular crystalline structure of the fuel. In this regard, this thesis work proposes to develop a reduced order model for each of these situations in order to involve different nuclear systems in the discussion.

Keywords: Fuel Performance Codes, Fission gases, Models Order Reduction, Proper orthogonal decomposition, Galerkin projection.

Sommario

Durante il normale funzionamento di un impianto nucleare di potenza, l'irraggiamento del combustibile determina la produzione di prodotti di fissione gassosi (xenon e krypton) il cui comportamento rappresenta un fattore limitante la vita del combustibile stesso. In particolare, la loro bassa solubilità ne determina la diffusione e il loro conseguente rilascio nel volume libero della barra di combustibile. I gas di fissione rilasciati nell'intercapedine del combustibile aumentano la pressione interna e la temperatura del combustibile degradando la conducibilità termica del gas di riempimento. Di conseguenza, la comprensione del processo di rilascio dei prodotti di fissione è essenziale per analizzare il comportamento termo-meccanico della barra di combustibile. A tal fine risulta necessario simulare il comportamento intra-granulare dei gas di fissione tramite i codici di performance del combustibile.

Le simulazioni numeriche su scala ingegneristica della barra di combustibile richiedono elevati sforzi computazionali, di conseguenza in questo contesto è essenziale il compromesso tra accuratezza della soluzione numerica e costo computazionale. In virtù di ciò, questo lavoro di tesi si propone di sviluppare un modello di ordine ridotto del processo di diffusione dei gas di fissione, da integrare con i codici di performance del combustibile. Questo è stato reso possibile utilizzando: (i) la tecnica Proper Orthogonal Decomposition (POD) che è stata impiegata per definire il sottospazio di dimensione minore su cui proiettare, mediante la proiezione di Galerkin, l'equazione alle derivate parziali (EDP) che governa il fenomeno (ii) la tecnica di discretizzazione a volumi finiti necessaria per realizzare la simulazione ad alta fedeltà e ricavare gli snapshots, cioè le soluzioni della EDP in corrispondenza di diversi istanti temporali, necessari per costruire le autofunzioni che popolano il sottospazio e (iii) una procedura Offline/Online. In questo modo, il sistema EDP originale viene approssimato da un sistema di equazioni differenziali ordinarie (EDO).

Il modello maggiormente adottato per studiare il rilascio diffusionale dei gas di fissione consiste nell'assumere i grani di forma sferica in cui la temperatura risulti uniforme lungo il grano. Queste rappresentano approssimazioni più che valide nel caso dei reattori ad acqua leggera ma non possono essere adottate nel caso dei reattori veloci in cui il fenomeno della ristrutturazione, causato dagli elevati valori di temperatura, determina la formazione di grani di forma cilindrica in cui la dipendenza spaziale della temperatura non è più trascurabile. Oltre a ciò, il comportamento diffusivo dei gas di fissione, che può essere isotropo o anisotropo, dipende dalla particolare struttura cristallina del combustibile. A tal proposito questo lavoro di tesi si propone di sviluppare un modello di ordine ridotto per ciascuna di queste situazioni in modo da coinvolgere nella trattazione diversi sistemi nucleari.

Parole chiave: Codici di prestazioni del combustibile, Gas di fissione, Modelli di riduzione d'ordine, Proper orthogonal decomposition, Proiezione di Galerkin.

Extended abstract

Multi-scale modelling enables a complete understanding of fuel behavior and provides computational components for Fuel Performance Codes (FPCs) for the development of advanced fuel systems and for predicting in-reactor performance. Among the peculiar phenomena occurring in fuel and in cladding caused by irradiation, there is the creation of Fission Products (FPs) which alter the fuel chemical composition and affect its microstructure inducing atomic displacements and disturbances of the crystallographic structure. Their presence in the fuel can also lead to two complementary phenomena, gaseous swelling and fission gas release which in turn can cause Pellet-Cladding Mechanical Interaction (PCMI), cladding creep and cladding failure. Consequently, fission gas behaviour is a potential life-limiting factor for the operation of nuclear fuel in light water and fast reactors. To predict these phenomena the modelling of fission gas behaviour is typically the first and fundamental part of models in nuclear FPC.

Two different approaches are possible to describe fission gas behaviour in the frame of fuel performance codes: physics-based approaches [1, 2] and correlation-based approaches [3, 4]. Physics-based approaches are often represented by a set of Partial Differential Equations (PDEs) with parametric dependence, which can either be physical or geometrical. Therefore, numerical simulations on engineering-scale of the integral fuel rod requires high computational efforts, also considering the very high number of calls of each local model (such as the fission gas behavior model) in a fuel performance code during the analysis of a detailed fuel rod irradiation history. Accordingly, in addition to the requirement of suitable accuracy for the numerical solution, there is a requirement of low computational cost [5].

Focusing on the fission gas release phenomenon, this occurs mainly by diffusion of the gases through the grains that populate the fuel matrix due to their low solubility. Therefore in physics-based approach of fission gas release, the first step is to model the gas atom transport from inside to boundaries of the grains which takes the name of intra-granular fission gas release. The state-of-art algorithms implemented to describe this transport process have been developed and optimized to solve a specific problem and therefore there is no possibility to apply them under different conditions. Consequently, it is necessary develop techniques that can be extended to more complex models.

A possible solution is to adopt Reduce Order Model (ROM) techniques [6]. The computational reduction techniques identify any approach aimed at replacing a high-fidelity problem with one featuring a much lower complexity trying to preserve the accuracy of the solution as much as possible. The main idea standing at the basis of the reduction strategies is that the behavior of the system with respect to a parameter or the time can be well described by a small number of dominant modes [7]. The

typical requirements of the reduced order modelling are to preserve the relationship between input-output, to guarantee the stability of the ROM and be computationally efficient. These techniques can be divided into two groups: *Computational Reduction Technique (CRT)* and *Surrogate Response Surface (SRS)*. While the latter are based on the interpolation of data obtained through numerical simulations, the former are based on the projection of the system of equations on a subspace of smaller dimension, generated by basic functions representative of the problem considered. For that reason, the CRTs, unlike the SRSs, are built with reference to the mathematical and physical model of departure, and can be used for systems for which numerical data are not available.

Among the CRTs, the POD is the most used procedure in fluid-dynamics. With it, the dimensionality of the problem is reduced by passing from the starting degrees of freedom to a new set consisting of N elements, the modes of the POD, through the expansion of the solution $y = y(\mathbf{x}, t)$ of a PDE on these modes $\varphi_i(\mathbf{x})$:

$$y(\mathbf{x}, t) \approx \sum_{i=1}^{N} a_i(t)\varphi_i(\mathbf{x}) \tag{1}$$

In particular, in the POD based on the *Snapshots Method* [8], the N modes are calculated starting from the snapshots, that is the N_s values y_k assumed by the solution of the complete problem in N_s certain time instants t_k, minimizing the norm of the difference between the snapshots and their projection on the subspace X^{POD} generated by the modes themselves, $X^{POD} = \text{span}\{\varphi_1, \varphi_2, \ldots, \varphi_N\}$:

$$X^{POD} = \text{argmin}\frac{1}{N_s}\sum_{n=1}^{N_s}\left\| y_n - \sum_{i=1}^{N_c}\langle y_n, \varphi_i(\mathbf{x})\rangle\varphi_i(\mathbf{x})\right\|_{L^2}^2 \tag{2}$$

$$\langle\varphi_i(\mathbf{x}), \varphi_j(\mathbf{x})\rangle_{L^2} = \delta_{ij} \tag{3}$$

Once the spatial modes have been computed, replacing theme in the governing equations (1), the original PDE system is approximated by an Ordinary Differential Equation (ODE) system.

This thesis focuses on developing a reduced order model based on POD procedure of the fission gas diffusion phenomenon. The equations are discretized through the Finite Volume (FV) discretization on which the most common codes of fluid-dynamics are based and finally the equations are projected according to Galerkin, i.e. first multiplied by the test functions, in this case the modes of the projection subspace, and then integrated over the volume. The POD technique used in this thesis takes shape starting from the adaptation of the FV methodology developed in [9] (POD-FV-ROM).

The most adopted model to study the diffusional release is the one proposed by Booth [10] which consists in assuming the grain of spherical shape and in which the temperature is supposed to be uniform along the grain. This represents a good approximation in the case of Light Water Reactors (LWRs) in which the morphological alterations due to temperature values are not so significant as to cause an intense restructuring process. On the contrary, in Fast Reactors (FRs) the levels of temperature are such as to cause an intense phenomenon of recrystallization with consequent formation of cylindrical-shaped grains in which the spatial dependence

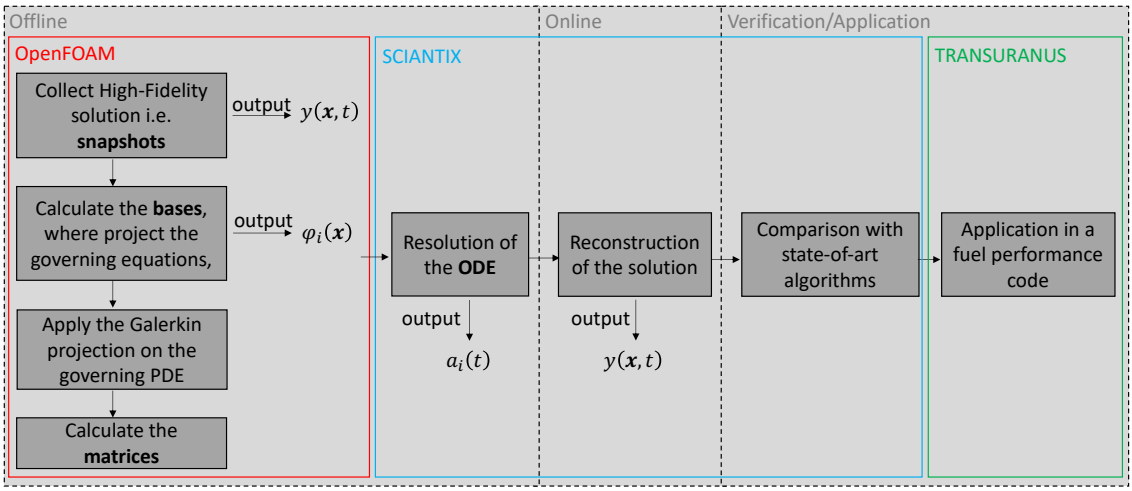

Figure 1. The workflow structure adopted in the present work.

of the temperature is no longer negligible [11]. In addition, the diffusive behavior of fission gases, which can be isotropic or anisotropic, depends on the particular crystalline structure of the fuel. In this regard, this thesis work aims to develop a reduced order model for each of these situations in order to involve the greatest number of nuclear systems in the discussion.

The work presented has been done using OpenFOAM, an open-source Computational Fluid Dynamics (CFD) software that make use of the FV discretization, SCIANTIX, an open source 0D stand-alone computer code designed to be coupled as a module in existing fuel performance codes and the fuel performance code TRANSURANUS. In Figure 1 are summarized the main steps performed in each software/code.

The intra-granular diffusion problem in oxide fuel spherical grains can be written in this way:

$$\frac{\partial c_t\left(r,t\right)}{\partial t} = D_{\text{eff}} \frac{1}{r^2} \frac{\partial}{\partial r}\left(r^2 \frac{\partial}{\partial r} c_t\left(r,t\right)\right) + S \tag{4}$$

adopting the equivalent sphere model proposed by Booth [10], thus exploiting the spherical symmetry of the problem, and the quasi-stationary approach proposed by Speight [12] which consists in lumping the trapping and resolution rate into an effective diffusion coefficient, restating the mathematical problem as purely diffusive. In the equation, $c_t\,(at\ m^{-3})$ is the total intra-granular gas concentration considering both the concentration of single gas atoms dissolved in the lattice and the concentration of gas atoms in intra-granular bubbles, r is the coordinate of the spherical grain, $S\,(\text{at m}^{-3}\ \text{s}^{-1})$ is the production rate of fission gas which is in turn given by the fission rate $\dot{F}\,(\text{fiss m}^{-3}\ \text{s}^{-1})$ multiplied by the total yield of fission gas atoms $y\,(\text{at fiss}^{-1})$ and $D_{\text{eff}}\,(\text{m}^2\ \text{s}^{-1})$ is the effective gas diffusion coefficient, a single parameter lumping the diffusion towards the grain boundaries, the trapping/re-solution rate of atoms in/from intra-granular bubbles:

$$D_{\text{eff}} = \frac{b}{b+g} D \tag{5}$$

The Xe-diffusion coefficient D in irradiated oxide nuclear fuels is made up of three terms, each one describes a distinct physical process that influences different temperature ranges [13]:

$$D = 7.6 \times 10^{-10} e^{-35217/T} + 5.64 \times 10^{-25} \sqrt{\dot{F}} e^{-13840/T} + 2 \times 10^{-40} \dot{F} \tag{6}$$

where $T(K)$ and $\dot{F}\,(\text{fiss m}^{-3}\text{s}^{-1})$.

Each individual grain presents the boundary surface which acts as a perfect sink: upon arrival at the boundary, a gas atom is given a virtually zero probability of returning to the matrix. This defines a mathematical Boundary Condition (BC) of a zero gas concentration immediately adjacent to the grain boundary, i.e., $c_t\,(R,t) = 0$ for $t > 0$ with $R\,(\text{m})$ being the radius of the spherical grain. As initial condition have been considered $c_t\,(r,t) = 0$.

For the purpose of modelling intra-granular fission gas release, the figure of merit is the weighted volume average in the grain of the total gas concentration along time, $\bar{c}_t(t)$. This equation has been implemented in OpenFOAM in order to solve the diffusion problem under constant conditions, i.e. the source term S and the diffusion coefficient D are assumed as constant in time and uniform in space. For the sake of simplicity in the implementation, the quasi-stationary term, i.e. $b/(b+g)$, was not considered in the equation and will be possible to introduce later during the SCIANTIX implementation. Therefore the high fidelity full order simulation refers to this equation:

$$\frac{\partial c\,(r,t)}{\partial t} = D \frac{1}{r^2} \frac{\partial}{\partial r} \left(r^2 \frac{\partial}{\partial r} c\,(r,t) \right) + S \tag{7}$$

It is possible to operate in this way because as shown in Equation 13 the diffusion coefficient is outside the matrix term, consequently during the online stage, that can be run many times as require, is possible change this parameter. Furthermore, to simplify implementation, a dimensionless mesh has been adopted, consequently the Equation 7 have been transformed into a dimensionless form:

$$R^2 \frac{\partial c}{\partial t} = D \nabla^2 c + R^2 S \tag{8}$$

This adimensionalization allows to adopt a spherical mesh of unitary radius expressed in meters and to introduce the radius of the grain directly in the equation.

The simulation was run for $7.5 \times 10^8\,\text{s}$, this was chosen on the basis of the time taken by the phenomenon to reach equilibrium. The frequency of snapshot sampling was set to $1.333 \times 10^{-6}\,\text{Hz}$, therefore in the $7.5 \times 10^8\,\text{s}$-simulation, 1000 snapshots have been collected. The distribution of concentration field at equilibrium resulting from the Full Order Model (FOM) implemented in OpenFOAM is showcased in Figure 2.

The first step in applying the Proper Orthogonal Decomposition (POD) technique, briefly discussed above, to this fission gas diffusion problem in spherical grains is to expressed the approximate solution of the problem $c_r(\mathbf{x},t)$ as linear combination of spatial modes $\phi_i(\mathbf{x})$ multiplied by temporal coefficients $a_i(t)$, thus resulting in the following form:

$$c(\mathbf{x},t) \approx c_r(\mathbf{x},t) = \sum_{i=1}^{N_c} a_i(t) \phi_i(\mathbf{x}) \tag{9}$$

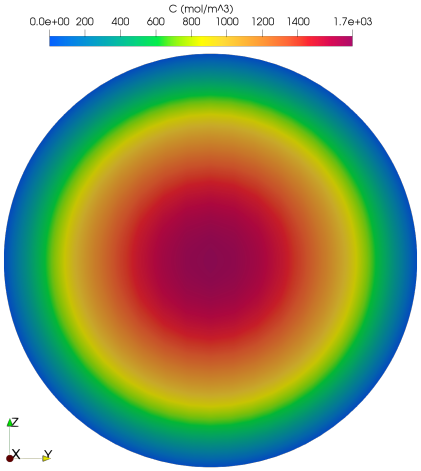

Figure 2. Concentration distribution at 6×10^8 s resulting from the full order simulation implemented in OpenFOAM.

where N_c is the number of basis adopted. Replacing the concentration c with c_r in Equation 8 and projecting according to Galerkin:

$$R^2 \frac{\mathrm{d}a_j(t)}{\mathrm{d}t} = D \sum_{i=1}^{N_c} a_i(t) \int_\Omega \phi_j(\mathbf{x}) \cdot \nabla^2 \phi_i(\mathbf{x}) d\Omega + R^2 S \int_\Omega \phi_j(\mathbf{x}) d\Omega \quad j = 1, ..., N_c \tag{10}$$

By defining the matrices:

$$A_{ji} = \langle \phi_j(\mathbf{x}), \nabla^2 \phi_i(\mathbf{x}) \rangle_{L^2} \tag{11}$$

$$B_j = \langle \phi_j(\mathbf{x}) \rangle_{L^2} \tag{12}$$

The original PDE system is replaced by this ODE system in which the unknowns are the time-dependent coefficients $a_i(t)$:

$$\dot{\mathbf{a}} = \frac{D}{R^2} \mathbf{a}\mathbf{A} + S\mathbf{B} \tag{13}$$

where the dot denotes the time derivative. This ODE system is then solved in SCIANTIX by means an Implicit Euler Scheme in order to derive the time coefficients and finally reconstruct the solution. As can be seen in Equation 13, the diffusion coefficient D is outside the matrix term. In this way during the resolution of the ODE system in SCIANTIX is possible to adopt any diffusion coefficient, based on the type of diffusion phenomenon to be studied.

The procedure to implement the reduction of the model, thus going from a set of PDEs to a set of ODEs, in OpenFOAM follows two main steps: (i) the set of orthonormal modes, which in this thesis is composed by two bases, is computed from the set of snapshots collected during the performing of the full-order model which consist in the minimization of Equation 2, performed through a library implemented in the FOAMextend environment [14] and (ii) this set of orthonormal modes was used to perform the integrations (Equations 11 and 12) so as to obtain the matrices (Equations 11 and 12).

The ODE system (Equation 13) was solved in SCIANTIX by means an iterative procedure based on Backward Euler Scheme:

$$\begin{bmatrix} a_1^{i+1} \\ a_2^{i+1} \end{bmatrix} = \left(I - \frac{D}{R^2} \Delta t \mathbf{A} \right)^{-1} \begin{bmatrix} a_1^i + S\Delta t B_1 \\ a_2^i + S\Delta t B_2 \end{bmatrix} \tag{14}$$

where I is the identity matrix. Once the time coefficients have been obtained, it is possible to reconstruct the solution. For the purpose of modelling intra-granular fission gas release, the figure of merit is the average concentration:

$$\bar{c}(\mathbf{x}, t) \approx \sum_{i=1}^{N_c} a_i(t) \bar{\phi}_i(\mathbf{x}) \tag{15}$$

where $\bar{\phi}_i$ are the weighted volume average of the two set of bases. I have called this numerical algorithm, implemented in SCIANTIX, REDUCE.

The verification of the implemented algorithm was carried out in several ways. The first step was to compare the outcomes of the reduction algorithm in terms of average concentration with the analytical solution and the high-fidelity result. In Figure 3a is possible to see the comparison between this three results. The maximum relative errors between the SCIANTIX and the high-fidelity solution, obtained at the initial time, stands at 6.25%. Through an uncertainty analysis on the parameters that define the concentration (Table 1) is possible conclude that the error obtained is comparable with the uncertainty associated with the diffusion coefficient and therefore can be considered reasonable. Reconstructing the entire concentration distribution in OpenFOAM (Figure 3b) at 6×10^8 s the same result is obtained as shown in Figure 2.

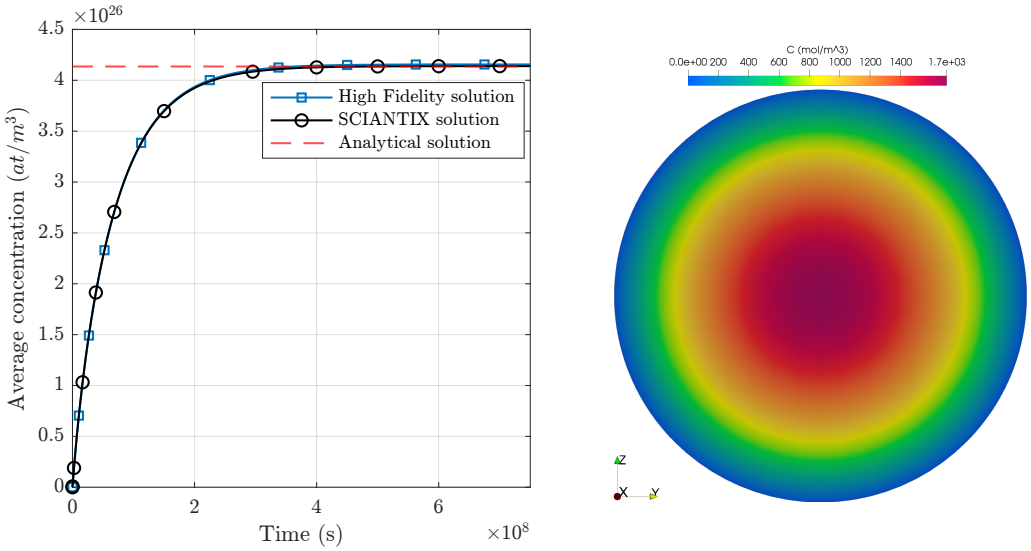

(a) *Online phase implemented in SCIANTIX* **(b)** *Online phase implemented in OpenFOAM*

Figure 3. In (a) is shown the comparison between the SCIANTIX solution, the high fidelity solution and the analytical solution at equilibrium in terms of average concentration. In (b) is shown the reconstruction of the spatial distribution of the concentration field at 6×10^8 s.

Table 1. Values of the uncertainties related to the diffusion coefficient and the radius, obtained from [37], and to the asymptotic value of the average concentration which has been obtained by means of the uncertainty propagation formula.

Parameter	Scaling factors		Variance	Reference
	Low	High		
Grain radius	$0.4R$	$1.6R$	$0.12R^2$	[15]
Diffusion coefficient	$0.4R$	$10R$	$8D^2$	[15]
Average concentration	$-3\sqrt{3}\bar{c}_\infty$	$3\sqrt{3}\bar{c}_\infty$	$9\bar{c}_\infty^2$	

The second part of the verification phase consisted in adopt the Method of Manufactured Solutions (MMS) in order to test that the algorithm is able to scale the error correctly, as the time step varies, in physical and non-physical situations so as to control its behavior even in complex situations in which the parameters could assume unexpected values. The procedure is briefly structured as follows: (i) As the name suggests a specific solution is manufactured and assumed to satisfy the PDE of interest (ii) the solution is replaced in the PDE and the equation is rearranged such that a forcing source term appears and (iii) the PDE is numerically solved with the forcing source term and the two solutions are compared. In Figures 4 and 5 the estimate of the convergence order p of the method is showcased. As expected, it asymptotically approaches to two, since the time derivative is discretized with implicit Euler method of order one and the algorithm performs also the spatial average.

Lastly, different numerical experiments were performed aimed to (i) verify the

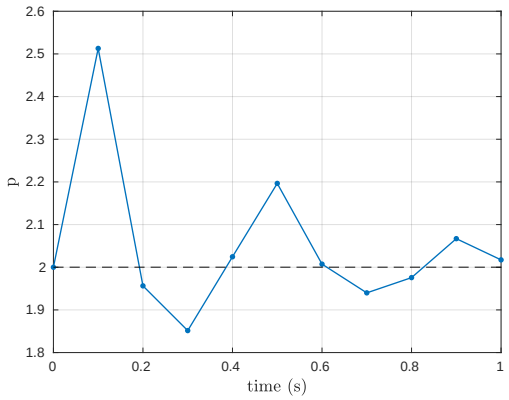

Figure 4. Behaviour of the estimated order of convergence p in the case of physical diffusion coefficient. Despite the initial oscillations, the method shows an order of convergence equal to two.

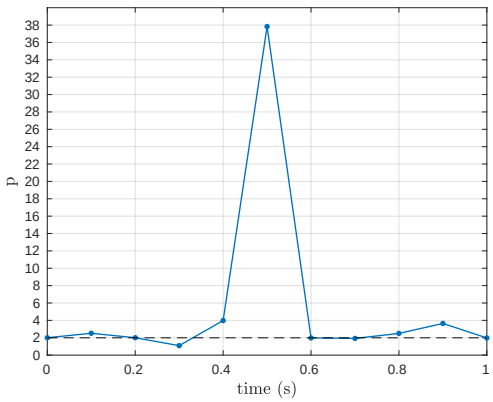

Figure 5. Behaviour of the estimated order of convergence p in the case of non-physical diffusion coefficient. Also in this case is reached an order of convergence of two.

solution of the algorithm (ii) compare the accuracy of the algorithm solutions and computational time to other state-of-art algorithms currently used in fuel performance codes and (iii) compare the accuracy of the algorithm to a reference algorithm which provides quasi-exact solution. As state-of-art algorithms were used FORMAS and ANS-5.4 which, unlike the REDUCE algorithm, have been implemented to solve the

diffusion equation under time-varying conditions, i.e. $D_{\text{eff}}(t)$ and $S(t)$. As reference algorithm a refined version of ANS-5.4 obtained adopting a number of modes high enough that the truncation error is negligible and each time interval was discretized in more sub-steps than the other algorithms. The numerical experiment consists of application of each algorithm to the numerical solution of Equation 4 for 1000 randomly generated operation histories. In each individual history, the quantities: number of linear steps, time duration of each linear step, temperature and fission rate are considered as random variables (sampled from uniform distributions). These features ensure that all possible situations are covered. The figure of merit adopted to compare the REDUCE algorithm with FORMAS and ANS-5.4 are: (1) the intra-granular average fission gas concentration, (2) the fractional intra-granular fission gas release and (3) the computational time taken by the three algorithms. While the comparison with the reference algorithm was made only through the intra-granular average fission gas concentration.

***Intra-granular average fission gas concentration*:** The results are reported in Figure 6. For this type of graphic representation, any deviation from the 45° diagonal is a measure of the accuracy: the closer the results are to the 45° diagonal, the better the algorithm is. As can be seen, the REDUCE algorithm is able to calculate the intra-granular average concentration with good accuracy indeed only a slight deviation is perceived. The only data point that deviates very far from the 45° diagonal is the red one. The history related to this point is characterized by a sharp change in the parameters, consequently it is possible to conclude that the discrepancy is due to the fact that FORMAS and ANS-5.4 have been implemented to solve the diffusion equation under time-varying conditions while the REDUCE algorithm under constant conditions.

***Intra-granular fission gas release*:** The intra-granular fission gas release is defined as:

$$f := \frac{\bar{c}_{created}(t_{end}) - \bar{c}_t(t_{end})}{\bar{c}_{created}(t_{end})} \tag{16}$$

where $\bar{c}_{created}$ (at m^{-3}) is the concentration of gas created (i.e. the time integral of $S(t)$) and t_{end}(s) is the final time of the operation history. The results are reported in Figure 7. Was adopted this type of graphic representation in order to show the range, in terms of release, covered by each algorithm. As can be seen, the REDUCE algorithm covers approximately the same intra-granular fission gas release interval as the FORMAS and American Nuclear Society (ANS)-5.4 algorithms except for the very low values. Consequently this algorithm has good coverage of the range of interest, $0 \div 0.8$, related to application in light water reactors where the fission gas release is not very high.

***Computational time*:** The results are reported in Figure 8. As can be seen, the REDUCE algorithm takes the same computational time as FORMAS (Figure 1.17a) which is reasonable since FORMAS solves four decoupled ODEs that are equivalent to solve a system of two coupled ODEs as the REDUCE algorithm does. On the other side, the REDUCE algorithm takes less time than ANS-5.4 (Figure 1.17b), this is due to the fact that ANS-5.4 solves thirty spatial modes that correspond to thirty decoupled ODEs, resulting in a higher computational cost than REDUCE.

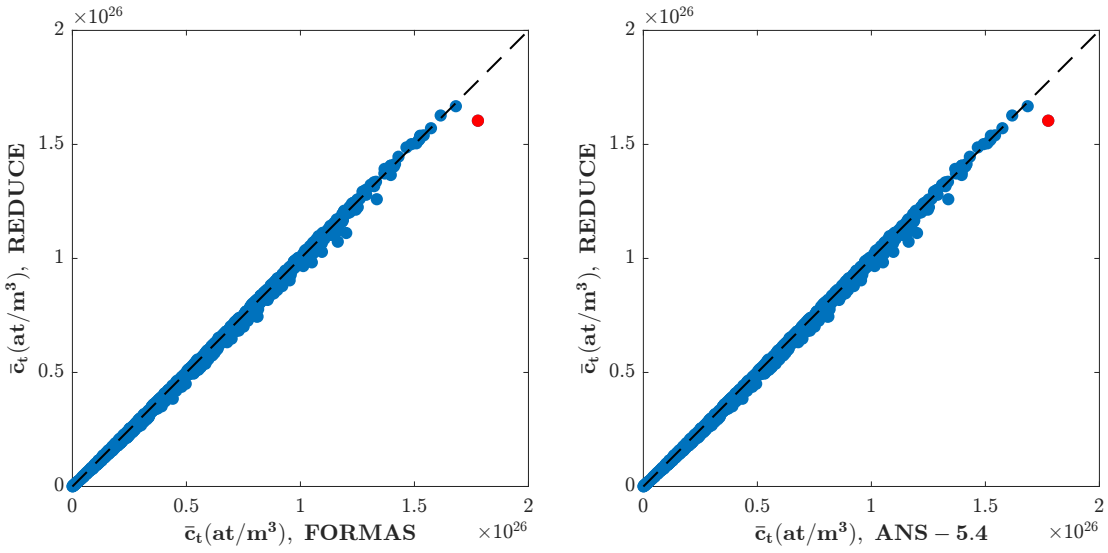

Figure 6. Comparison between the values of intra-granular average fission gas concentration calculated by the REDUCE algorithm and by the FORMAS algorithm (a) and calculated by the REDUCE algorithm and by the ANS-5.4 algorithm (b). The red data point in each figure corresponds to a story characterized by sharp change in the parameters and indeed this point turns out to be the one most diverged from the 45° diagonal due to the implementation characteristics of the REDUCE algorithm which do not allow to detect properly a similar situation.

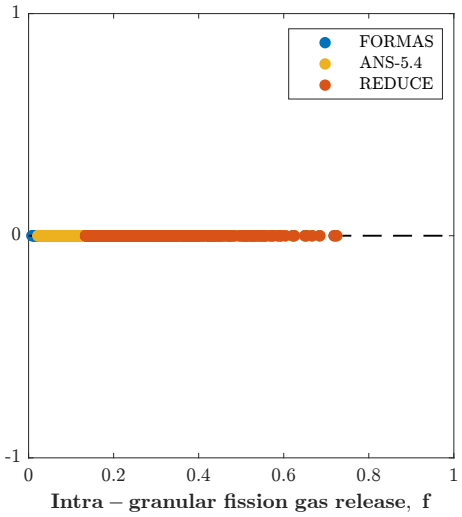

Figure 7. Comparison between the interval covered in terms of intra-granular fission gas release by the three algorithm.

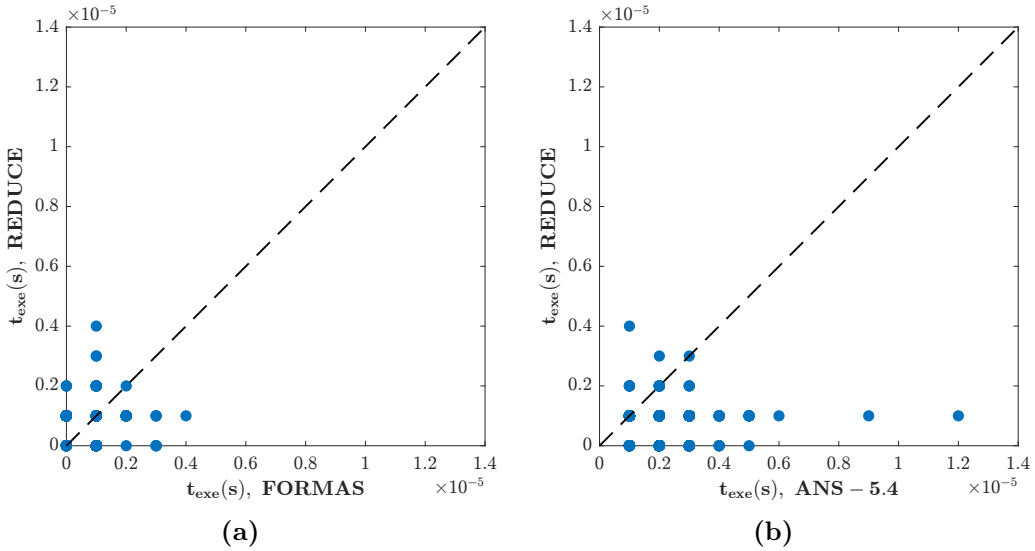

Figure 8. Comparison between the values of execution time calculated by the REDUCE, FORMAS and ANS-5.4 algorithms.

***Reference algorithm*:** The results are reported in Figure 9. As can be seen, the accuracy of the REDUCE algorithm is lower than FORMAS and ANS-5.4. indeed in Figures 9a is possibile to see a slight deviation from the 45° diagonal while in Figures 9b and 9c the deviation is imperceptible. This is due to the fact that FORMAS and ANS-5.4 have been implemented to solve the diffusion equation under time-varying conditions while the REDUCE algorithm under constant conditions. Moreover, FORMAS ans ANS-5.4, are methods that have been optimized from the point of view of the number of bases to be used while REDUCE is still in a preliminary phase in which no optimization work has been done. To investigate in finer detail the accuracy of the three algorithms, in Figure 9d is showcased the relative error of the solution obtained with each algorithm with respect to the reference algorithm solution. The results are consistent with the conclusions just drawn, namely that the overall accuracy of REDUCE is less than FORMAS and ANS-5.4.

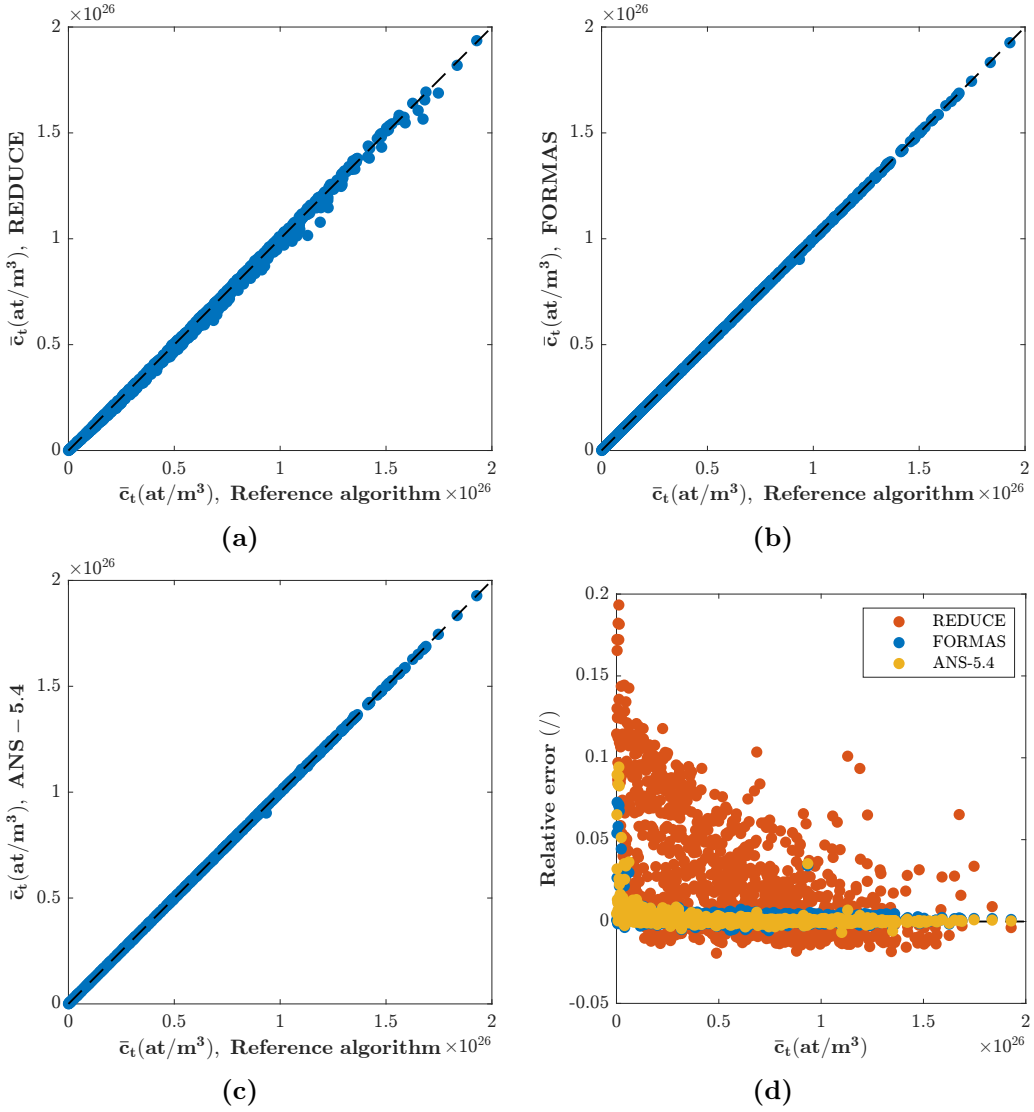

Figure 9. Comparison between the values of intra-granular average fission gas concentration calculated by the reference algorithm and by the other three algorithms. In (d) is shown the comparison between the REDUCE, FORMAS and ANS-5.4 algorithms in terms of relative error with respect to the reference algorithm.

The application of the algorithm to integral fuel rod analysis was carried out by coupling SCIANTIX with the fuel performance code TRANSURANUS in order to demonstrate that, firstly, the REDUCE algorithm is able to work if applied to a case of integral irradiation without ever crashing and to have a stable behavior for the entire duration of the irradiation and, secondly, is able to correctly predict the fission gases behavior. In this regard, I simulated the GE7 rod irradiation experiment carried out during the third Risø Transient Fission Gas Release program in 1989. The test fuel rod consisted of pellets of UO_2 at 95.2% theoretical density with 2-dimensional average grain diameter of approximately 18.8 μm. The cladding is in Zircaloy-2 with an outer diameter of 12.26 mm and was stress relieved with a bonded zirconium liner. The experiment involves a fuel rod base irradiation up to about 40 GWd t_U^{-1} and subsequent a power transient test. The power history during the bump included a 6-hour conditioning period at approximately 30 W mm^{-1}, a 15 minute power ramp, and then a 4-hour hold, where the the linear heat rate at the end of the hold period was 48 W mm^{-1}.

Figures 1.24 and 1.25 compares the results obtained by the three algorithm in terms of intra-granular average fission gas concentration and fractional fission gas release as a function of the time, during the base irradiation and the power ramp. The underestimation of the gas concentration in the grain, and on the other hand the overestimation of the gas release, operated by the REDUCE algorithm is due to the number of bases adopted during the implementation of the POD procedure. Since only two bases are adopted, these do not allow a complete knowledge of the phenomenon and therefore lead to underestimate the real concentration value present in the grain. Accordingly, what can be done to reduce the discrepancy is to increase the number of bases that populate the subspace of smaller dimension 1.18 in order to have a more complete characterization of the phenomenon.

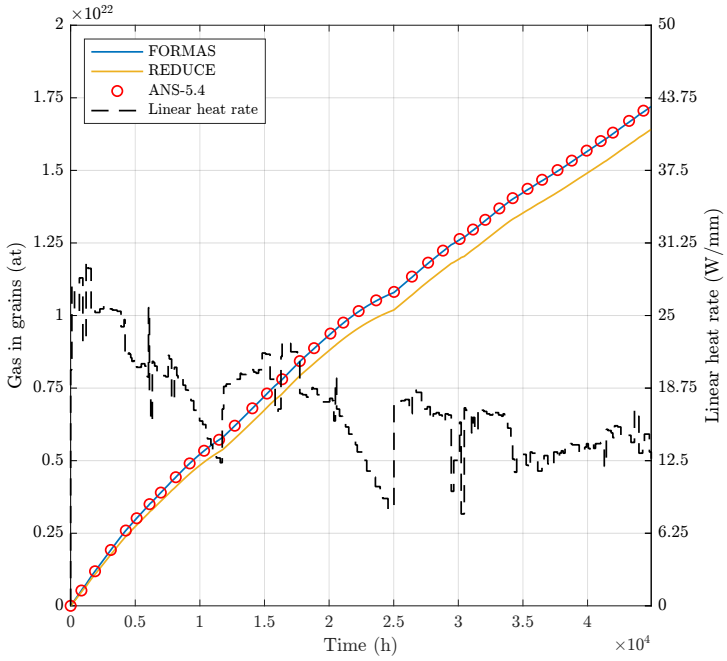

(a) Base irradiation

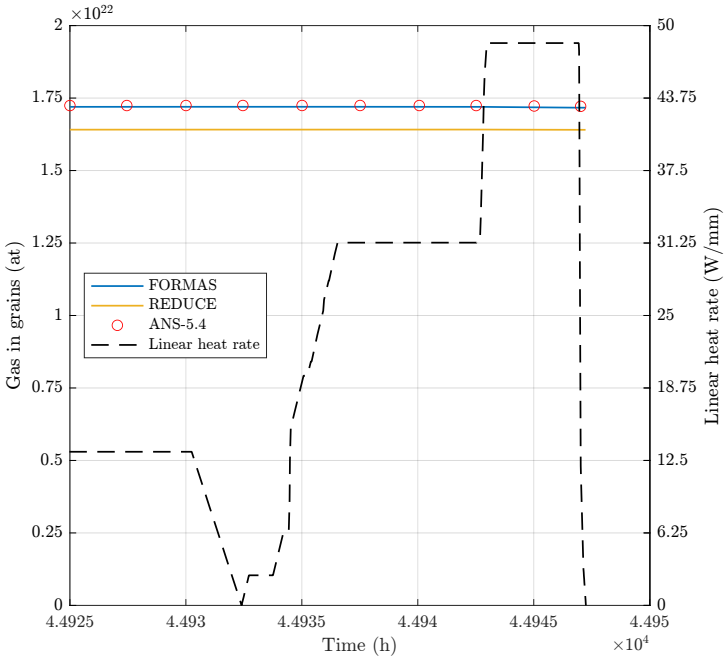

(b) Zoom on the ramp test

Figure 10. Comparison between the values of intra-granular average fission gas concentration along time calculated by the REDUCE, FORMAS and ANS-5.4 algorithms during the base irradiation (a) and ramp test (b).

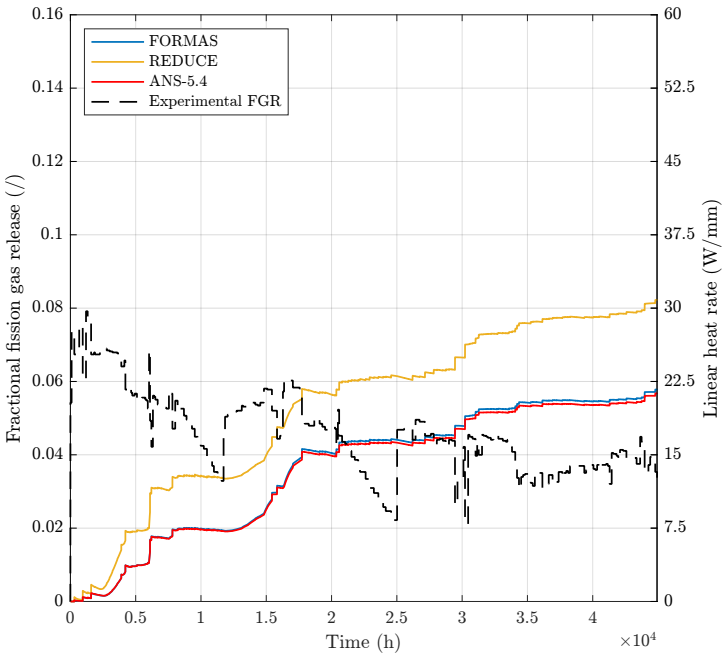

(a) Base irradiation

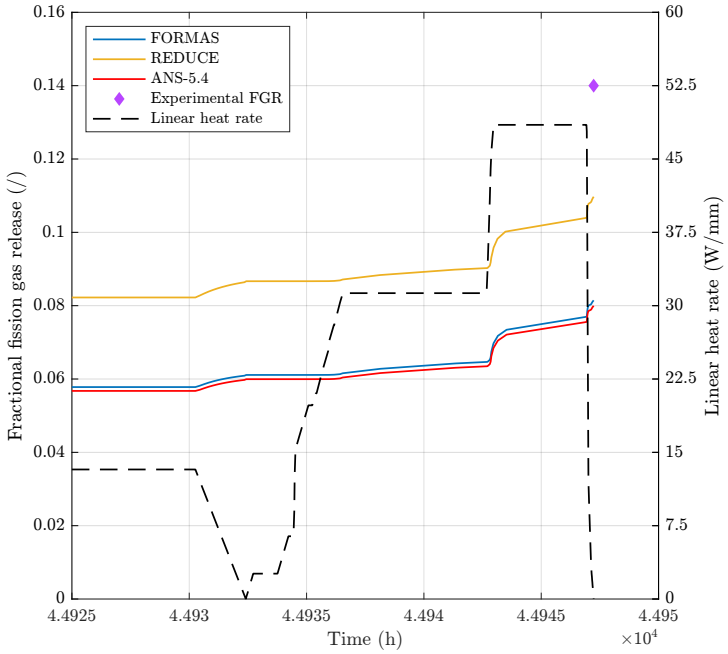

(b) Zoom on the ramp test

Figure 11. Comparison between the values of intra-granular fission gas release along time calculated by the REDUCE, FORMAS and ANS-5.4 algorithms during the base irradiation (a) and ramp test (b).

At the conclusion of the isotropic diffusion analysis in spherical grains, the order reduction procedure was further enriched in order to consider the anisotropic behavior of diffusion. Such situation occurs with uranium silicide fuel, as U_3Si_2, promising Accident Tolerant Fuel (ATF) and candidates to substitute uranium dioxide in LWR thanks to their interesting thermophysical properties and high uranium densities. The Xe-diffusivity is anisotropic due to the tetragonal crystal structure of U_3Si_2, accordingly the intra-granular diffusion problem has to be written in this way:

$$\frac{\partial c_t(r,t)}{\partial t} = \frac{1}{r^2}\frac{\partial}{\partial r}\left(\underline{\underline{D}}_{\text{eff}}\, r^2 \frac{\partial}{\partial r} c_t(r,t)\right) + S \tag{17}$$

adopting the equivalent sphere model proposed by Booth [10] and the quasi-stationary approach proposed by Speight [12], analogously to the isotropic case. Now the Xe-diffusion coefficient D is a tensor with components $D_{Xe}^{aa} = D_{Xe}^{bb}$ in the basal $a-b$ plane and D_{Xe}^{cc} along the c axis. The equation implemented in OpenFOAM, neglecting the quasi-stationary term and adopting a dimensionless mesh, is:

$$R^2 \frac{\partial c}{\partial t} = \nabla \cdot \left(\underline{\underline{D}} \nabla c\right) + R^2 S \tag{18}$$

The strategy necessary to be adopt in the POD procedure in order to deal with anisotropy correctly was to rewrite the Equation 18 by separating the diffusion coefficient from the matrix containing the anisotropy of the problem, $\underline{\underline{G}}$:

$$R^2 \frac{\partial c}{\partial t} = \nabla \cdot \left(D_{Xe}^{aa} \begin{bmatrix} 1 & 0 & 0 \\ 0 & 1 & 0 \\ 0 & 0 & \frac{D_{Xe}^{cc}}{D_{Xe}^{aa}} \end{bmatrix} \cdot \nabla c \right) + R^2 S \tag{19}$$

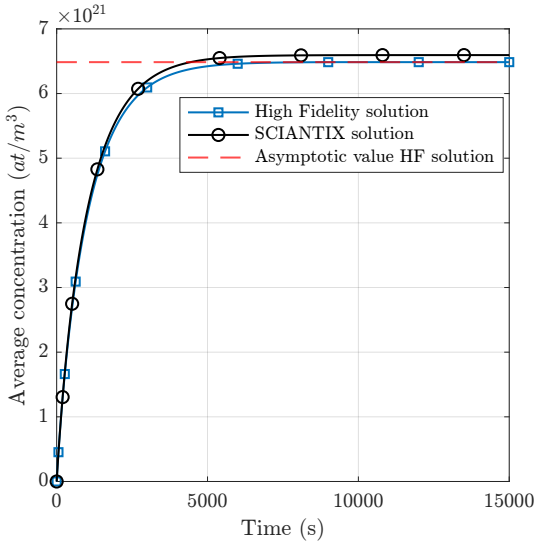

Figure 12. Comparison between the SCIANTIX solution and the high fidelity solution in terms of average concentration. The red dashed line identify the asymptotic value of the high fidelity solution.

in order to get rid of the anisotropy of the problem in online phase by involving it in the calculation of the matrix (Equation 21). Going on with the POD procedure, carried out analogously to the isotropic case, the following ODE system was obtained:

$$\dot{\mathbf{a}} = \frac{D_{Xe}^{aa}}{R^2}\mathbf{a}\mathbf{E} + S\mathbf{F} \tag{20}$$

where:

$$E_{ji} = \langle \phi_j(\mathbf{x}), \nabla \cdot \left[\underline{\underline{G}}\nabla\phi_i(\mathbf{x})\right]\rangle_{L^2} \tag{21}$$

$$F_j = \langle \phi_j(\mathbf{x})\rangle_{L^2} \tag{22}$$

The only verification that has been performed for this anisotropic diffusion case was to compare the solution obtained from the SCIANTIX code with the high-fidelity solution. In Figure 2.5 is possible to see the comparison between this two results. The initial relative error stands at 6% and reaches 1.7% at equilibrium. Referring to the uncertainty analysis on the parameters previously seen, is possible conclude that the reduced order model reproduces with good accuracy the solution relative to the FOM unless a negligible error, comparable to the uncertainty on the parameters.

Finally, the order reduction procedure used for the anisotropic diffusion problem in spherical grains has been extended to cylindrical grains. In Mixed Oxides (MOX) fuels adopted in FRs not only spherical but also cylindrical grains are formed due to the restructuring process. For this type of grains it is no longer possible to adopt the hypothesis of spherical grain and uniform temperature along the grain defined by

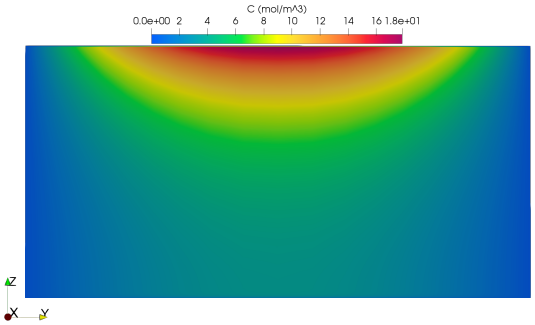

Figure 13. Concentration distributions at 6×10^6 s resulting from the full order simulation implemented in OpenFOAM.

Booth [10] making the diffusion problem highly non-linear:

$$\begin{cases} \dfrac{\partial}{\partial t}T(z,t) = \dfrac{1}{r}\dfrac{\partial}{\partial r}\alpha\left(T(z,t)r\dfrac{\partial}{\partial r}T(z,t)\right) + \dfrac{\partial}{\partial z}\alpha\left(T(z,t)\dfrac{\partial}{\partial z}T(z,t)\right) + Q \\ \dfrac{\partial}{\partial t}c_t(r,z,t) = \dfrac{1}{r}\dfrac{\partial}{\partial r}\left(D_{\text{eff}}\left(T(z)\right)r\dfrac{\partial}{\partial r}c_t(r,z,t)\right) + \dfrac{\partial}{\partial z}\left(D_{\text{eff}}\left(T(z)\right)\dfrac{\partial}{\partial z}c_t(r,z,t)\right) + S \end{cases} \tag{23}$$

where z (m) is the longitudinal coordinate, α (m^2 s^{-1}) is the thermal diffusivity and Q (K s^{-1}) is the heat generation rate. For concentration problem was set the same BC as before while for temperature problem was set an initial condition of 2000 K, a Dirichlet boundary condition of 2000 K on one of the cylinder basis and a null Neumann boundary condition on the other basis and on the lateral surface. The equations implemented in OpenFOAM, neglecting the quasi-stationary term and adopting a dimensionless mesh, are:

$$\begin{cases} L^2\dfrac{\partial T(\mathbf{x},t)}{\partial t} = \alpha\nabla^2 T(\mathbf{x},t) + L^2 Q \\ L^2\dfrac{\partial c}{\partial t} = L^2\nabla\cdot(\underline{\underline{D}}\nabla c) + L^2 S \end{cases} \tag{24}$$

where the anisotropy of the problem has been exploited through the tensor representation of the Turnbull diffusion coefficient (Equation 6) where D_x and D_y have been divided by the squared length of the radius, R, and D_z has been divided by the squared length of the height of the cylinder, L. The result of the simulation in terms of distribution of concentration field at equilibrium is showcased in Figure 13.

Having to deal with a system of coupled Partial Differential Equations (PDEs), the first step of POD procedure is to express not only the concentration field but also the temperature field as linear combination of spatial modes, $\varphi_i(\mathbf{x})$ and $\phi_i(\mathbf{x})$, multiplied by temporal coefficients, $a_i(t)$ and $b_i(t)$:

$$T(\mathbf{x},t) \approx T_r(\mathbf{x},t) = \sum_{i=1}^{N_T} a_i(t)\varphi_i(\mathbf{x}) \tag{25}$$

$$c(\mathbf{x},t) \approx c_r(\mathbf{x},t) = \sum_{i=1}^{N_c} b_i(t)\phi_i(\mathbf{x}) \tag{26}$$

By introducing the following matrices:

$$H_{ji} = \langle \varphi_j(\mathbf{x}), \nabla^2 \varphi_i(\mathbf{x}) \rangle_{L^2} \tag{27}$$

$$L_j = \langle \varphi_j(\mathbf{x}) \rangle_{L^2} \tag{28}$$

$$J_{ji} = \langle \varphi_j(\mathbf{x}), \varphi_i(\mathbf{x}) \rangle_{L^2,\Gamma_1} \tag{29}$$

$$K_j = \langle \varphi_j(\mathbf{x}) \rangle_{L^2,\Gamma_1} \tag{30}$$

$$X_{ji} = \langle \phi_j(\mathbf{x}), \nabla \cdot \left[\underline{\underline{\mathrm{G}}} \nabla \phi_i(\mathbf{x}) \right] \rangle_{L^2} \tag{31}$$

$$M_{jki} = \langle \phi_j(\mathbf{x}), \left(\varphi_k(\mathbf{x}), \nabla \cdot \left[\underline{\underline{\mathrm{G}}} \nabla \phi_i(\mathbf{x}) \right] \right) \rangle_{L^2} \tag{32}$$

$$N_{jki} = \langle \phi_j(\mathbf{x}), \left[\nabla \varphi_k(\mathbf{x}), \underline{\underline{\mathrm{G}}} \nabla \phi_i(\mathbf{x}) \right] \rangle_{L^2} \tag{33}$$

$$P_j = \langle \phi_j(\mathbf{x}) \rangle_{L^2} \tag{34}$$

The system of reduced equations is composed by the following equations:

$$\begin{cases} \dot{\mathbf{a}} = \dfrac{\alpha}{L^2} \mathbf{a}\mathbf{H} + Q\mathbf{L} + \tau_T \left[\dfrac{1}{L^2} \mathbf{J}\mathbf{a} - \dfrac{T_{BC}}{L^2} \mathbf{K} \right] \\ \dot{\mathbf{b}} = \dfrac{1}{R^2} \left(D^0 - \alpha^D T^0 \right) \mathbf{b}\mathbf{X} + \dfrac{1}{R^2} \alpha^D \mathbf{a}^T \mathbf{b}\mathbf{M} + \dfrac{1}{R^2} \alpha^D \mathbf{a}^T \mathbf{b}\mathbf{N} + S\mathbf{P} \end{cases} \tag{35}$$

where τ_T is the Penalty factor introduced in order to enforce explicitly the Dirichlet BC on temperature. The dependence on temperature by the diffusion coefficient has been modeled by means of the linear relation:

$$D = D^0 + \alpha^D (T - T^0) \tag{36}$$

The maximum relative error deriving from the comparison between the SCIANTIX solution and the high fidelity solution (Figure 14a), obtained at equilibrium, stands at 13.10% is negligible and comparable to the uncertainty on the parameters. Reconstructing the entire concentration distribution in OpenFOAM (Figure 14b) at 6×10^6 s is obtained a result comparable, except for a negligible error, with the distribution relative to the FOM (Figure 13).

In conclusion, in this Master Thesis a reduced order modeling approach for fission gas behaviour has been developed. In particular, the focus was on the diffusion of fission gases in the grains of different nuclear fuels and operating under different conditions. This work is aimed at tackling the need of nuclear engineering field to have a fast-running simulation tool. The global goal has been to demonstrate that reduced order modeling is suited to be applied in more complex industrial problems in order to introduce competitive computational performance. The goal has been

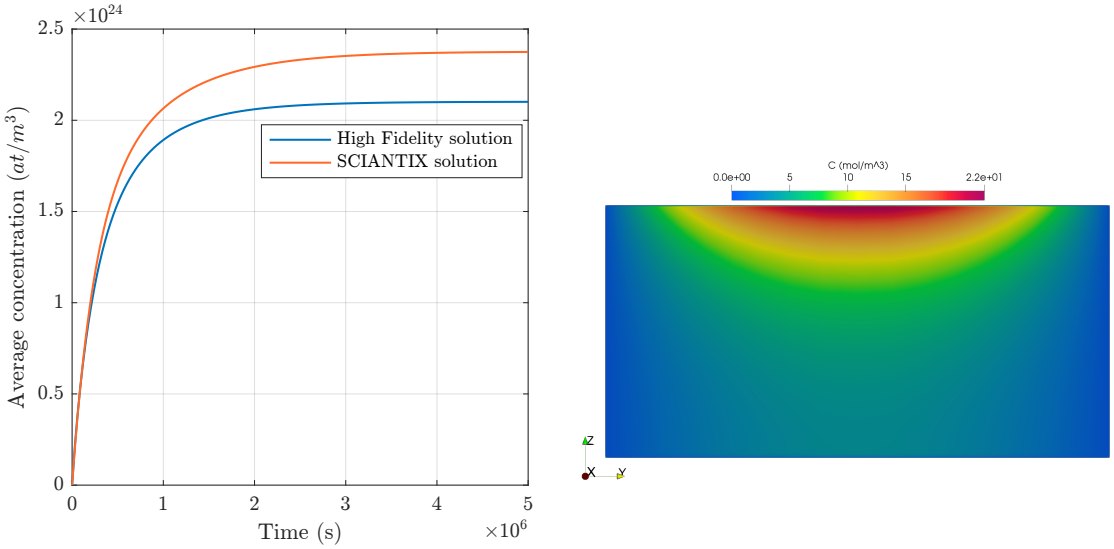

(a) *Online phase implemented in SCIANTIX* **(b)** *Online phase implemented in OpenFOAM*

Figure 14. In (a) is shown the comparison between the SCIANTIX solution, the high fidelity solution and the analytical solution at equilibrium in terms of average concentration. In (b) is shown the reconstruction of the spatial distribution of the concentration field at 6×10^6 s.

pursued with a three-step procedure in which the ROM technique was progressively enriched. The present work may represent a starting point for future developments of ROM techniques in the framework of fission gas behaviour. What could be done to further enrich the discussion is, for example, consider that: (i) for some systems it may be useful to solve not a single diffusion equation but to take into account the two coupled equations relating to the gas in the bubbles and the gas in solution, (ii) there could be a diffusion term on the bubbles, i.e. a mobility of the intra-granular bubbles, which comes into play beyond 1800 °C and (iii) an advective term could be introduced in order to more accurately describe the transport of fission gases in the fuel matrix. Despite the many other features that could be considered, the models implemented up to now with this thesis work still allow to deal with a good number of nuclear systems. Furthermore, the development of the ROM has focused on the diffusion of fission gases but in a FPC there are many other physics, for example the gap conductance, on which such an approach could work. Consequently, this thesis can be considered more generally a "demonstrator" of using a ROM approach to sub-modules in an FPCs.

Acronyms

AFC	Advanced Fuel Campaign
ATF	Accident Tolerant Fuel
ANS	American Nuclear Society
BC	Boundary Condition
BWR	Boiling Water Reactor
CFD	Computational Fluid Dynamics
CRT	Computational Reduction Technique
DFT	Density Functional Theory
FE	Finite Elements
FGR	Fission Gas Release
FOM	Full Order Model
FP	Fission Product
FPC	Fuel Performance Code
FR	Fast Reactor
FV	Finite Volume
JRC	Joint Research Center
LWR	Light Water Reactor
MMS	Method of Manufactured Solutions
MOX	Mixed Oxides
ODE	Ordinary Differential Equation
PDE	Partial Differential Equation
PCMI	Pellet-Cladding Mechanical Interaction
POD	Proper Orthogonal Decomposition
PWR	Pressurized Water Reactor
RB	Reduced Basis
ROM	Reduce Order Model
SRS	Surrogate Response Surface
SVD	Singular Value Decomposition
TD	Theoretical Density

Symbols

a_i	(/)	temporal coefficient
$\mathbf{a}$	(/)	vector of ROM temporal coefficient
$\mathbf{A}$	(/)	ROM matrix
b	(s^{-1})	resolution rate
b_i	(/)	temporal coefficient
$\mathbf{B}$	(/)	ROM matrix
c	(at m^{-3})	intra-granular gas concentration
c_p	(J kg^{-1} K^{-1})	specific heat
c_r	(at m^{-3})	approximated intra-granular gas concentration
$\bar{c}_{created}$	(at m^{-3})	concentration of gas created
$\bar{c}_\infty$	(at m^{-3})	analytical weighted volume average concentration at equilibrium
$\bar{c}_\infty^{HF}$	(at m^{-3})	weighted volume average concentration computed with OpenFOAM
c_b	(at m^{-3})	in-bubble intra-granular single gas atoms concentration
c_s	(at m^{-3})	in-solution intra-granular single gas atoms concentration
c_t	(at m^{-3})	total intra-granular gas concentration
d	(m)	atomic jump distance
D	(m^2 s^{-1})	single gas atom diffusion coefficient
D_{eff}	(m^2 s^{-1})	effective gas atom diffusion coefficient
D_{Xe}^{aa}	(m^2 s^{-1})	xenon diffusion coefficient along x coordinate in U_3Si_2
D_{Xe}^{bb}	(m^2 s^{-1})	xenon diffusion coefficient along y coordinate in U_3Si_2
D_{Xe}^{cc}	(m^2 s^{-1})	xenon diffusion coefficient along z coordinate in U_3Si_2
$\mathbf{E}$	(/)	ROM matrix
f	(/)	intra-granular fission gas released
$\dot{F}$	(fiss m^{-3} s^{-1})	fission rate density
$\mathbf{F}$	(/)	ROM matrix
g	(s^{-1})	trapping rate
$\mathbf{G}$	(/)	matrix containing the anisotropy of the problem
H	(J)	activation energy
$\mathbf{H}$	(/)	ROM matrix
$\mathbf{I}$	(/)	identity matrix
j_v	(s^{-1})	thermally activated vacancy jump rate

$\mathbf{J}$	(/)	ROM matrix
k	(W m^{-1} K^{-1})	thermal conductivity
k_B	(J K^{-1})	Boltzmann constant
$\mathbf{K}$	(/)	ROM matrix
L	(m)	cylindrical grain length
$\mathbf{L}$	(/)	ROM matrix
$\mathbf{M}$	(/)	ROM matrix
N_s	(/)	number of snapshots
$\mathbf{N}$	(/)	ROM matrix
p	(/)	convergence error of a numerical method
$\mathbf{P}$	(/)	ROM matrix
q	(K fiss^{-1})	fission heat
q'''	(W m^{-3})	power density
S	(at m^{-3} s^{-1})	fission gas production rate
y	(at fiss^{-1})	total yield of fission gas atoms
r	(m)	radial coordinate
R	(m)	spherical and cylindrical grain radius
t	(s)	time
t_{end}	(s)	final time of the operation history
t_n	(s)	snapshot collection time
t_{exe}	(s)	execution time of the algorithm
T	(K)	temperature
T_r	(K)	approximated temperature
u_∞	(/)	relative error between SCIANTIX and high-fidelity at equilibrium
$u_{\max}$	(/)	maximum relative error between SCIANTIX and high-fidelity
u_∞^{HF}	(/)	relative error between the high-fidelity simulation and the analytical solution at equilibrium
u_∞^{SC}	(/)	Relative error between SCIANTIX and analytical solution at equilibrium
$\mathbf{x}$	(m)	vector of spatial coordinate
X_c^{POD}	(/)	reduced subspace of concentration field
X_T^{POD}	(/)	reduced subspace of temperature field
$\mathbf{X}$	(/)	ROM matrix
z	(m)	longitudinal coordinate
α	(m^2 s^{-1})	thermal diffusivity
Γ	(/)	boundary function
ρ	(kg m^{-3})	density
τ	(s)	characteristic time of the phenomenon
$\varphi_i(\mathbf{x})$	(s)	temperature spatial modes
$\phi_i(\mathbf{x})$	(at m^{-3})	concentration spatial modes
Ω	(m^3)	spatial domain

Contents

List of Figures

List of Tables

Introduction

Multi-scale modelling enables a complete understanding of fuel behavior and provides computational components for Fuel Performance Codes (FPCs) for the development of advanced fuel systems and for predicting in-reactor performance. Among the peculiar phenomena occurring in fuel and in cladding caused by irradiation, there is the creation of Fission Products (FPs) which alter the fuel chemical composition and affect its microstructure inducing atomic displacements and disturbances of the crystallographic structure. Their presence in the fuel can also lead to two complementary phenomena, gaseous swelling and fission gas release which in turn can cause Pellet-Cladding Mechanical Interaction (PCMI), cladding creep and cladding failure. Consequently, fission gas behaviour is a potential life-limiting factor for the operation of nuclear fuel in light water and fast reactors. To predict these phenomena the modelling of fission gas behaviour is typically the first and fundamental part of models in nuclear FPCs.

Two different approaches are possible to describe fission gas behaviour in the frame of fuel performance codes: (1) physics-based approaches, which are based on mechanistic models and aim at describing the physical mechanisms of fission gas behaviour within the fuel [1, 2], and (2) correlation-based approaches, in which mechanistic models are replaced with simplified empirical descriptions, consequently fission gas release and gaseous swelling are calculated via expressions directly related to macroscopic variables of the fuel rod (e.g., fuel temperature and burnup) and tuned on experimental data [3, 4]. Physics-based approaches are often represented by a set of Partial Differential Equations (PDEs) with parametric dependence, which can either be physical or geometrical. Therefore, numerical simulations on engineering-scale of the integral fuel rod requires high computational efforts, also considering the very high number of calls of each local model (such as the fission gas behavior model) in a fuel performance code during the analysis of a detailed fuel rod irradiation history. Accordingly, in addition to the requirement of suitable accuracy for the numerical solution, there is a requirement of low computational cost [5].

Focusing on the Fission Gas Release (FGR) phenomenon, this occurs mainly by diffusion of the gases through the grains that populate the fuel matrix due to their low solubility. Therefore in physics-based approach of fission gas release, the first step is to model the gas atom transport from inside to boundaries of the grains which takes the name of intra-granular fission gas release. The state-of-art algorithms implemented to describe this transport process have been developed and optimized to solve a specific problem and therefore there is no possibility to apply them under different conditions. Consequently, it is necessary to develop techniques that can be extended to more complex models.

A possible solution is to adopt Reduce Order Model (ROM) techniques [6]. The

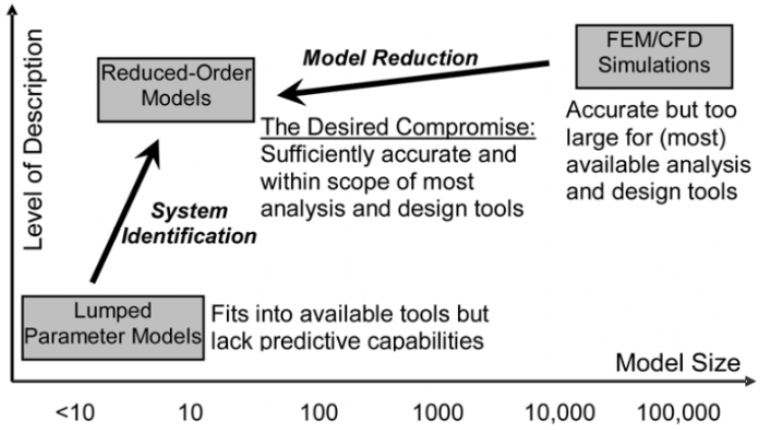

Figure 1. Scheme of the reduced order modelling approach underling the trade-off between the level of accuracy and the model size [16].

computational reduction techniques identify any approach aimed at replacing a high-fidelity problem with one featuring a much lower complexity trying to preserve the accuracy of the solution as much as possible. The main idea standing at the basis of the reduction strategies is that the behavior of the system with respect to a parameter or the time can be well described by a small number of dominant modes [7]. The typical requirements of the reduced order modelling are to preserve the relationship between input-output, to guarantee the stability of the ROM and be computationally efficient. This means finding the best compromise between accuracy and the size of the model (Fig. 1). It is important clarify that reduced order modelling do not replace high-fidelity discretization technique but there is a kind of algorithmic collaboration between them since the reduced order model are usually built upon and compared to the Full Order Model (FOM) [20].

The use of techniques focused on this scope are not recent, the earliest attempt of reduction approximation can be considered the truncated Fourier series [21] and the Lagrange Polynomial Interpolation in the 18th century, however their development has increased in recent years in parallel with the increase of computational resources required in numerical simulations. A classification of ROM methods defines two paradigms mainly based on projection or interpolation and which can be seen as the evolutions of Fourier Series and Lagrange Polynomial Interpolation respectively. To the first family belongs all the *Computational Reduction Technique (CRT)* and are based on the definition of a basis of reduced size and on the projection of the full system onto its span. The basis functions are global and specific for the problem under consideration. On the other side the *Surrogate Response Surface (SRS)* family rely, rather than on projection, on interpolation of data obtained through numerical simulations [7]. The main difference between the two approaches is that the CRTs are problem-dependent and this means that require a physical modeling of the particular problem that is analyzed and consequently are capable in accurately reproducing scenarios far from those used for building the model, contrary to the SRSs which are problem-transparent. Given these characteristics for this thesis work was adopted the CRT approach instead of the SRS one.

All CRTs are characterized by some common features [7]. First, as this group of

strategies is based on projection, it is necessary to define the set of basis functions that generate the subspace onto which such projection will take place. To this purpose, a high-fidelity technique is always needed for discretizing the problem (e.g. Finite Elements (FE), Finite Difference (FD), Finite Volume (FV) or Spectral Methods) and for computing the Snapshots, i.e. the PDE solutions that will be used to build the basis functions. Second, a technique for projecting the equations onto the subspace is needed. Such projection, the so-called Galerkin projection, involves the multiplication of a test function and the volume integration of the equations. Third, a key point for an efficient ROM evaluation is the capability to decouple the Offline phase, which involves (i) the expensive simulations of the full model to generate the snapshots, (ii) construction of the reduced-order space and (iii) Galerkin projection of the full model onto the reduced subspace, followed by an Online phase which consists in the parametric evaluation. The Offline phase is performed only once per problem instead the Online phase can be run many times as required with low computational efforts. This is called offline/online decomposition.

Among the CRTs the two main algorithms historically used in fluid dynamics for choosing the basis on which to build ROMs are Proper Orthogonal Decomposition (POD), introduced by Lumley [22] and Sirovich [8] in the context of turbulent flows, and Greedy algorithms for Reduced Basis (RB), introduced by Noor and Peters [23]. In this thesis, a POD technique has been used since the RB technique demand a more intense Online procedure and is less used than POD in fluid-dynamics. A discussion of RB features can be found in [20, 24, 25].

The POD techniques are based on the idea that a problem solution can be defined in a subspace of smaller dimension with respect to the space dimension of the original full-order model. This is done identifying a certain number of dominant modes associated with most of the energy of the system. For this aim, the POD begins with the construction of the snapshots [8] generated by a discrete evaluation of the problem solution for different values of the problem parameters, as well as for the time coordinate. According to [6], the space-time dependent PDE solution $y = y(\mathbf{x}, t)$ is approximated through a linear combination of spatial modes $\varphi_i(\mathbf{x})$ multiplied by temporal coefficients $a_i(t)$, thus resulting in the following form:

$$y(\mathbf{x}, t) \approx \sum_{i=1}^{N} a_i(t)\varphi_i(\mathbf{x}) \tag{37}$$

The set of modes $\{\varphi_i\}_{i=1}^{N}$ is computed from a set of snapshots i.e., values of the field $y(\mathbf{x}, t)$ at prescribed times t_n for $n = 1, \ldots, N_s$. The POD approach handles the calculation of the spatial set of modes in terms of an optimization problem, minimizing the norm of the least square difference between the high-fidelity solution and their projection in the subspace X^{POD} generated by the modes themselves, $X^{POD} = \text{span}\{\varphi_1, \varphi_2, \ldots, \varphi_N\}$:

$$X^{POD} = \text{argmin} \frac{1}{N_s} \sum_{n=1}^{N_s} \left\| y_n - \sum_{i=1}^{N_c} \langle y_n, \varphi_i(\mathbf{x}) \rangle \varphi_i(\mathbf{x}) \right\|_{L^2}^2 \tag{38}$$

$$\langle \varphi_i(\mathbf{x}), \varphi_j(\mathbf{x}) \rangle_{L^2} = \delta_{ij} \tag{39}$$

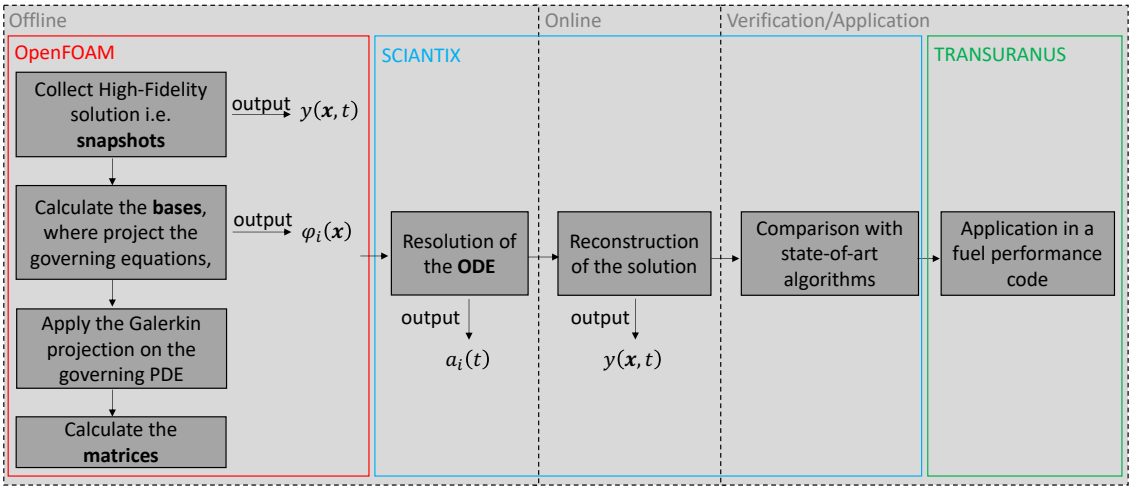

Figure 2. The workflow structure adopted in the present work.

Once the spatial modes have been computed, replacing theme in the governing equation (37), the original PDE system is approximated by an Ordinary Differential Equation (ODE) system. For more details about POD theory [26].

This thesis focuses on developing a reduced order model based on POD procedure of the fission gas diffusion phenomenon. The equations are discretized through the FV discretization on which the most common codes of fluid-dynamics are based and finally the equations are projected according to Galerkin, i.e. first multiplied by the test functions, in this case the modes of the projection subspace, and then integrated over the volume. The POD technique used in this thesis takes shape starting from the adaptation of the FV methodology developed in [9] (POD-FV-ROM).

The most adopted model to study the diffusional release is the one proposed by Booth [10] which consists in assuming the grain of spherical shape and in which the temperature is supposed to be uniform along the grain. This represents a good approximation in the case of Light Water Reactors (LWRs) in which the morphological alterations due to temperature values are not so significant as to cause an intense restructuring process. On the contrary, in Fast Reactors (FRs) the levels of temperature are such as to cause an intense phenomenon of recrystallization with consequent formation of various microstructures [11]. So, in the case of FRs, we are not only dealing with spherical grains but also with columnar-shaped grains. With this type of grains it is no longer possible to adopt the Booth's hypothesis but it is necessary to adopt a more complex model which also considers the intense temperature gradient that is determined along the grain itself. In addition to the difference in shape of some grains, it is also necessary to take into account the fact that the diffusion of fission gases in the fuel matrix can be isotropic or anisotropic depending on the type of crystalline structure that characterizes the fuel adopted. In the case of uranium dioxide we are dealing with an isotropic diffusion while in the case of uranium silicide, a promising Accident Tolerant Fuel (ATF), the diffusion is anisotropic [19].

As it is necessary to adopt different models based on the type of fuel and reactor studied this thesis work has been conceived to develop and implement a ROM technique for these three situations. The principal novelty brought by the research

presented in this thesis work consists in the development of a technique that can be extended to any situation unlike the state-of-art algorithms implemented in FPC which are intrinsically limited to a specific problem. A second novelty is that this work represents the first case of applying a reduce order algorithm in a FPC.

The work presented has been done using OpenFOAM, an open-source Computational Fluid Dynamics (CFD) software that make use of the FV discretization, SCIANTIX, an open source 0D stand-alone computer code designed to be coupled as a module in existing fuel performance codes and the fuel performance code TRANSURANUS. OpenFOAM was adopted to: (i) Collect a limited number of high-fidelity solutions of the governing PDE. For the high-fidelity solution I used the in-house developed solver in OpenFOAM (ii) Calculate the bases on which to project the governing equation, generating a reduced solution of the PDE (iii) Apply the Galerkin projection on the governing PDE and (iv) Calculate the matrices which correspond to the coefficients of the ODE system. These four steps are performed offline instead the resolution of the ODE (offline), the reconstruction of the solution (online) and the verification process were performed via the SCIANTIX module. In the end, the application part to a fuel performance code was performed in TRANSURANUS. In Figure 2 are summarized the main steps performed in each software/code.

Chapter 1

Reduced order model of fission gas diffusion in oxide fuel spherical grains

Abstract

In this Chapter, the attention is focused on the development of the Proper Orthogonal Decomposition technique, discussed briefly in the introduction, for the diffusion problem of fission gas in oxide fuel spherical grains. After an introduction on the models that describe the intra-granular fission gas behavior, we move on to the implementation of the ROM technique in OpenFOAM and in SCIANTIX. Following the implementation of the reduced order algorithm on a meso-scale computer code, there is an intense verification phase which aims to test the correct functioning of the algorithm, even in non-physical situations, comparing its behavior with the state-of-art algorithms. Finally, the algorithm is applied in a fuel performance code in order to verify that is able to work also at the engineering scale of the integral fuel rod. This chapter aims also to define the workflow to be applied to subsequent chapters and, in the future, to other models.

The main results of this Chapter are to be published in:

> Di Gennaro, M., Pizzocri, D., Luzzi, L., 2021. A multi-scale reduced order model of intra-granular fission gas diffusion in oxide fuel spherical grains: Application in fuel performance codes. In preparation for *Nuclear Engineering and Design*.

1.1 Intra-granular fission gas behaviour

Under nominal condition, in light water reactors and fast reactors, radioactive FPs are generated from fission events in uranium oxide (UO_2) and uranium-plutonium oxide, also known as Mixed Oxides (MOX), grains. Their low solubility make them diffuse toward grain boundaries involving their release in the free volume of the rod. An understanding of the release process of the gaseous fission products (xenon and krypton) during the irradiation of oxide nuclear fuels is essential for analyzing the thermal-mechanical behavior of the nuclear fuel rods employed in all reactor systems. This phenomenon is so relevant because the fission gases released from the fuel to the fuel-cladding gap increase the internal pressure and fuel temperature by degrading the thermal conductivity of the filling gas due to the mixing of heavy gas atoms in the gap. The fission gases which remain in the fuel form fission gas bubbles on both intra-granular and inter-granular regions, resulting in fuel swelling. The release occurs mainly by diffusion of the gases from the interior of the grains of the sintered fuel into grain boundaries, and from the boundaries to the free volume of the rods through inter-linkage of the inter-granular bubbles. It follows that modeling of this transport process is a fundamental component of any fission gas behavior model in a fuel performance code [27–31].

Even at high burn-up, the dominant mechanism of release is generally supposed to be the diffusional release, i.e. the diffusion of fission product atoms to open porosity [32]. It is possible to ignore other minor release mechanisms active at low burn-ups (knockout, recoil ad evaporation) given their negligible contribution (contribute less than 1%) and given their behavior not yet well understood [33–35].

Physics-base modelling [36] of FPs release must include: intra-granular diffusion of gas atoms to grain boundary, intra-granular bubble behavior, nucleation, growth, trapping and re-solution phenomena, coalescence, interconnection and subsequent release. The first step of FGR is gas atom transport from the inside to the boundaries of the grains, which takes the name of intra-granular fission gas release. Fission gas transport to the grain boundaries occurs by thermal and irradiation-enhanced diffusion of single gas atoms, coupled with trapping in and irradiation-induced re-solution from intra-granular bubbles. Thus, modelling intra-granular fission gas release calls for the treatment of different concomitant mechanisms, namely, diffusion coupled with trapping and re-solution of gas atoms. Assuming that fission gas atoms born in the fuel grains, diffuse through the UO_2 lattice with a single gas atom diffusion coefficient $D\,(\mathrm{m}^2\ \mathrm{s}^{-1})$ and that the trapping sites (bubbles) are effectively immobile[1], the problem of gas atom diffusion during trapping and re-solution can be stated mathematically with this system of partial differential equations where we have a coupling between the diffusion equation and the equation for the gas balance in the bubbles:

$$\begin{cases} \dfrac{\partial c_s}{\partial t} = D\nabla^2 c_s - g c_s + b c_b + S \\ \dfrac{\partial c_b}{\partial t} = g c_s - b c_b \end{cases} \tag{1.1}$$

where $c_s\,(\text{at m}^{-3})$ is the concentration of single gas atoms dissolved in the lattice, $c_b\,(\text{at m}^{-3})$ is the concentration of gas atoms in intra-granular bubbles, $g\,(\mathrm{s}^{-1})$ is the

[1] This is true up to 1800 °C [37].

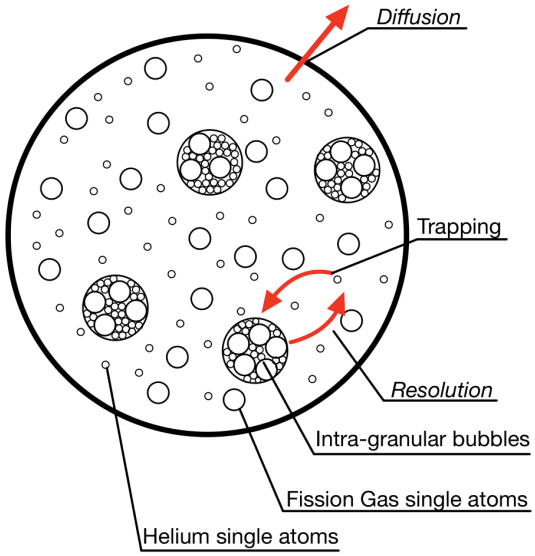

Figure 1.1. Sketch representing the mechanisms involved in intra-granular fission gas release (courtesy of [17]).

trapping rate of a gas atom in solution by a bubble, $b\,(\mathrm{s}^{-1})$ is the re-solution rate of a gas atom within a bubble, and $S\,(\mathrm{at\ m}^{-3}\ \mathrm{s}^{-1})$ is the production rate of fission gas which is in turn given by the fission rate $\dot{F}\,(\mathrm{fiss\ m}^{-3}\ \mathrm{s}^{-1})$ multiplied by the total yield of fission gas atoms $y\left(\mathrm{at\ fiss}^{-1}\right)$ $\left(S = y\dot{F}\right)$. The processes described by Equation 1.1 are represented in Figure 1.1.

Among all the fission products generated during the normal operation, the focus of this work is mainly on noble gases, xenon and krypton. If pure Xenon is considered, without taking into account the decay of volatile fission products such as Tellurium, Iodine and Cesium, approximately 0.26 stable gases atoms are produced for each fission event [38]. In this thesis work has been considered the decay of volatile FPs in Xenon then the fission yield y is around 0.30 [27]. The xenon and krypton nuclides can considered long-lived, except for the Xe^{133} and Xe^{135} isotopes, therefore is not necessary to consider their decay rate in the Equation 1.1. Other models are needed to determine the release of unstable or short-lived FPs.

Speight [12] proposed a simplified mathematical description of intra-granular fission gas release during irradiation of UO_2. He assumed that, for times of engineering interest, trapping and re-solution are in equilibrium (bubbles are saturated), i.e., $gc_s - bc_b = 0$ (quasi-stationary approach). The concept of the quasi-stationary approximation is illustrated in graphical form in Figure 1.2. With this assumption he lumped the trapping and re-solution rate into an effective diffusion coefficient, restating the mathematical problem as purely diffusive. Consequently the intra-granular gas diffusion in presence of trapping and irradiation-induced re-solution may be evaluated by solving a single diffusion equation:

$$\frac{\partial c_t(r,t)}{\partial t} = D_{\mathrm{eff}}\nabla^2 c_t(r,t) + S \tag{1.2}$$

where now $c_t = c_s + c_b\,(at\ m^{-3})$ is the total intra-granular gas concentration considering both the concentration of single gas atoms dissolved in the lattice and the concentration

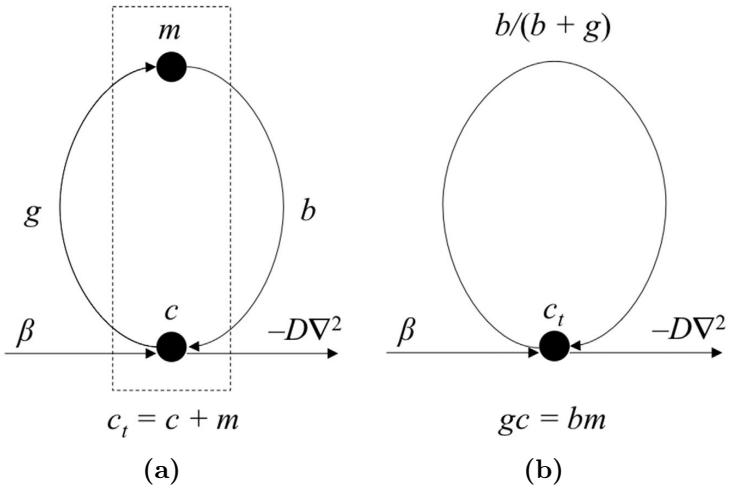

Figure 1.2. Graphical representation of (a) the general formulation of the intra-granular fission gas release problem and (b) the quasi-stationary approximation [18].

of gas atoms in intra-granular bubbles, and $D_{\text{eff}}\,(\text{m}^2\ \text{s}^{-1})$ is the effective gas diffusion coefficient, a single parameter lumping the diffusion towards the grain boundaries, the trapping/re-solution rate of atoms in/from intra-granular bubbles:

$$D_{\text{eff}} = \frac{b}{b+g} D \tag{1.3}$$

A further assumption is that the diffusion coefficient D for the nuclides of interest are assumed to be the same as xenon or a multiple of that for xenon, i.e., $D\,(\text{Xe}) = D\,(\text{Kr}) = D\,(\text{I}) = D\,(\text{Br})\,/20 = D\,(\text{Te})\,/4$. The Xe-diffusion coefficient in irradiated oxide nuclear fuels is made up of three terms, each one describes a distinct physical process that influences different temperature ranges [13].

$$D(T, \dot{F}) = D_1(T) + D_2(T, \dot{F}) + D_3(\dot{F}) \tag{1.4}$$

1. $D_1\,(T)$ is the intrinsic diffusion coefficient which depends only on the fuel temperature. It predominates at $T > 1400\,^{\circ}\text{C}$ and, since it describes a thermally activated volume diffusion, is written in the usual Arrhenius form:

$$D_1\,(T) = D_{10} e^{-\Delta H / k_B T} \tag{1.5}$$

   where $D_{10}\ (\text{s}^{-1})$ is the pre-exponential factor, ΔH (J) is an activation energy and $k_B\ (\text{J K}^{-1})$ is the Boltzmann constant;

2. $D_2\left(T, \dot{F}\right)$ depend on both temperature and fission rate. Describes diffusion via thermal and irradiation induced cation vacancies and dominates for temperatures between $1000\,^{\circ}\text{C}$ and $1400\,^{\circ}\text{C}$. Based on random walk model:

$$D_2\left(T, \dot{F}\right) = d^2 j_v c_v = D_{20} \sqrt{\dot{F}} e^{-E_{10}/T} \tag{1.6}$$

   where d is the atomic jump distance, j_v is the thermally activated vacancy jump rate, c_v is the cation vacancy concentration [13, 39], $D_{20}\ (\text{s}^{-1})$ is the pre-exponential factor and E_{10} (K) the exponential factor.

3. $D_3\left(\dot{F}\right)$ is the athermal diffusion coefficient and dominates down to 250°C because when $T < 250\,°\text{C}$ the vacancy jump rate is negligible and diffusion occurs by atomic collision cascades. Turnbull follows Matzke [40] in adopting a term proportional to the fission rate and scaled to agree with the low temperature plateau. This athermal contribution is empirically written as:

$$D_3\left(\dot{F}\right) = D_{30}\dot{F} \tag{1.7}$$

where D_{30} (s^{-1}) is the pre-exponential factor.

Finally the diffusion coefficient is [13]:

$$D = 7.6 \times 10^{-10} e^{-35217/T} + 5.64 \times 10^{-25}\sqrt{\dot{F}} e^{-13840/T} + 2 \times 10^{-40}\dot{F} \tag{1.8}$$

$T(K)$ and $\dot{F}\,(\text{fiss m}^{-3}\text{s}^{-1})$. In general the parameters of Equation 1.2 vary in time as temperature and fission rate vary during irradiation, in particular D present a rapid variation during transient owing to their exponential dependence on temperature as shown in Equation 1.8. This thesis work deal to solve the diffusion problem under constant conditions, i.e. the source term S and the diffusion coefficient D are assumed as constant in time and uniform in space. Derivation of Equation (1.2) requires the additional assumption that parameters b and g are uniform in space across the domain (grain).

Most of the mechanistic FGR models for LWR fuel exploit the equivalent sphere model [10] to describe the diffusional release. Booth modeled the polycrystalline oxide nuclear fuel sinter as a collection of uniform sphere with an equivalent radius a. The equivalent radius a is related to the surface-to-volume ratio by the following:

$$\frac{\text{surface}}{\text{volume}} = \frac{4\pi a^2}{4/3\pi a^3} = \frac{3}{a} \tag{1.9}$$

The intra-granular diffusion problem Equation 1.2 is so written by taking advantage of the spherical symmetry of the problem:

$$\frac{\partial c_t\,(r,t)}{\partial t} = D_{\text{eff}}\frac{1}{r^2}\frac{\partial}{\partial r}\left(r^2\frac{\partial}{\partial r}c_t\,(r,t)\right) + S \tag{1.10}$$

where r is the coordinate of the spherical grain. Each individual grain presents the boundary surface which acts as a perfect sink: upon arrival at the boundary, a gas atom is given a virtually zero probability of returning to the matrix. This defines a mathematical Boundary Condition (BC) of a zero gas concentration immediately adjacent to the grain boundary, i.e., $c_t\,(R,t) = 0$ for $t > 0$ with $R\,(\text{m})$ being the radius of the spherical grain. As initial condition have been considered $c_t\,(r,t) = 0$. Consequently $c_t\,(r,t)$ satisfy the following well-posed problem:

$$\begin{cases} \dfrac{\partial c_t(r,t)}{\partial t} = D_{\text{eff}}\dfrac{1}{r^2}\dfrac{\partial}{\partial r}\left(r^2\dfrac{\partial}{\partial r}c_t(r,t)\right) + S & \\ c_t(r,0) = 0 & 0 < r < R \\ c_t(R,t) = 0 & t \geq 0 \end{cases} \tag{1.11}$$

For the purpose of modelling intra-granular fission gas release in FPCs, the figure of merit is the weighted volume average in the grain of the total gas concentration along time, $\bar{c}_t(t)$. The analytic solution of Equation 1.10 for constant conditions in spherical grain geometry is well known and is obtained by integrating the solution of Equation 1.10, $c_t(r,t)$, over the spherical domain [41, 42].

1.2 Implementation of the Full Order Model

In this work, the high fidelity-full order simulation of the partial differential equation (1.10) have been performed in OpenFOAM® environment, an open-source finite volume code written in C++ that allows finite volume discretization, PDE modeling and solution [43].

The domain has a 3D spherical geometry in which was defined a Dirichlet BC in correspondence of the whole boundary surface that acts as a perfect sinks and the gas concentration within the grain is set to be initially equal to zero[2]. For the simulation was used the default 3D spherical mesh of OpenFOAM with a discretization of $20 \times 20 \times 200$ cells (Figure 1.3). The number of cells for each direction was chosen through a sensitivity analysis which led to the choice of the combination that allows to obtain the average concentration value closest to the analytical solution.

For the sake of simplicity in the implementation, the equation solved in OpenFOAM doesn't consider the quasi-stationary term, i.e. $b/(b+g)$, which will be possible to introduce into the equation later during the SCIANTIX implementation. Consequently in OpenFOAM was implemented this equation:

$$\frac{\partial c\,(r,t)}{\partial t} = D\frac{1}{r^2}\frac{\partial}{\partial r}\left(r^2\frac{\partial}{\partial r}c\,(r,t)\right) + S \tag{1.12}$$

It is possible to operate in this way because as shown in Equation 1.28 the diffusion coefficient is outside the matrix term, consequently during the online stage, that can be run many times as require, is possible change this parameter. This concept will be explained better in Section 1.3.

Furthermore, to simplify implementation, a dimensionless mesh has been adopted, consequently the Equation 1.12 have been transformed into a dimensionless form:

$$R^2\frac{\partial c}{\partial t} = D\frac{1}{\rho^2}\frac{\partial}{\partial \rho}\left(\rho^2\frac{\partial}{\partial \rho}c\right) + R^2 S \tag{1.13}$$

where $\rho = r/R$. Rewritten in generic form results:

$$R^2\frac{\partial c}{\partial t} = D\nabla^2 c + R^2 S \tag{1.14}$$

[2]The boundary conditions are assigned in the `boundaryField` section of the field files within each time directory for each mesh patch.

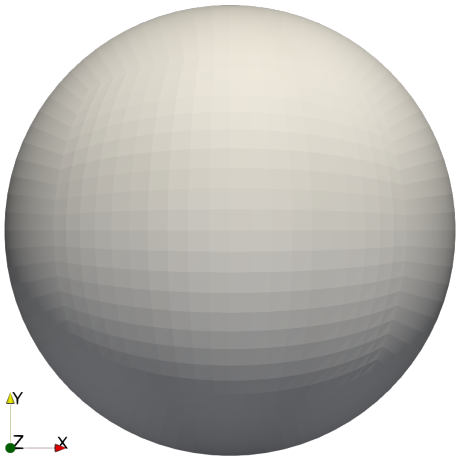

Figure 1.3. Representation of the spherical adimensional mesh used in OpenFOAM.

Table 1.1. List of values and u.o.m adopted in the simulation

Symbol	Definition	Value	u.o.m (original)	u.o.m (simulation)
c	Concentration		mol m^{-3}	-
R	Radius	5×10^{-6}	m	m
T	Temperature	1200	K	K
$\dot{F}$	Fission rate	3×10^{19}	fiss $m^{-3}s^{-1}$	-
y_F	Fission yield	5×10^{-25}	mol $fiss^{-1}$	s^{-1}
D	Diffusion coefficient	[13]	m^2 s^{-1}	s^{-1}
∇^2	Laplacian term		m^{-2}	-

This adimensionalization allows to adopt a spherical mesh of unitary radius expressed in meters and to introduce the radius of the grain directly in the equation[3]. The parameters adopted for the simulation are shown in table 1.1 where is possible to see the units of measurement that have been adopted for the simulation. Regarding the pre-exponential and exponential factors of the diffusion coefficient, the values have been defined in Section 1.1 and their unit of measurement has remained unchanged.

The simulation was run for 7.5×10^8 s, this was chosen on the basis of the time taken by the phenomenon to reach equilibrium which, for the equation under study, is in the order of:

$$\tau = \frac{R^2}{D} = 6.9 \times 10^8 \, \text{s} \tag{1.15}$$

The computational time required by a intel Core i5-5300U CPU @ 2.30GHz and 8GB RAM was in the order of 5 minutes. The frequency of snapshot sampling was set to 1.333×10^{-6} Hz, therefore in the 7.5×10^8 s-simulation, 1000 snapshots have been collected. These snapshots are the several time folders resulting from the performing of the FOM. The distribution of concentration field for different time steps resulting

[3]To solve this diffusion equation has been implemented a specific solver using the *LaplacianFoam* solver as starting point. In the header file *createFields.H* each field was defined. The concentration and temperature fields was defined as volume fields to guarantee an accurate description per unit volume of the diffusion problem, the diffusion coefficient were defined as tensor field and the other parameters of the equation was defined as scalar fields.

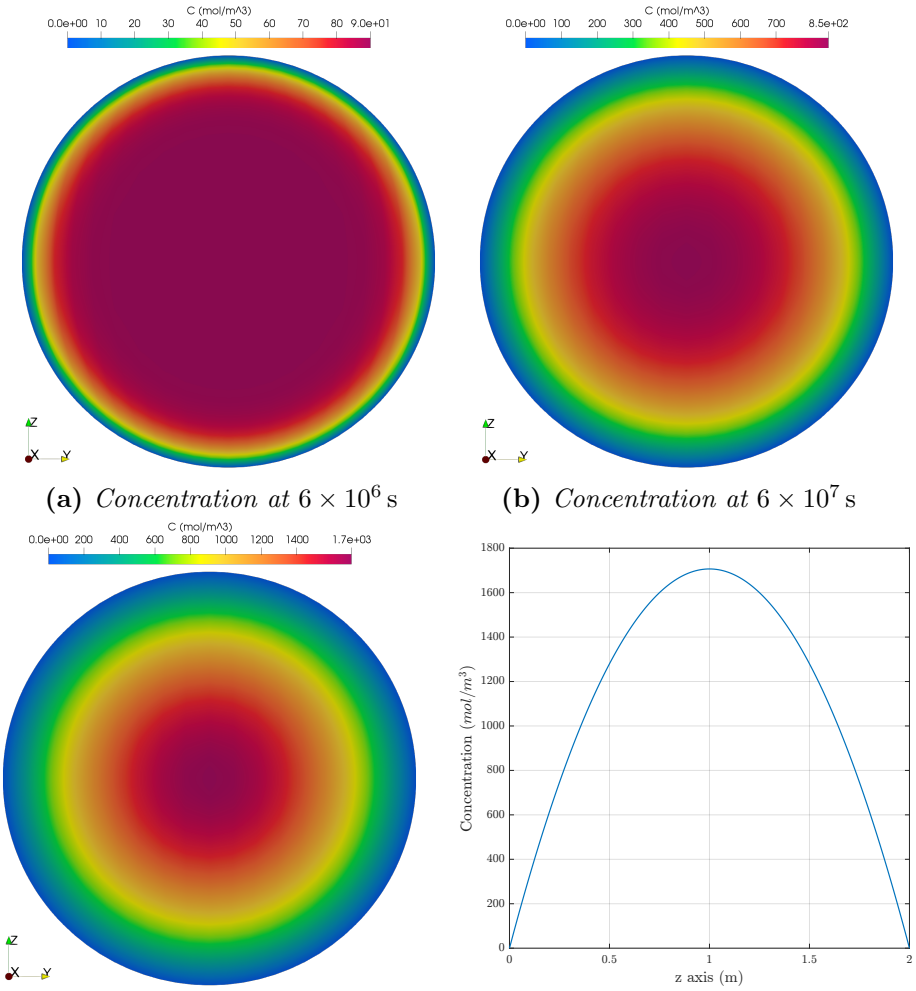

(a) *Concentration at* 6×10^6 s **(b)** *Concentration at* 6×10^7 s

(c) *Concentration at* 6×10^8 s **(d)** *Concentration trend along the z axis*

Figure 1.4. In (a), (b) and (c) are reported the concentration distributions in correspondence of three time steps resulting from the full order simulation implemented in OpenFOAM. In (d) is reported the concentration trend along the spatial coordinates at equilibrium. Since this is a case of isotropic diffusion and symmetrical geometry, whatever plane is adopted to slice the sphere the same results are obtained. I have chosen to depict the trend along the z axis because the mesh is finer so as to have a smoother graph.

from the FOM implemented in OpenFOAM are showcased in Figure 1.4 and, as expected, the concentration assumes a parabolic trend along the spatial coordinates.

In addition to snapshots, the computed quantity of interest is the weighted volume average concentration along time which in OpenFOAM is calculated by carrying out the weight average on the volume of each cell of the mesh[4]. It is actually useful for a quantitative evaluation of the inert gas distribution, hence it is exactly the quantity to be considered as relevant. These values are showcased in Fig.1.5 compared with the analytical asymptotic value. The weighted volume average concentration computed with OpenFOAM, $\bar{c}_{\infty}^{HF}$, reaches the correct analytical asymptotic value,

[4]For this purpose was exploited the Function objects utilities of OpenFOAM to collect this value for all the time steps in a *.dat* file so that they can then be post-processed at a later time.

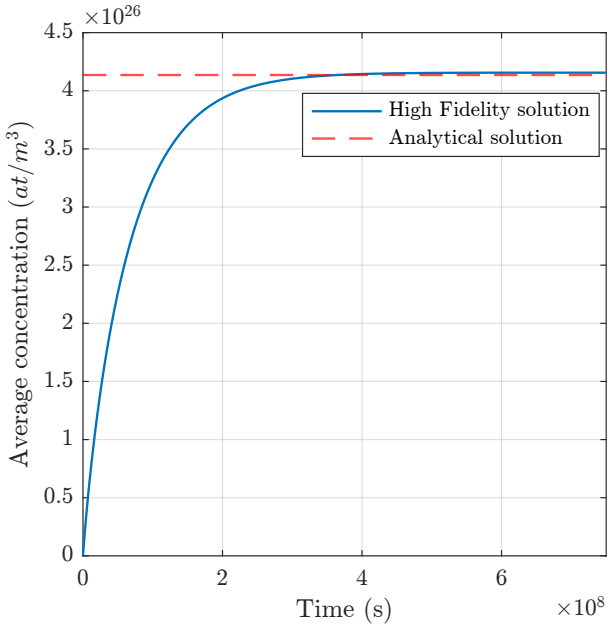

Figure 1.5. Average concentration along time against the analytical solution.

$\bar{c}_\infty$ by committing a small relative error u_∞^{HF}:

$$u_\infty^{HF} = \frac{\bar{c}_\infty^{\,HF}}{\bar{c}_\infty} - 1 = 0.48\% \tag{1.16}$$

1.3 POD-FV-ROM of diffusion equation

In this section the POD technique discussed briefly in the introduction is applied directly to the problem of fission gas diffusion in spherical grains with the purpose of obtaining a POD-ROM of Equation 1.14 considering the Finite Volume approximation (POD-FV-ROM). In order to do this the procedure followed by [9] is adopted here. The main assumption, in the reduced order techniques based on projection method, is that the approximated solution of the problem $c_r(\mathbf{x}, t)$ can be expressed as linear combination of spatial modes $\phi_i(\mathbf{x})$ multiplied by temporal coefficients $a_i(t)$, thus resulting in the following form:

$$c(\mathbf{x}, t) \approx c_r(\mathbf{x}, t) = \sum_{i=1}^{N_c} a_i(t)\phi_i(\mathbf{x}) \tag{1.17}$$

where N_c is the number of bases adopted. To this purpose a set of basis functions $\{\phi_i(\mathbf{x})\}_{i=1}^{N_c}$ is used for the concentration. For an efficient ROM is essential to select the correct spatial modes so as to be able to reduce the simulation time in the online phase or increase the accuracy with respect to the FOM. Different method are available to achieve this purpose. In this thesis work, and in general in fluid flow computation, the POD procedure is adopted due to its capability to select the most energetic modes. This results into a very cost-effective solution to retain all the fundamental information

of the model, while reducing its complexity.
The subspace is the span of the set of basis functions introduced for concentration:

$$X_c^{POD} = \text{span}\{\phi_1, \phi_2, ..., \phi_{N_c}\} \tag{1.18}$$

Being the member of each set of basis functions orthogonal one to each other, they can be normalized in order to obtain:

$$\langle \phi_i(\mathbf{x}), \phi_j(\mathbf{x}) \rangle_{L^2} = \delta_{ij} \tag{1.19}$$

The set of spatial modes $\{\phi_i(\mathbf{x})\}_{i=1,...,N_c}$ can be built starting from the *snapshots*, i.e. the values of the field $c(\mathbf{x}, t)$ at prescribed times t_n for $n = 1, ..., N_s$:

$$c_n = c(\mathbf{x}, t_n) \quad n = 1, ..., N_s \tag{1.20}$$

where N_s is the number of snapshots adopted. The snapshots can be obtained through numerical simulations or through experimental measurements. The spatial set of modes is built so as to minimize the norm of the least square difference between the snapshots and the projection of the snapshots in the subspace X_c^{POD} in the X-norm, given the orthonormality of the modes (Equation 1.19). If the L^2-norm is chosen, the POD basis is optimal considering the energy contained in the snapshots.

$$X_c^{POD} = \arg\min \frac{1}{N_s} \sum_{n=1}^{N_s} \left\| c_n - \sum_{i=1}^{N_c} \langle c_n, \phi_i(\mathbf{x}) \rangle \phi_i(\mathbf{x}) \right\|_{L^2}^2 \tag{1.21}$$

These minimization can be achieved either with Singular Value Decomposition (SVD) (described in [44] and adopted in [45]) or with the introduction of the correlation matrices (described in [7] and adopted in [9]). With the latter approach, the following eigenvalue-eigenvector problem is considered:

$$K\boldsymbol{\chi}_j = k_j \boldsymbol{\chi}_j \quad j = 1, ..., N_s \tag{1.22}$$

where k_j are the eigenvelues, $\boldsymbol{\chi}_j$ are the eigenvectors and $K \in \mathbb{R}^{N_s \times N_s}$ is the correlation matrix whose components are calculated as follows:

$$[K]_{ml} = \frac{1}{N_c} \langle c_m(\mathbf{x}), c_l(\mathbf{x}) \rangle_{L^2} \tag{1.23}$$

where $c_m(\mathbf{x}) = c(t_m, \mathbf{x})$ and $c_l(\mathbf{x}) = c(t_l, \mathbf{x})$ are the m-th and l-th concentration snapshots. The $\left(k_j, \boldsymbol{\chi}_j\right)$ eigenvalue–eigenvector pair is used to build the basis modes as:

$$\phi_i(\mathbf{x}) = \frac{1}{\sqrt{k_i}} \sum_{n=1}^{N_s} \chi_{i,n} c_n(\mathbf{x}) \quad i = 1, ..., N_c \tag{1.24}$$

Since the eigenvalues, which are associated to the energies transported by the modes, are sorted in descending order, the first modes are those retaining most of the energy of the complete solution [46]. This ensure that however the series in Equation (1.17) is truncated and the most energetic modes are saved.
Replacing the concentration c with c_r (Equation 1.17) in Equation 1.14 we obtain:

$$R^2 \sum_{i=1}^{N_c} \phi_i(\mathbf{x}) \frac{\partial a_i(t)}{\partial t} = D \sum_{i=1}^{N_c} \left(a_i(t) \nabla^2 \phi_i(\mathbf{x}) \right) + R^2 S \tag{1.25}$$

Applying the Galerkin projection over the test functions $\phi_j(\mathbf{x})$:

$$R^2 \sum_{i=1}^{N_c} \frac{\partial a_i(t)}{\partial t} \int_\Omega \phi_j(\mathbf{x}) \cdot \phi_i(\mathbf{x}) d\Omega = D \sum_{i=1}^{N_c} a_i(t) \int_\Omega \phi_j(\mathbf{x}) \cdot \nabla^2 \phi_i(\mathbf{x}) d\Omega + \\ + R^2 S \int_\Omega \phi_j(\mathbf{x}) d\Omega \quad j = 1, ..., N_c \tag{1.26}$$

where Ω is the local control volume. Being the members of each set of basis functions orthonormal one to each other (Equation 1.19), the integration on the left hand side brings to a unitary term:

$$R^2 \frac{\mathrm{d}a_j(t)}{\mathrm{d}t} = D \sum_{i=1}^{N_c} a_i(t) \int_\Omega \phi_j(\mathbf{x}) \cdot \nabla^2 \phi_i(\mathbf{x}) d\Omega + R^2 S \int_\Omega \phi_j(\mathbf{x}) d\Omega \quad j = 1, ..., N_c \tag{1.27}$$

Rewriting the equation in matrix terms and dividing everything by R^2, the following POD-Galerkin ROM (POD-G-ROM) for Finite Volume discretization (POD-FV-ROM) is obtained:

$$\frac{\mathrm{d}a_j(t)}{\mathrm{d}t} = \frac{D}{R^2} \sum_{i=1}^{N_c} a_i(t) A_{ji} + S B_j \quad j = 1, ..., N_C \tag{1.28}$$

where:

$$A_{ji} = \langle \phi_j(\mathbf{x}), \nabla^2 \phi_i(\mathbf{x}) \rangle_{L^2} \tag{1.29}$$

$$B_j = \langle \phi_j(\mathbf{x}) \rangle_{L^2} \tag{1.30}$$

In this way, the original PDE system is replaced by an ODE system in which the unknowns are the time-dependent coefficients $a_i(t)$. The ODE system can be expressed as the following autonomous dynamical system:

$$\dot{\mathbf{a}} = \frac{D}{R^2} \mathbf{a}\mathbf{A} + S\mathbf{B} \tag{1.31}$$

where the dot denotes the time derivative. This ODE system is then solved in SCIANTIX by means an implicit Euler scheme in order to derive the time coefficients and finally reconstruct the solution (Section 1.5). Although, from a mathematical point of view, the unknowns $a_i(t)$ depends exclusively on time, the system also provides a spatial description, as the spatial character is included in the matrices that have been calculated by the orthonormal modes.
In general in deriving the POD-G-ROM a relevant assumption is made: the term A_{ij}, representing the diffusive term, is derived keeping into account that $\nabla^2 c = \nabla \cdot (\nabla c)$ and applying the Green formula for the divergence operator. In this way we should have:

$$\int_\Omega \phi_j(\mathbf{x}) \cdot \nabla^2 \phi_i(\mathbf{x}) d\Omega = - \int_\Omega \nabla \phi_j(\mathbf{x}) : \nabla \phi_i(\mathbf{x}) d\Omega + \int_{\partial\Omega} \frac{\partial \phi_i(\mathbf{x})}{\partial \mathbf{n}} \cdot \phi_j(\mathbf{x}) d\gamma \tag{1.32}$$

where $\mathbf{n}$ denotes the outward normal of $\partial\Omega$, consequently the matrix A_{ij} would be:

$$A_{ji} = \langle \nabla \phi_j(\mathbf{x}), \nabla \phi_i(\mathbf{x}) \rangle_{L^2} \tag{1.33}$$

and the first term in the right hand side should have a minus sign in front. This procedure is typical of the weak formulation of differential problems in the FE approach and it is extended also to POD-G-ROM. Note that, for the term A_{ij} in 1.29 the Green's formula has not been applied. This is due to the fact that the Green's formula cannot be exploited in the POD-FV-ROM procedure since it would introduce discretization discrepancies between the full order model and the reduced order one as shown in [9]. As additional consequence, the boundary conditions cannot be explicitly incorporated in the ROM as in the POD-G-ROM case. Therefore, writing the A_{ij} term as in 1.29, the BCs are "embedded" in the term itself and not explicit present in the ROM formulation.

As can be seen in Equation 1.31, the diffusion coefficient D is outside the matrix term. In this way, during the resolution of the ODE system in SCIANTIX, it is possible to adopt any diffusion coefficient, based on the type of diffusion phenomenon has to be studied. In Section 1.6.3 and 1.6.4, where the reduce algorithm will be compared with the state-of-art algorithms, will be adopted the effective diffusion coefficient. If, on the contrary, the diffusion coefficient had taken part in the calculation of the matrix A_{ij} carried out in OpenFOAM:

$$A_{ji} = \langle \phi_j(\mathbf{x}), D\nabla^2\phi_i(\mathbf{x}) \rangle_{L^2} \tag{1.34}$$

the ODE system would have been:

$$\dot{\mathbf{a}} = \frac{1}{R^2}\mathbf{a}\mathbf{A} + S\mathbf{B} \tag{1.35}$$

Following this modus operandi the diffusion coefficient would no longer appear explicitly in the online phase, resulting in being forced to reconstruct a solution with the diffusion coefficient adopted in the offline phase, thus having to restart from the offline phase whenever one wanted to adopt a different parameter.

1.4 Implementation of the POD-FV-ROM

In this section the reduction of the model, thus going from a set of PDEs to a set of ODEs, is implemented in OpenFOAM. The procedure follows two main steps. First, the set of orthonormal modes is computed from the set of snapshots collected during the performing of the full-order model (Section 1.2). This computation consists in minimizing the equation 1.21 performed through a library implemented in FOAMextend environment [14]. In particular, this minimization is articulated in: (i) the calculations of the eigenvalues-eigenvectors (Equation 1.22) (ii) the inner product (Equation 1.19) and (iii) the projection of the snapshots in the subspace (Equation 1.21). For this thesis work have been adopted two bases and a decomposition accuracy of 1.1[5]. Subsequently, this set of orthonormal modes was used to perform the integrations (Equations 1.29 and 1.30) in order to obtain the matrices. This last step has taken place in OpenFOAM environment.

The outcomes are the two set of orthonormal bases (Figures 1.6a and 1.6b) and

[5]The number of modes and the accuracy that they must guarantee are set by the user through the dictionary file *PODsolverDict*, provided by the case directory in OpenFOAM.

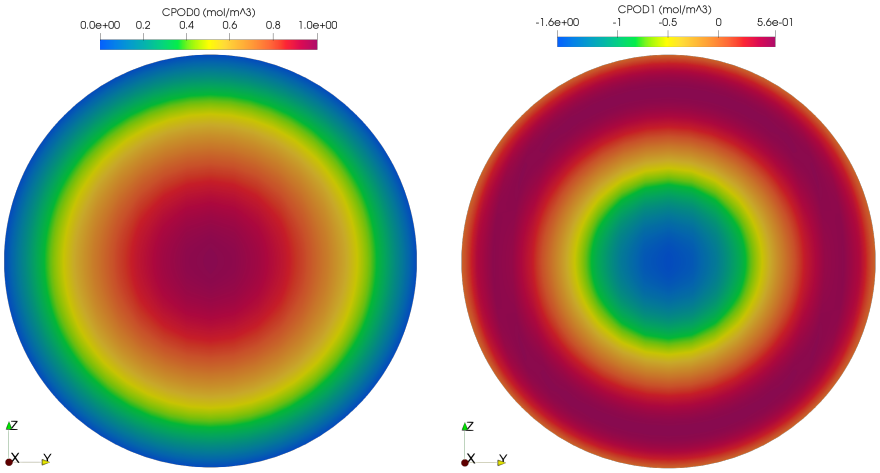

(a) *First POD basis* **(b)** *Second POD basis*

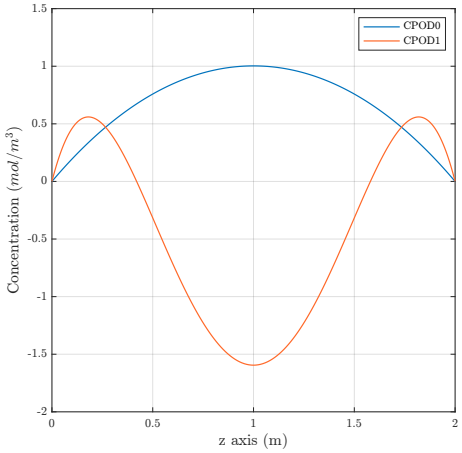

(c) *Concentration trend along the z axis for the two POD bases.*

Figure 1.6. The POD bases resulting from the POD-FV-ROM implementation in OpenFOAM. Being a case of isotropic diffusion and symmetrical geometry, the trend of the two basic functions is the same along any spatial coordinate.

the matrices:

$$\mathbf{A} = \begin{bmatrix} -10.5568 & -5.3065 \\ -5.3582 & -50.4583 \end{bmatrix} \quad \mathbf{B} = \begin{bmatrix} 1.7195 \\ 0.8155 \end{bmatrix} \tag{1.36}$$

As expected, the eigenfunctions trend along the spatial coordinates (Figure 1.6c) correspond to a parabolic and cardinal sine trend.

For the purpose of modelling intra-granular fission gas release, the figure of merit is the average concentration. Therefore are necessary the weighted volume average of the two set of bases:

$$\bar{\phi}_i = \begin{bmatrix} 0.4113 \\ 0.1951 \end{bmatrix} \tag{1.37}$$

In this way, in the implementation of the online phase in SCIANTIX (Section 1.5) will be performed the calculation expressed by Equation 1.39.

1.5 Implementation of the algorithm in SCIANTIX

In this section the resolution of the ODE system (Equation 1.31) and then the reconstruction of the solution are implemented in the physics-based meso-scale code SCIANTIX [36]. SCIANTIX is a 0D stand-alone computer code designed at Politecnico di Milano which covers the description of intra- and inter-granular inert gas behaviour in UO_2. The 0D approach means that the output of the code consists in a time-dependent local computation of the quantities of interest, e.g. the isotope released concentration or the local intra- and inter-granular swelling. This code can be used as a stand-alone code for the simulation of separate effect experiments at the fuel-grain scale involving inert gas behaviour. It arises from the need to bridge lower length-scale calculations with the engineering-scale simulations of FPC such as TRANSURANUS which we will see in Section 1.7.

The ODE system was solved by means an iterative procedure based on Backward Euler Scheme:

$$\begin{bmatrix} a_1^{i+1} \\ a_2^{i+1} \end{bmatrix} = \left(I - \frac{D}{R^2} \Delta t \mathbf{A} \right)^{-1} \begin{bmatrix} a_1^i + S\Delta t B_1 \\ a_2^i + S\Delta t B_2 \end{bmatrix} \tag{1.38}$$

where I is the identity matrix. At each time step the code solve the two ODE and stores in a vector the time coefficients a_1^{i+1} and a_2^{i+1}. This procedure is then iterated until a_1^{i+1} and a_2^{i+1} converges onto a solution. At the end of the simulation the code uses the time coefficients calculated and the volume weighted average of the basis (Figure 1.6a and 1.6b) to reconstruct the volume weighted average concentration along time:

$$\bar{c}(\mathbf{x}, t) \approx \sum_{i=1}^{N_c} a_i(t) \bar{\phi}_i(\mathbf{x}) \tag{1.39}$$

I have called this numerical algorithm, implemented in SCIANTIX, REDUCE.

1.6 Algorithm verification

To be able to assess confidence in modeling and simulation it is important to verify and validate (V&V) that the computational simulations are performed properly. This thesis work focuses on verification which is the assessment of the accuracy of the solution of a computational model. Verification is important in order to ensure that the algorithm works according to its specifications. The verification of the implemented algorithm was carried out in several ways. The first step was to compare the outcomes of the reduction algorithm in terms of average concentration with the analytical solution and the high-fidelity result. After, the algorithm was also verified via the Method of Manufactured Solutions (MMS), a technique for testing the consistency of numerical algorithms. Subsequently, different numerical experiments were performed aimed to (i) verify the solution of the algorithm and (ii) compare the accuracy of the algorithm solutions and computational time to other state-of-art algorithms currently used in fuel performance codes. Lastly, the algorithm was compared to a reference algorithm which provides quasi-exact solution of the problem.

1.6.1 Method of Exact solution and comparison with High Fidelity

The first step was to compare the solution obtained from the SCIANTIX code with the analytical solution and the high-fidelity solution. In Figure 1.7 is possible to see the comparison between this three results and in Figure 1.8 the relative error along time between the result obtained with the SCIANTIX code and the result obtained with the high-fidelity simulation implemented in OpenFOAM. The maximum relative error is obtained at the initial time and it stands at 6.25%. In Table 1.2 are summarized the relative errors encountered at each implementation step.

Focusing on u_{∞}^{HF} and u_{∞}^{SC} we notice that the error has been significantly reduced in correspondence with the last implementation step. In the implementation in OpenFOAM, since this is characterized by a finite volume discretization, the quantity of gas that exits the sphere depends on the discretization as this influences the concentration gradient at the surface. An incorrect discretization involves having a lower gradient than the real one. Therefore, on average, with high-fidelity there should be a lower release of gas and therefore retains a greater quantity of gas than expected by the analytic and this can also be seen in Figure 1.7. It is possible to reduce the error through mesh refinement but the discretization error on the cells at the boundary will always lead to an overestimation with respect to the analytic solution. Through the implementation of the ROM, gas is always lost because a finite number of bases are chosen on which to represent the problem, which a priori would have infinite. Therefore, the solution obtained in SCIANTIX will always have a lower average concentration value than the solution obtained with high-fidelity. Consequently, the overestimate that occurs with high-fidelity is balanced by the subsequent intrinsic underestimate of the ROM, resulting in a reduction of the error with respect to the analytical solution.

Through an uncertainty analysis on the parameters that define the concentration, $c = c(D, R)$, is possible to have a greater sensitivity on the results obtained with the aim of understanding how much role the parameters involved plays on the concentration. The uncertainty associated with the asymptotic average concentration can be obtained throughout the uncertainty propagation formula normalized over the equilibrium value

Table 1.2. Relative errors

Symbol	Definition	Value (%)
u_{∞}^{HF}	Relative error between high-fidelity and analytical solution at equilibrium	0.48 %
u_{∞}	Relative error between SCIANTIX and high-fidelity at equilibrium	0.39 %
u_{max}	Maximum relative error between SCIANTIX and high-fidelity	6.25 %
u_{∞}^{SC}	Relative error between SCIANTIX and analytical solution at equilibrium	0.09 %

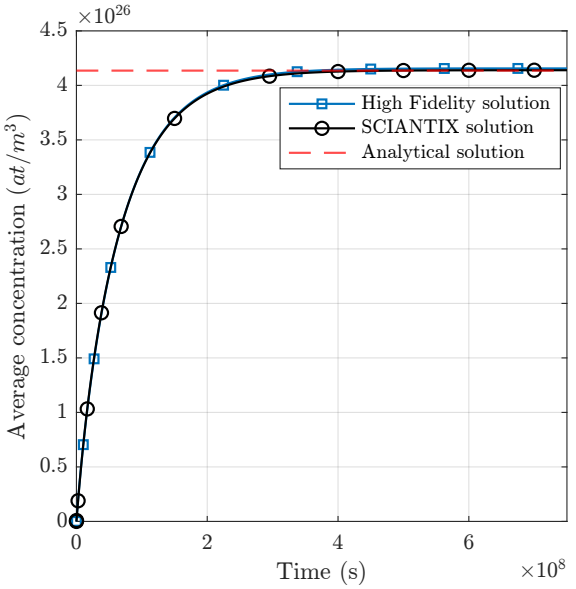

Figure 1.7. Comparison between the SCIANTIX solution, the high fidelity solution and the analytical solution at equilibrium in terms of average concentration.

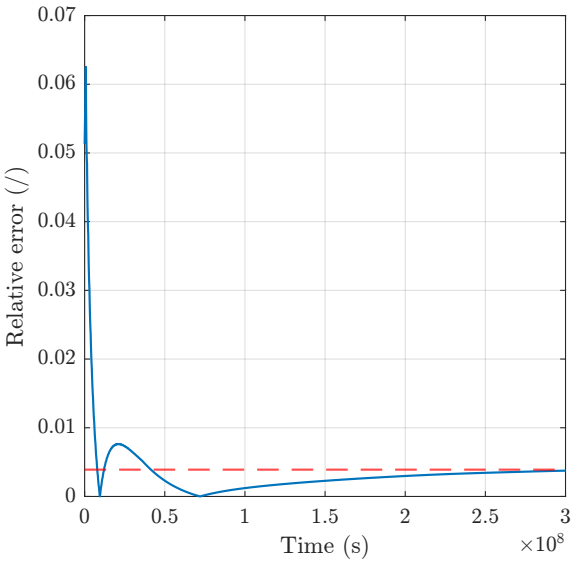

Figure 1.8. The relative error u between the SCIANTIX solution and the high fidelity solution along time. The red dashed line identify the final value.

of the average concentration, $\bar{c}_\infty$

$$\frac{\sigma_{\bar{c}}}{\bar{c}_\infty} \simeq \sqrt{\left(\frac{\partial \bar{c}}{\partial D}\right)^2 \frac{\sigma_D^2}{\bar{c}_\infty} + \left(\frac{\partial \bar{c}}{\partial R}\right)^2 \frac{\sigma_R^2}{\bar{c}_\infty}} \tag{1.40}$$

The uncertainties relating to diffusion coefficient, σ_D, and the radius, σ_R, were taken from [15] and are reported in Table 1.3, from these values is clear that the uncertainty associated with the diffusion coefficient dominates over the uncertainty associated with the asymptotic value of average concentration. Consequently, a variation of two orders of magnitude on the diffusion coefficient involves approximately a variation of an order of magnitude on the asymptotic value of the average concentration. In this way is possible conclude that the errors obtained (Table 1.2) are comparable with the uncertainty associated with the diffusion coefficient and therefore can be considered reasonable.

For completeness, the online phase was also carried out in OpenFOAM with the

Table 1.3. Values of the uncertainties related to the diffusion coefficient and the radius, obtained from [37], and to the asymptotic value of the average concentration which has been obtained by means of the uncertainty propagation formula.

Parameter	Scaling factors		Variance	Reference
	Low	High		
Grain radius	$0.4R$	$1.6R$	$0.12R^2$	[15]
Diffusion coefficient	$0.4R$	$10R$	$8D^2$	[15]
Average concentration	$-3\sqrt{3}\bar{c}_\infty$	$3\sqrt{3}\bar{c}_\infty$	$9\bar{c}_\infty^2$	

aim of reconstructing the entire spatial distribution of the concentration field. To do this, are necessary the time coefficients obtained through the resolution of the ODE system on SCIANTIX (Section 1.5) and the entire spatial field of the bases (Figure 1.6a and 1.6b), not only their average value (Equation 1.39). Comparing the distributions in Figure 1.6 and the distributions in the Figure 1.9, it can be seen that the error decreases as the time step advances both in terms of the spatially assumed values and in terms of the maximum concentration value reported on the color map. The trend of the error over time is in complete agreement with the Figure 1.8.

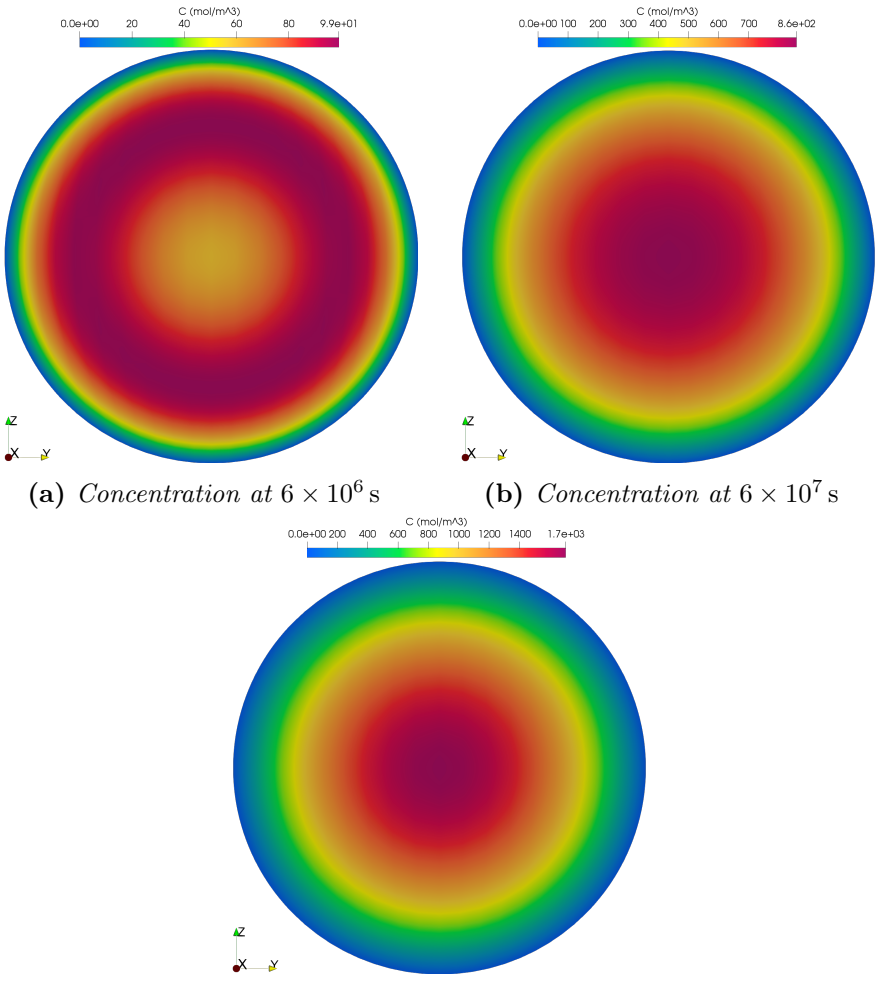

(a) *Concentration at* 6×10^6 s **(b)** *Concentration at* 6×10^7 s

(c) *Concentration at* 6×10^8 s

Figure 1.9. Reconstruction of the spatial distribution of the concentration field.

1.6.2 Method of Manufactured Solutions

When the analytical solution is not available, it is possible to develop a special type of analytical solution to be used as benchmark. The Method of Manufactured Solutions (MMS) [47] is a technique can be used for developing an exact analytical solution from the governing equation of the mathematical model to be used for testing the consistency of numerical algorithms. The procedure is briefly structured as follows.

1. As the name suggests a specific solution is manufactured and assumed to satisfy the PDE of interest;
2. The solution is replaced in the PDE and the equation is rearranged such that a forcing source term appears;
3. The PDE is numerically solved with the forcing source term and the two solutions are compared.

In this case, in which the analytical solution is known, the MMS was used to verify that the algorithm is able to scale the error correctly, as the time step varies, in non-physical situations so as to control its behavior even in complex situations in which the parameters could assume unexpected values.

Let's suppose that a solution of the form $c(r,t) = X(r)Y(t)$, satisfies Equation 1.10. The boundary conditions for $X(r)$ are $X(R) = 0$ and $X'(0) = 0$, while the initial condition is modeled by $Y(0) = 0$. The problem becomes:

$$XY' = D_M Y \nabla^2 X + S_M \tag{1.41}$$

where the subscript M stands for Manufactured. Indeed the manufactured source is written as:

$$S_M = XY' - D_M Y \nabla^2 X \tag{1.42}$$

If $R_M = 1$ and $X = 15/6(1 - r^2)$, then $\nabla^2 X = 1/5$. Finally the equation to be solved turns out to be:

$$S_M = \frac{15}{6}(1 - r^2)Y' - \frac{1}{5}D_M Y \tag{1.43}$$

The expression chosen for Y is a damped exponential (Figure 1.10a)

$$Y(t) = \frac{\exp(1 - 1.247t)}{1.3478}\sin(15t - 1.7) + 2 \tag{1.44}$$

Instead, for the diffusion coefficient, two different functions have been used (Figures 1.10b and 1.10c) in order to study a physical and non-physical situation:

$$\begin{cases} D_{M1}(t) = e^t \sin(t + 1) \\ D_{M2}(t) = 7\exp(-0.2t)\sin(15t + 5) \end{cases} \tag{1.45}$$

The function D_{M2} represents the non-physical situation since in this case the diffusion coefficient assumes also negative values. The numerical solution, evaluated by the code

$$C_N = \frac{3}{4\pi R^3}\int_0^R C(r,t)4\pi r^2 dr \tag{1.46}$$

where $R = R_M = 1$, has to be compared to the manufactured average concentration

$$C_M = \frac{3}{4\pi R_M^3}\int_0^{R_M} X(r)Y(t)4\pi r^2 dr \tag{1.47}$$

By defining the error between the manufactured average concentration $C_M(t_k)$ and the computational solution $C_N(t_k)$, at time t_k and with a constant time step Δt, as

$$e(\Delta t) = |C_M(t_k) - C_N(t_k)| \tag{1.48}$$

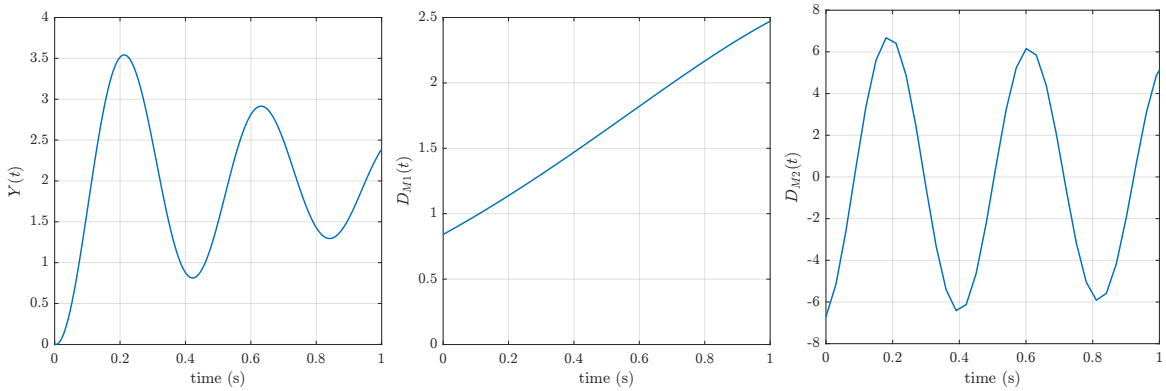

(a) **(b)** *Physical diffusion coefficient* **(c)** *Non-physical diffusion coefficient*

Figure 1.10. The three functions adopted for the MMS method.

the numerical solution C_N converges to the exact manufactured solution C_M , with order p if

$$e(\Delta t) < C\Delta t^p \tag{1.49}$$

To give an estimate of p, two numerical solutions are computed, respectively with time step Δt and $2\Delta t$. Since roughly $e(\Delta t) \approx \Delta t^p$

$$\frac{2e(\Delta t)}{e(2\Delta t))} = 2^{1-p} \tag{1.50}$$

and an estimate of p may be given by

$$p = 1 - \log_2 \left(\frac{2e(\Delta t)}{e(2\Delta t))} \right) \tag{1.51}$$

The MMS is carried from t = 0 to t = 1. In Figures 1.11 and 1.12 the estimate of the convergence order p of the method is showcased. As expected, they asymptotically approaches to two, since the time derivative is discretized with Backward Euler Method of order one and the algorithm performs also the spatial average.

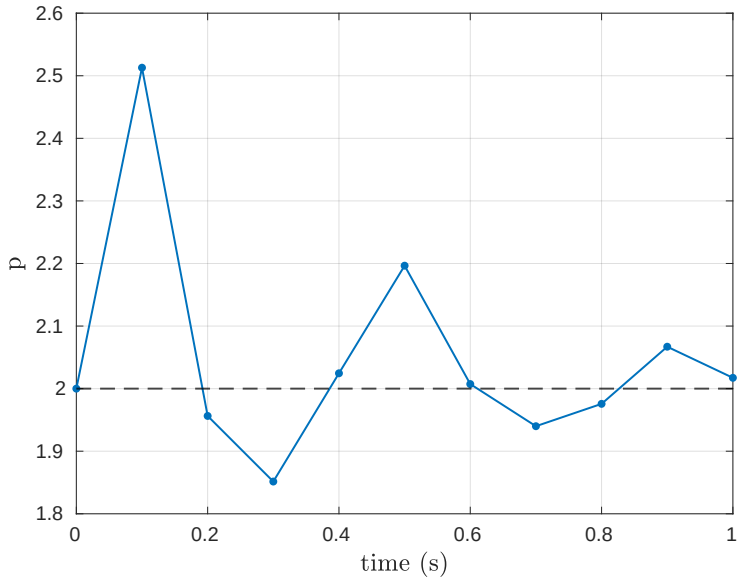

Figure 1.11. Behaviour of the estimated order of convergence p in the case of physical diffusion coefficient. Despite the initial oscillations, the method shows an order of convergence equal to two.

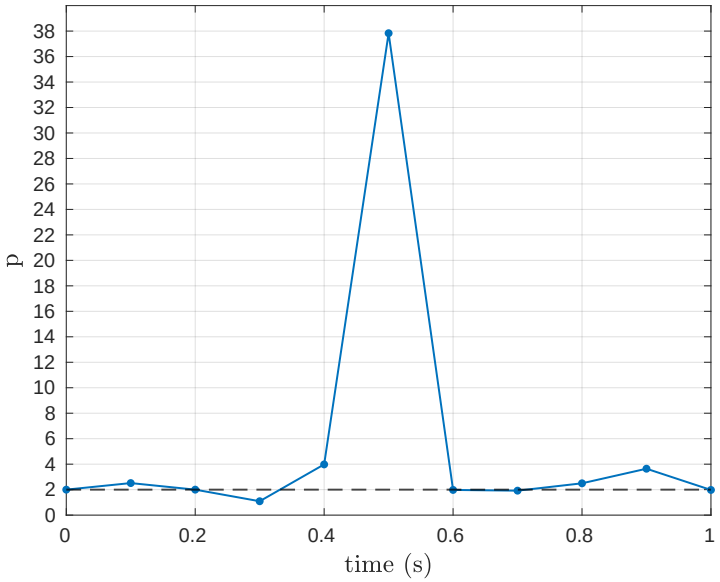

Figure 1.12. Behaviour of the estimated order of convergence p in the case of non-physical diffusion coefficient. Also in this case is reached an order of convergence of two.

1.6.3 Random Numerical Experiments

In SCIANTIX some algorithms are currently available with the purpose of solving the diffusion equation and two of these, FORMAS and the ANS *Method for Calculating the Fractional Release of Volatile Fission Products from Oxide Fuel*, ANS-5.4, were used to verify the accuracy and to compare the computational time of the REDUCE algorithm implemented in this thesis work.

- FORMAS algorithm was developed by [48], then revised by [41], and later by [49][6]. This algorithm is based on the separation of the time and the spatial parts: the time coordinate is transformed to the standard dimensionless time which is the integral of the product of the effective diffusion coefficient and the time interval divided by the square of the sphere radius while the radial part is given by the expansion of the complete set of eigenfunctions. The resulting series solution is approximated by the the sum of the four exponential functions which define the current radial gas distribution. Integrating the gas distribution function over an interval of dimensionless time gives four terms, the sum of which is the current average gas concentration in the grain. The FORMAS's solution, as [41] states, can be considered an exact solution adopting fission gas release above ≈ 0.05.

- The quasi-exact ANS-5.4 algorithm was developed by the Working Group ANS-5.4 of the American Nuclear Society [50] and is derived directly from the analytic solution of the diffusion equation for constant conditions. The main drawback of this algorithm is that it is non-incremental, thus it requires a computational effort exponentially increasing with the number of time steps. Nevertheless, this algorithm is only affected by discretization errors consequently the solution is exact for constant (or piecewise constant) operation histories. For this reason, it has been used as reference solution in several numerical experiment [41,42,51,52] and it was considered as a reference also in the present work[7].

These two algorithms, unlike the REDUCE one, have been implemented to solve the diffusion equation under time-varying conditions, i.e. $D_{\text{eff}}(t)$ and $S(t)$, so that they can be applied to realistic problems[8].

The numerical experiment consists of application of each algorithm to the numerical solution of Equation 1.2 for 1000 randomly generated operation histories. Each individual operation history is piecewise-linear with varying temperature and fission rate from which the parameters of Equation 1.2, i.e., D_{eff} and the time-dependent parameters of the same equation, i.e., $D_{\text{eff}}(t)$ and $S(t)$, are calculated and applied to the numerical algorithms by the program. In each individual history, the quantities shown in table 1.4 are considered as random variables (sampled from uniform distributions), the effect of hydrostatic stress on fission gas behaviour is not considered. These features ensure that all possible situations are covered.

[6] Among the various versions of the FORMAS algorithm, I used the FORMAS algorithm with four exponential terms from [49]

[7] I used the ANS-5.4 algorithm with thirty spatial modes

[8] From this moment on the diffusion coefficient adopted was the effective diffusion coefficient, D_{eff}, in order to simulate more realistic situations and to demonstrate what is stated in Section 1.3.

Parameter	Range of values
Number of linear steps	2-10
Time duration of each linear step	10-10000 (h)
Temperature	1000-3000 (K)
Fission rate	1×10^{18}-3×10^{19} (fiss $m^{-3}s^{-1}$)
Hydrostatic stress	0 (N m^{-2})

Table 1.4. List of parameters adopted in the simulations

Three different numerical experiments were performed each to test and compare the algorithms on the basis of three different figures of merit: (1) the intra-granular average fission gas concentration, (2) the fractional intra-granular fission gas release and (3) the computational time taken by the three algorithms. Each point in the following figures is the result of 1000 randomly generated histories.

1. **Intra-granular average fission gas concentration**
   This numerical experiment aimed to compare the final intra-granular average concentration predicted by the three algorithms. The results are reported in Figures 1.13 and 1.14 in which are also reported the same plots in logarithmic scale so as to highlight the areas with lower values. For this type of graphic representation, any deviation from the 45° diagonal is a measure of the accuracy: the closer the results are to the 45° diagonal, the better the algorithm is. Also the FORMAS and ANS-5.4 algorithms were compared with each other (Figure 1.15) in order to show their accuracy. As can be seen, the REDUCE algorithm is able to calculate the intra-granular average concentration with good accuracy indeed in Figures 1.13a and 1.14a only a slight deviation is perceived. These two figures are practically identical because FORMAS and ANS-5.4 have the same accuracy (Figure 1.15). The good accuracy is obtained even for low concentration values indeed also in logarithmic scale plots (Figures 1.13b and 1.14b) the deviation is practically imperceptible. The only data point that deviates very far from the 45° diagonal is the red one. Comparing the characteristics of this story with those of other stories related to data points fully superimposed on the diagonal, it is possible to conclude that the discrepancy is definitely due to the fact that FORMAS and ANS-5.4 have been implemented to solve the diffusion equation under time-varying conditions while the REDUCE algorithm under constant conditions. Indeed, the history related to the red data point is characterized by a sharp change in the parameters.

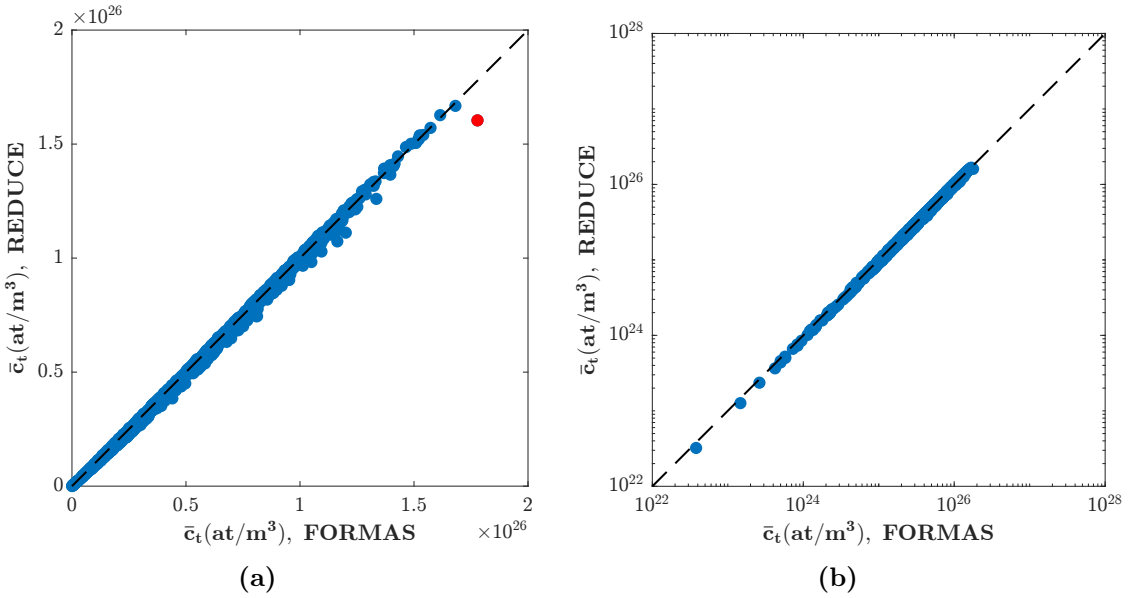

(a) **(b)**

Figure 1.13. Comparison between the values of intra-granular average fission gas concentration calculated by the REDUCE algorithm and by the FORMAS algorithm in linear (a) and logarithmic (b) scale. Each data point corresponds to a calculation with randomly generated conditions. The red data point corresponds to a story characterized by sharp change in the parameters and indeed this point turns out to be the one most diverged from the 45° diagonal due to the implementation characteristics of the REDUCE algorithm which do not allow to detect properly a similar situation.

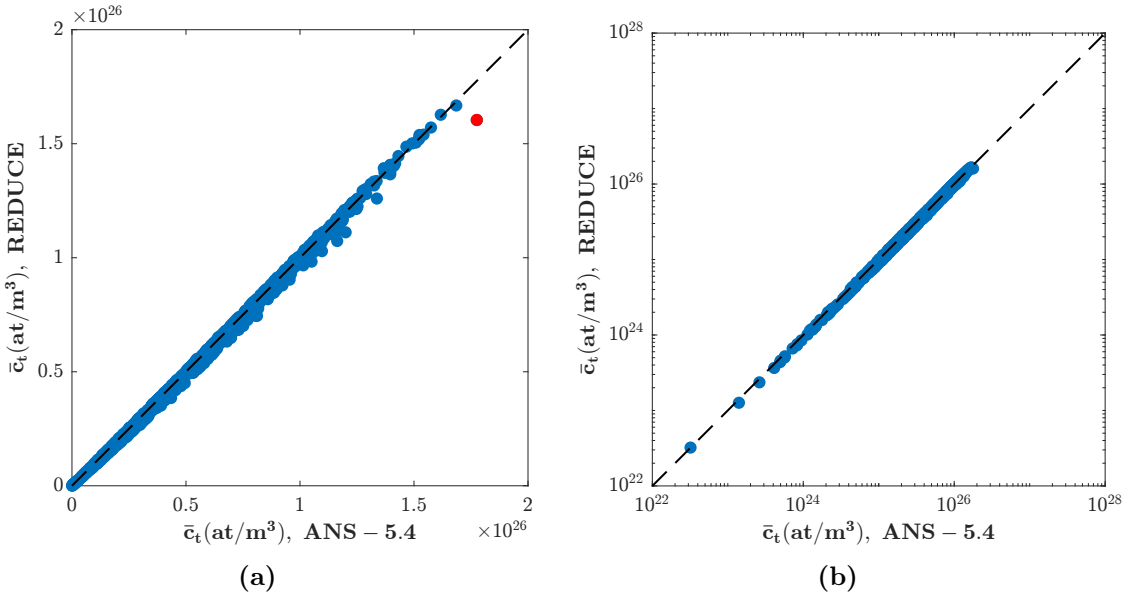

(a) **(b)**

Figure 1.14. Comparison between the values of intra-granular average fission gas concentration calculated by the REDUCE algorithm and by the ANS-5.4 algorithm in linear (a) and logarithmic (b) scale. Each data point corresponds to a calculation with randomly generated conditions. The red data point corresponds to a story characterized by sharp change in the parameters and indeed this point turns out to be the one most diverged from the 45° diagonal due to the implementation characteristics of the REDUCE algorithm which do not allow to detect properly a similar situation.

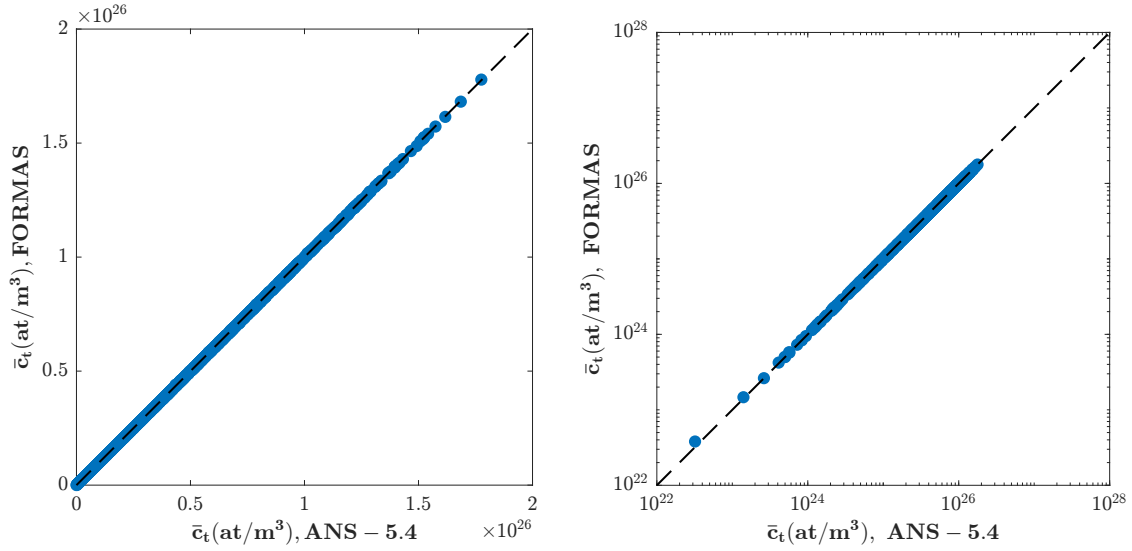

Figure 1.15. Comparison between the values of intra-granular average fission gas concentration calculated by the FORMAS algorithm and by the ANS-5.4 algorithm in linear (a) and logarithmic (b) scale. Each data point corresponds to a calculation with randomly generated conditions.

2. Intra-granular fission gas release

This numerical experiment aimed to compare the final intra-granular release predicted by the three algorithms. This parameter is defined as:

$$f := \frac{\bar{c}_{created}(t_{end}) - \bar{c}_t(t_{end})}{\bar{c}_{created}(t_{end})} \tag{1.52}$$

where $\bar{c}_{created}$ (at m^{-3}) is the concentration of gas created (i.e. the time integral of $S(t)$) and t_{end}(s) is the final time of the operation history. The results are reported in Figure 1.16. Was adopted this type of graphic representation in order to show the range, in terms of release, covered by each algorithm. As can be seen, the REDUCE algorithm covers approximately the same intra-granular fission gas release interval as the FORMAS and ANS-5.4 algorithms except for the very low values. Consequently this algorithm has good coverage of the range of interest, $0 \div 0.8$, related to application in light water reactors where the fission gas release is not very high. On the contrary, in fast breeder reactors the fission gas release is usually very high and therefore this algorithm should not be used.

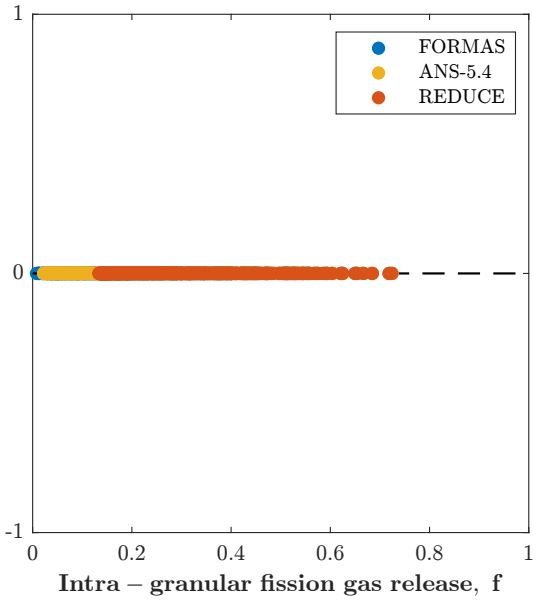

Figure 1.16. Comparison between the interval covered in terms of intra-granular fission gas release by the three algorithm. Due to the type of graphic representation adopted it is not clearly seen but the three algorithms reach the same extreme on the right of the interval. Each data point corresponds to a calculation with randomly generated conditions.

3. Computational time

This numerical experiment aimed to compare the computational times taken by the three algorithms. The execution time, $t_{exe}(s)$, considered refers only to the time taken by each algorithm without taking into account the other SCIANTIX routines, this is the reason why the values obtained are very low. The results are reported in Figure 1.17. Was adopted the same graphic representation of numerical experiment related to intra-granular average fission gas concentration. In this case, any deviation from the 45° is a measure of how far differ the computational times of the three algorithms. As can be seen, the REDUCE algorithm takes the same computational time as FORMAS (Figure 1.17a), this result is reasonable since FORMAS solves four decoupled ODEs that are equivalent to solve a system of two coupled ODEs as the REDUCE algorithm does. On the other side, the REDUCE algorithm takes less time than ANS-5.4 (Figure 1.17b), this is due to the fact that ANS-5.4 solves thirty spatial modalities that correspond to 30 decoupled ODEs, resulting in a higher computational cost than REDUCE.

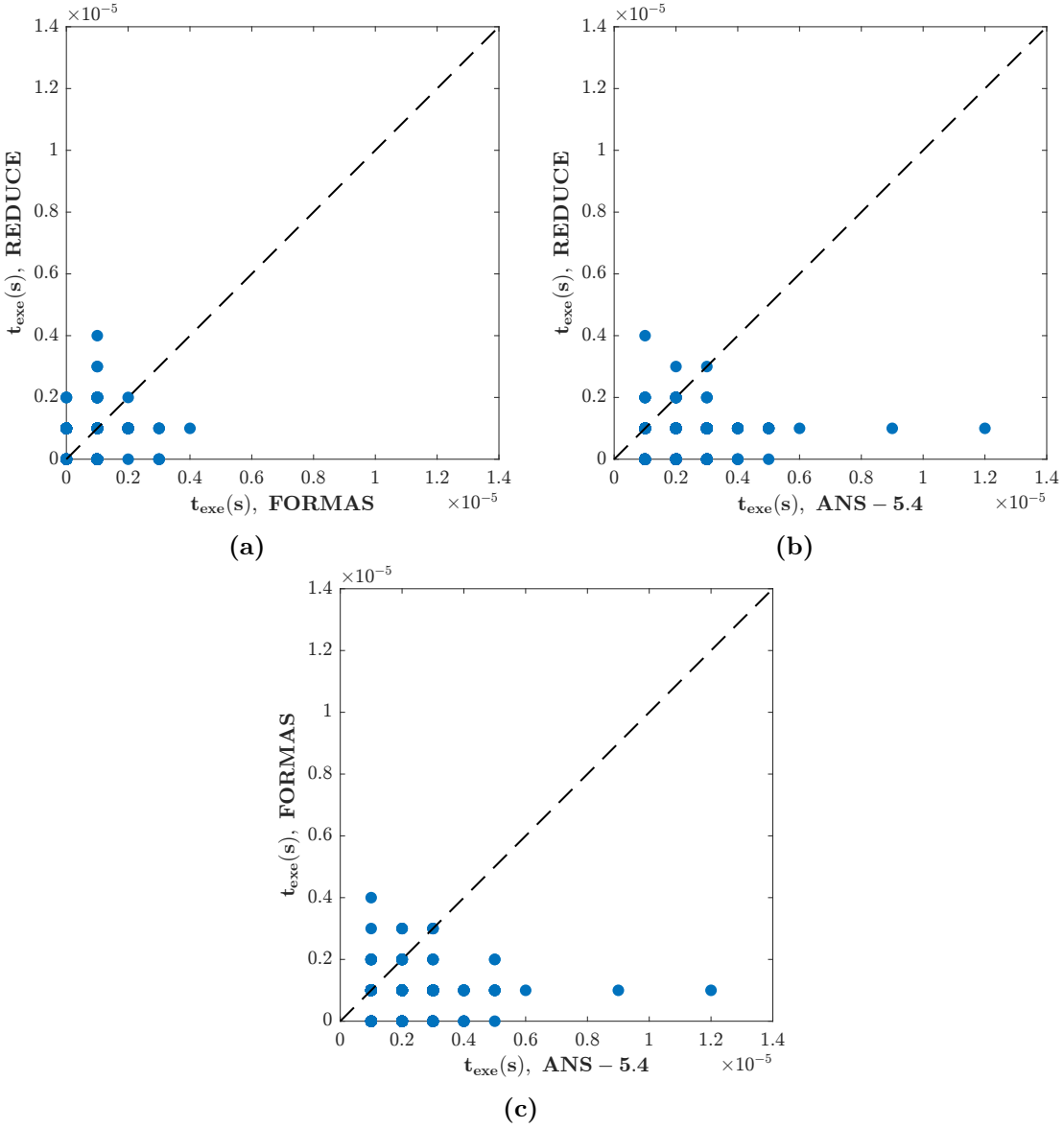

Figure 1.17. Comparison between the values of execution time calculated by the REDUCE, FORMAS and ANS-5.4 algorithms. Although 1000 stories have been simulated, the points on the graph are much less because the times required by the algorithms are practically always the same. Each data point corresponds to a calculation with randomly generated conditions.

1.6.4 Comparison to reference algorithm

As reference algorithm a refined version of the classical semi-analytic reference algorithm ANS-5.4 was used, which provides quasi-exact solution of the problem as the time-step tends to zero. To obtain this reference solution, each time interval was discretized in 5000 sub-steps compared to the 1000 sub-steps used for the solution via the proposed algorithms (FORMAS, ANS-5.4 with thirty spatial modes and REDUCE) and a number of modes high enough that the truncation error is negligible is considered, i.e. the higher modes are "empty" along the all history. Also in this case was implemented a numerical experiment of 1000 randomly generated operation histories with the random variables reported in Table 1.4 in order to go back the accuracy of the REDUCE algorithm, comparing it with the accuracy achieved by FORMAS and ANS-5.4. The figure of merit considered is the intra-granular average fission gas concentration.

The results are reported in Figures 1.18, 1.19 and 1.20. Was adopted the same graphic representation of some numerical experiments described above. As can be seen, the accuracy of the REDUCE algorithm is lower than FORMAS and ANS-5.4. indeed in Figures 1.18 is possibile to see a slight deviation from the 45° diagonal while in Figures 1.19 and 1.20 the deviation is imperceptible. This is due to the fact that FORMAS and ANS-5.4 have been implemented to solve the diffusion equation under time-varying conditions while the REDUCE algorithm under constant conditions, as already mentioned in the previous section. On the other hand is necessary to emphasize that, despite no correction is applied to the REDUCE algorithm in stories that have very wide variations in the parameters, there is still a reasonable accuracy. Moreover, FORMAS ans ANS-5.4, are methods that have been optimized from the point of view of the number of bases to be used, both as kernel expansion in FORMAS and as eigenfunctions in ANS-5.4, while REDUCE is still in a preliminary phase in which no optimization work has been done. From the point of view of the REDUCE optimization, one could increase the number of bases that populate the subspace of smaller dimension 1.18 so as to see how the accuracy and the computational time scales compared with an increase in the modes of FORMAS. I expect that going from two to three bases with REDUCE will be more efficient than going from four to nine spatial modes with FORMAS.

To investigate in finer detail the accuracy of the three algorithms, in Figure 1.21 is showcased the relative error of the solution obtained with each algorithm with respect to the reference algorithm solution. The results are consistent with the conclusions just drawn, namely that the overall accuracy of REDUCE is less than FORMAS and ANS-5.4.

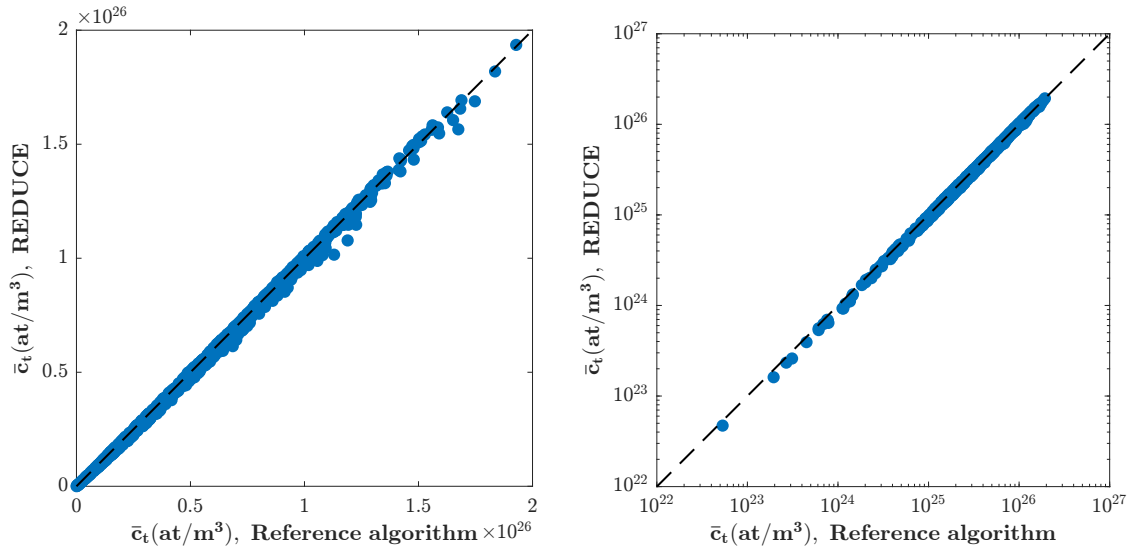

Figure 1.18. Comparison between the values of intra-granular average fission gas concentration calculated by the REDUCE algorithm and by the reference algorithm in linear (left) and logarithmic (right) scale. Each data point corresponds to a calculation with randomly generated conditions.

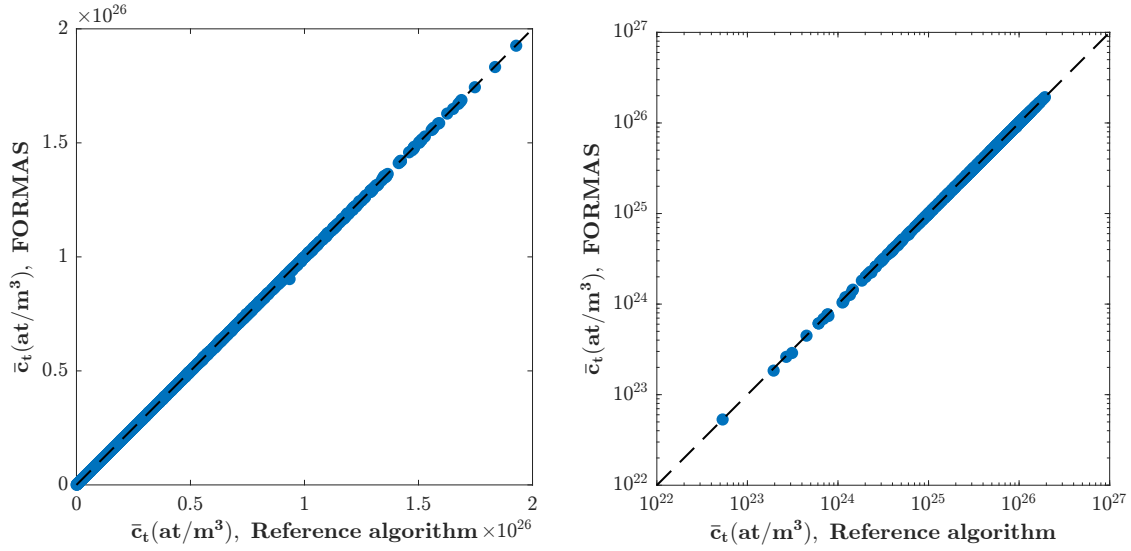

Figure 1.19. Comparison between the values of intra-granular average fission gas concentration calculated by the FORMAS algorithm and by the reference algorithm in linear (left) and logarithmic (right) scale. Each data point corresponds to a calculation with randomly generated conditions.

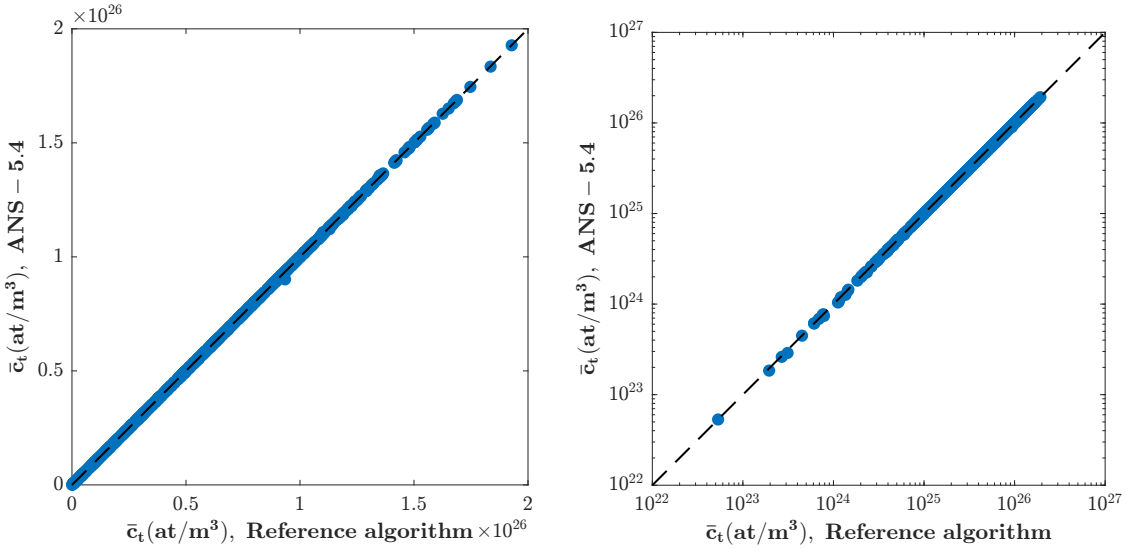

Figure 1.20. Comparison between the values of intra-granular average fission gas concentration calculated by the ANS-5.4 algorithm and by the reference algorithm in linear (left) and logarithmic (right) scale. Each data point corresponds to a calculation with randomly generated conditions.

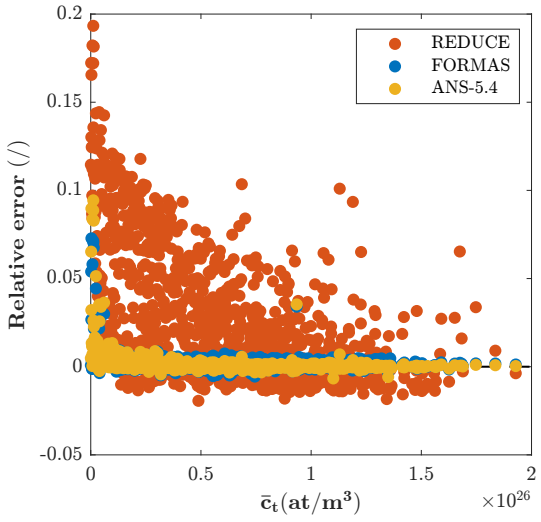

Figure 1.21. Comparison between the REDUCE, FORMAS and ANS-5.4 algorithms in terms of relative error with respect to the reference algorithm. Each data point corresponds to a calculation with randomly generated conditions.

1.7 Application in a fuel performance code

In this section, the applicability of the REDUCE algorithm to integral fuel rod analysis is presented, together with a comparison with the state-of-art solvers represented by FORMAS and ANS-5.4. This was done through implementation and testing in the length-scale fuel performance code TRANSURANUS [3]. The algorithms implemented in SCIANTIX were coupled with the TRANSURANUS subprograms for the calculation of intra-granular fission gas concentration and intra-granular fission gas release. The first step was to simulate a simple irradiation situation with the intent to test the correct coupling between SCIANTIX and TRANSURANUS and the behavior of the REDUCE algorithm in a fuel performance code by comparing it with the state-of-art solvers. Subsequently, the GE7 fuel rod irradiation experiment from the Risø-3 experimental program was then simulated in order to verify the applicability in a more realistic situation. The purpose of this section is not to show that the REDUCE algorithm is able to correctly predict the behavior of fission gases but to show that it is able to work if applied to a case of integral irradiation without ever crashing and to have a stable behavior for the entire duration of irradiation.

TRANSURANUS is a computer program for the thermal and mechanical analysis of fuel rods in nuclear reactors and was developed at the Joint Research Center (JRC) in Karlsruhe. Was specifically designed for the analysis of a whole nuclear fuel rod throught a 1.5D approach (superposition of a one-dimensional radial and axial analysis). The fuel rod is divided into axial slices and at a given time the rod is analysed slice per slice. This program is built into several subroutines which allow for the incorporation of different correlations, for the purposes of this thesis work the subroutine of interest[9] is the one that deals with calculating for each point in the fuel the intra-granular fission gas concentration and fission gas release. Through the coupling with SCIANTIX[10] this calculation is intended for the REDUCE, FORMAS or ANS-5.4 algorithm, consequently one of the three algorithms is used to solve the diffusion equation in that specific point of the mesh at each iteration and since the number of points is approximately a million each single algorithm returns a million results, each relating to different temperature and fission rates conditions. In this way, a simulation in TRANSURANUS is equivalent to a numerical experiment, like those implemented in Sections 1.6.3 and 1.6.4, in which a million random operation histories are generated.

Case study

In this preliminary analysis, I considered the irradiation of a single fuel pellet (without the cladding[11]) of UO_2 at 95.2% theoretical density with an outer diameter of 3 mm in a Pressurized Water Reactor (PWR). The power history is characterized by a constant linear heat rate at 30 W/mm and the duration of irradiation is of 10 000 h. In Tables 1.5a and 1.5b are summarized the geometrical characteristics of the fuel rod

[9] This subroutine is the FisPro3.f95 which deals with the analysis of the behavior of fission products using the SCIANTIX code.

[10] SCIANTIX is called by TRANSURANUS by setting in the input file: `Modfuel(4)`=1 and `FGMech`=3.

[11] Is possible to eliminate the presence of cladding by setting: `ifalll`=2.

Table 1.5. Main features of the preliminary analysis

Pellet stack length (mm)	25
Plenum length (mm)	120
Fuel diameter (mm)	3
Grain diameter (μm)	10

(a) *Fuel rod characteristics*

O/M (-)	1.99
Linear heat rate (W mm^{-1})	30
Fuel central temperature (K)	1082
Fuel surface temperature (K)	403.54

(b) *Irradiation conditions*

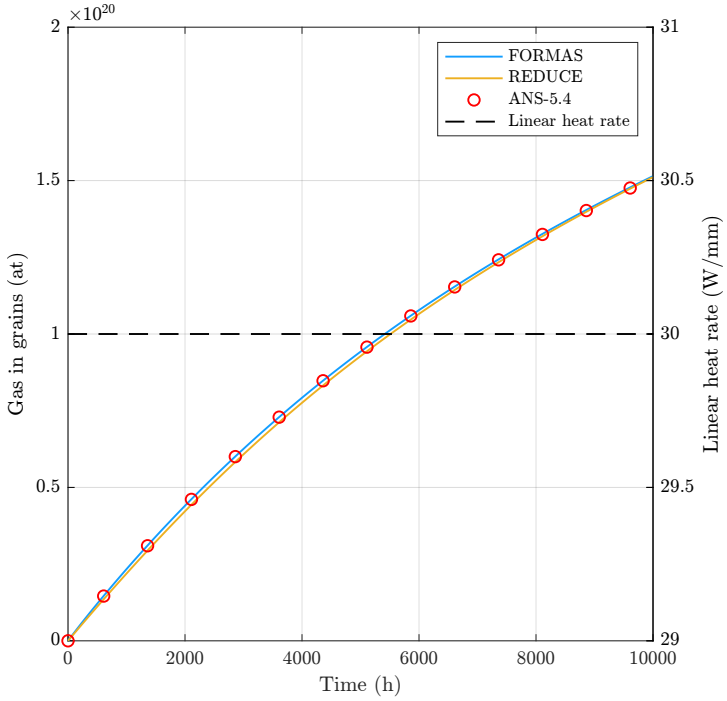

Figure 1.22. Comparison between the values of intra-granular average fission gas concentration along time calculated by the REDUCE, FORMAS and ANS-5.4 algorithms. Is also depicted the linear heat rate.

and the irradiation conditions.

Figure 1.22 compares the results obtained by adopting the REDUCE algorithm with those obtained by using the state-of-art algorithm in SCIANTIX, in terms of intra-granular average fission gas concentration as a function of the time. As can be seen, the result predicted by REDUCE differs slightly from what was predicted by FORMAS and ANS-5.4. The maximum relative error between the three algorithms stands at 14% and is, more or less, of the same order of magnitude as the relative error found in Figure 1.21. Consequently we can also conclude that the numerical experiment seen in Section 1.6.4 has returned representative results and is more than reasonable to estimate errors in the code.

In conclusion, this case study has allowed to demonstrate that the TRANSURANUS-SCIANTIX coupling works and that the REDUCE algorithm is able to predict the gas concentration in the grain unless a negligible error which is comparable with the uncertainty associated with the diffusion coefficient as seen in Section 1.6.1.

GE7 irradiation experiment

The GE7 rod bump test was carried out during the third Risø Transient Fission Gas Release program in 1989 and is included in the IAEA FUMEX-III Project [53–55]. The test fuel rod (designated as ZX115) consisted of pellets of UO_2 at 95.2% theoretical density with 2-dimensional average grain diameter of approximately 18.8 μm. The cladding is in Zircaloy-2 with an outer diameter of 12.26 mm and was stress relieved with a bonded zirconium liner. The fabrication characteristics of the fuel rod are given in Table 1.6. The experiment involved a fuel rod base irradiation up to about 40 GWd t_U^{-1} in the Quad Cities-1 Boiling Water Reactor (BWR) (USA) (Figure 1.23a). Subsequent, the power transient test was performed in the DR3 research reactor at Risø (Denmark). The power history during the bump included a 6-hour conditioning period at approximately 30 W mm^{-1}, a 15 minute power ramp, and then a 4-hour hold, where the the linear heat rate at the end of the hold period was 48 W mm^{-1} (Figure 1.23b). More details on fuel fabrication data and irradiation conditions are reported in [53, 55].

Table 1.6. Fabrication data of the ZX115 fuel rod

Pellet stack length (mm)	752.1
Diametral gap (mm)	0.22
Plenum length	143.4
Internal free volume (cm^3)	12
Fill gas	He
Fill gas pressure (MPa)	0.29
O/M (-)	1.997

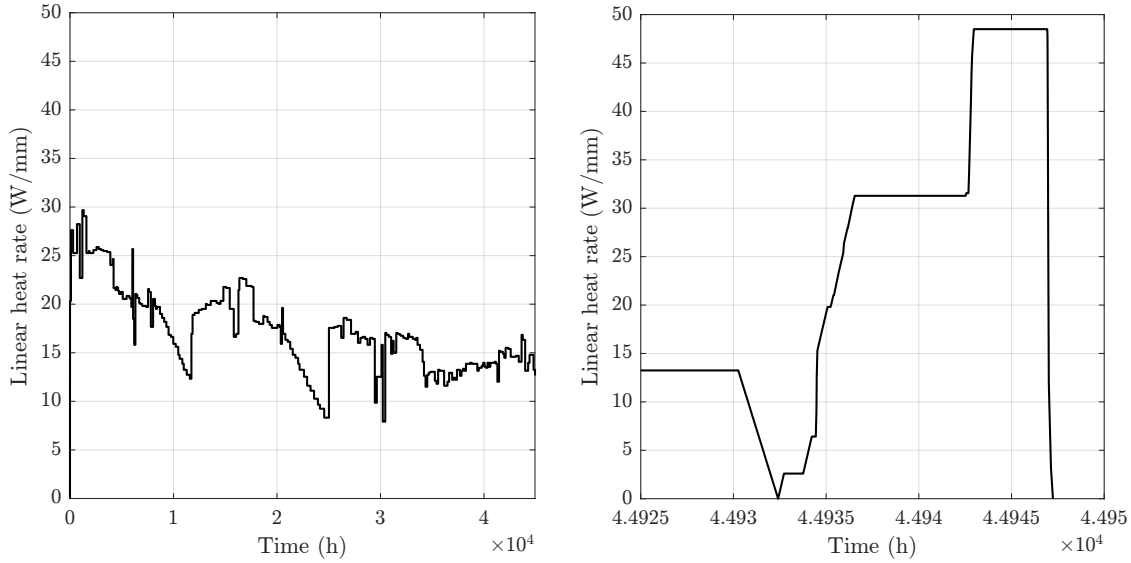

(a) *Base irradiation* **(b)** *Zoom on the ramp test*

Figure 1.23. GE7 linear power profile during the base irradiation (a) and bumb test (b).

I simulated this irradiation experiment in TRANSURANUS in order to verify the

applicability of the REDUCE algorithm in a more realistic situation. Figures 1.24 and 1.25 compares the results obtained by the three algorithm in terms of intra-granular average fission gas concentration and fractional fission gas release as a function of the time, during the base irradiation and the power ramp.

As can be seen in Figure 1.24a the REDUCE algorithm involves a greater diffusion during the base irradiation, indeed its curve is below that of the other two algorithms, which means that more fission gases come out of the grain and this is consistent with the Figure 1.25a in which the release is greater. Subsequently during the ramp (Figure 1.25b) there is an additional release contribution because there was a greater release during the base irradiation. This underestimation of the gas concentration in the grain operated by the REDUCE algorithm is due to the number of bases adopted during the implementation of the POD procedure. Since only two bases are adopted, these do not allow a complete knowledge of the phenomenon and therefore lead to underestimate the real concentration value present in the grain. Accordingly, what can be done to reduce the discrepancy is to increase the number of bases that populate the subspace of smaller dimension 1.18 in order to have a more complete characterization of the phenomenon, as has already been suggested in Section 1.6.4.

It is however worth emphasize that the REDUCE algorithm is able to keep the intra-granular average fission gas concentration constant during the ramp (Figure 1.24b) which qualitatively is the correct trend.

It might seem strange that during the ramp the intra-granular average fission gas concentration is constant while the fission gas release has an increasing trend (Figure 1.24b and 1.25b), this is because the release phenomenon foresees that the gas passes from the grain to the grain boundary and then from the grain boundary is released but during the ramp the times are so short that we are able to see only the release of the gas from the grain boundary, this explains the trends obtained.

The experimental fission gas release at the end of the power ramp stands at 14% [15] instead the values predicted by the REDUCE, FORMAS and ANS-5.4 algorithms stands, respectively, at 11%, 8.15% and 8%. From this result it is not possible to draw many conclusions regarding the accuracy of the algorithm in real situations because the analysis should be extended by evaluating the entire validation database.

The time taken by each simulation carried out with FORMAS, REDUCE and ANS-5.4 turns out to be respectively 40.5 s, 40 s and 59.4 s. As expected from the random numerical experiments carried out in Section 1.6.3, the reduction algorithm takes the same execution time as FORMAS and both are faster than ANS-5.4.

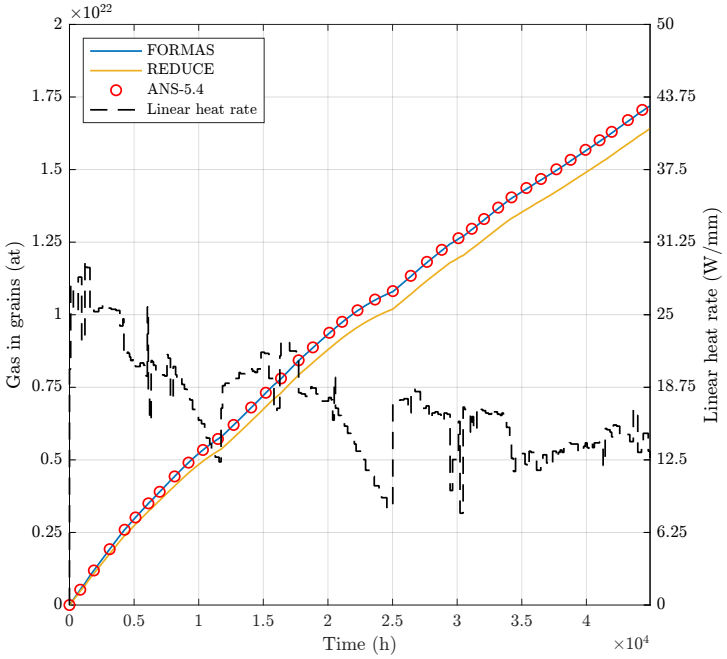

(a) *Base irradiation*

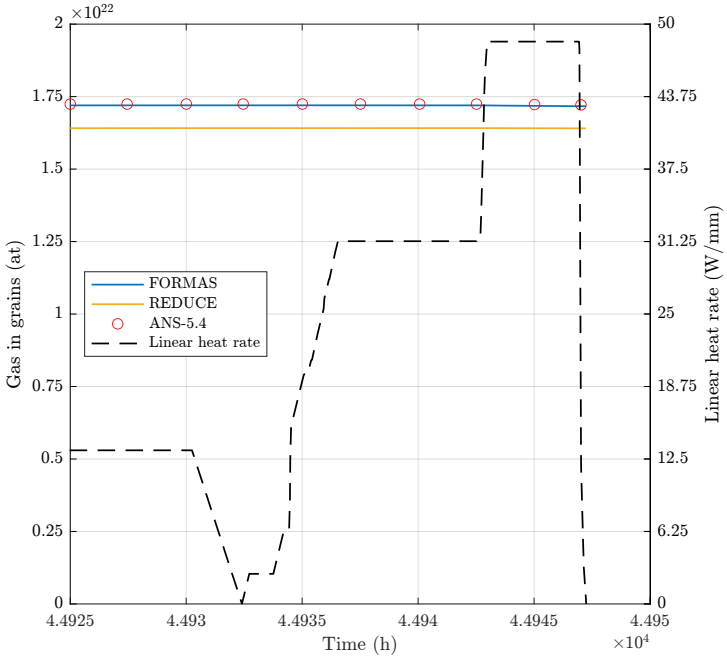

(b) *Zoom on the ramp test*

Figure 1.24. Comparison between the values of intra-granular average fission gas concentration along time calculated by the REDUCE, FORMAS and ANS-5.4 algorithms during the base irradiation (a) and ramp test (b).

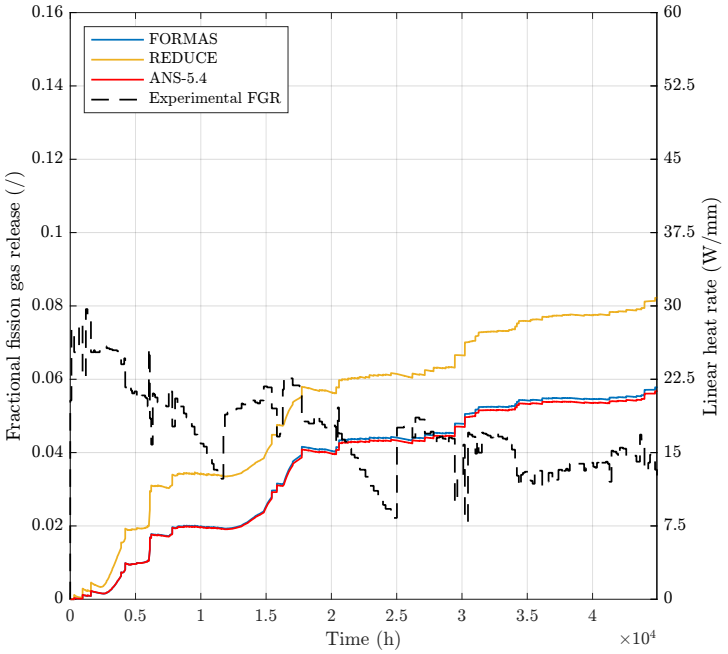

(a) *Base irradiation*

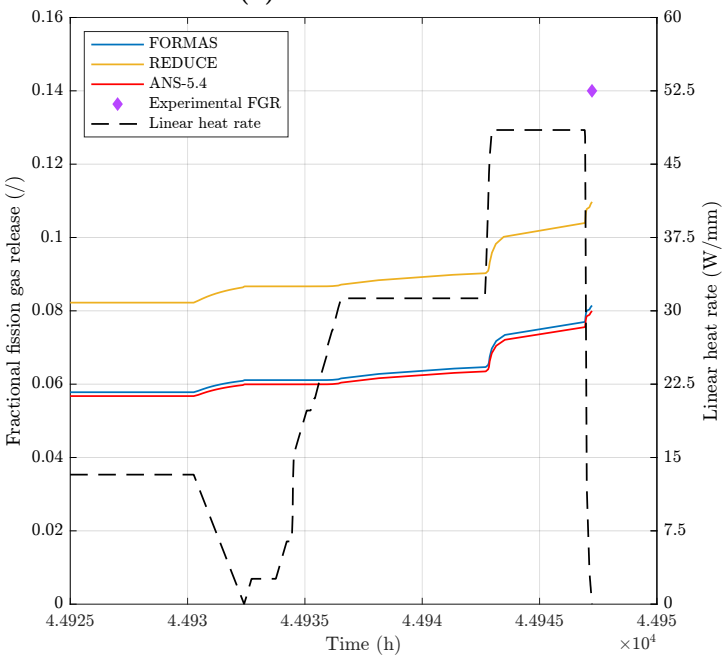

(b) *Zoom on the ramp test*

Figure 1.25. Comparison between the values of intra-granular fission gas release along time calculated by the REDUCE, FORMAS and ANS-5.4 algorithms during the base irradiation (a) and ramp test (b).

1.8 Closing remarks

In this Chapter, the POD-FV-ROM technique for the diffusion problem of fission gas in oxide fuel spherical grains was developed. The results obtained through the intense verification phase lead to the conclusion that, although the REDUCE algorithm has been implemented under constant conditions is able to accurately predict the solution even in transient conditions. Subsequently the application of the algorithm in a fuel performance code lead to the conclusion that the algorithm is able to correctly function even at the engineering scale. What is missing is an algorithm validation test to conclude that the model is accurate enough to represent and provide information about real physical applications.

Future developments foresee:

- The optimization of the algorithm in terms of accuracy and computational time. What should be done is increase the number of bases to see how the accuracy and computation times scale and then, through a sensitivity analysis, determine the number of optimal bases;

- Make corrections to the algorithm in order to extend the range of intra-granular fission gas release covered. The correction that will need to be made is conceptually identical to that made by Lassmann and Benk to the FORMAS algorithm in [41]. Basically it means correcting the algorithm in correspondence with the low fission gas release region where it is inaccurate, $f < 0.02$.

The implementation of the reduced order model for this simple case of fission gas diffusion in fuel grains represents a milestone for the implementation of more complex models in the framework of fission gas behaviour. This chapter has indeed made possible to lay the foundations and to define the workflow to be followed in the next chapters in which the discussion will be enhanced by adding further features so as to extend the discussion to other fuels.

Chapter 2

Reduced order model of fission gas diffusion in uranium silicide fuel spherical grains

Abstract

In the previous chapter, the attention was focused on developing an accurate and computationally economical reduced order model for diffusion problem in which the diffusion of the gaseous fission products was isotropic. In this chapter, the aim is to extend what has been done to the case in which diffusion in spherical grains is no longer isotropic but anisotropic. This case occurs, for example, in uranium silicide fuels due to its particular crystalline structure. The intent is to highlight how anisotropy must be treated during the offline phase so as not to encounter difficulties in the online phase. The treatment of anisotropy will be useful in the next chapter, which in addition to anisotropy is added a further degree of difficulty which is the non-linearity.

2.1 Intra-granular fission gas behaviour

All LWRs around the world are currently using fuel systems comprised of oxide fuels, such as UO_2 and MOX, encased within a zirconium-based alloy cladding. The oxide fuel-zircaloy system has been optimised over many decades and performs very well under normal operations and anticipated transients. However, because of the highly exothermic nature of zirconium-steam reactions, under some low frequency accidents – when core cooling is temporarily lost and part of the core is uncovered – low probability accidents may lead to an excess generation of heat and hydrogen, resulting in undesirable core damage [56].

After the 2011 Japan earthquake and tsunami, and the events that followed at the Fukushima Daiichi power plant, global interest has expanded in exploring fuels with enhanced performance during such rare events, with accident-tolerant fuel development programmes starting in many research institutions and industry teams. While there is broad consensus that a new fuel system alone is insufficient to mitigate accident consequences, fuels in combination with other systems are expected to give similar or better performance during frequent events and/or normal operations and improved

performance in accident scenarios. Improved performance in accidents has been interpreted to mean allowing more time for cooling to be applied before unacceptable oxidation or melting occurs. [57–60].

In this context, the United States Department of Energy has accelerated research in this area, promoting the Fuel Cycle Research and Development Advanced Fuel Campaign (AFC). The goal of the ATF program of the AFC is to guide the selection of promising fuel concepts to start a test rod irradiation in a commercial reactor by 2022.

Focusing on the nuclear fuel, uranium silicides are potential candidates to substitute uranium dioxide in LWR. Among uranium silicides compounds such as U_3Si, U_3Si_2, and U_3Si_5 emerge, thanks to their interesting thermophysical properties and high uranium densities [61]. They offers improved thermal conductivity, which results in lower centerline temperatures, and higher uranium density. Those characteristics make these compounds attractive from the economic and safety point of view in particular the latter besides being beneficial from operational and economic standpoints could also offset changes to the cladding material that give rise to higher neutron losses compared to the current Zr-based cladding, such as iron-chromium-aluminum (FeCrAl) alloys [62] and Cr-coated Zr alloys [59] with increased oxidation resistance at high temperature.

In order to license a new commercial nuclear fuel, it is necessary to be able to predict the fuel behavior during operation. A wide experience exists worldwide in using uranium U_3Si and U_3Si_2 as fuel for research and test reactors [63–65], however limited experimental testing of U_3Si_2 at power reactor conditions relevant to LWRs has been carried out [66]. This is due to the aggressive development schedule which makes impossible to perform a comprehensive set of experiments to provide material characterization data. For this reason the AFC is carrying out comprehensive experiments to characterize the innovative fuel systems, as well as computational analyses to investigate the proposed materials.

Out-of-pile experimental data has been reported for thermo-physical properties such as thermal and electronic conductivity, specific heat, oxidation reactions and phase stability, however little is known about either point defect diffusion, self-diffusion or fission gas diffusion, neither under intrinsic nor irradiation conditions. Therefore it is not possible to clearly explain the phenomenon of fuel swelling and of fission gas release which correspond to the two of the most important fuel performance behaviors in uranium silicide. In this framework, accurate modeling of fission gas behavior as part of the engineering analysis of fuel rods becomes of particular importance.

Among the uranium silicide fuels, the focus of this work is mainly on U_3Si_2 due to the greater amount of information available. The reduced order model derived in this Chapter requires the diffusivity of Xe atoms in the fuel and in order to derive it is necessary to rely on Density Functional Theory (DFT) as was done by Andersson in [19]. The Xe diffusivity is anisotropic due to the tetragonal crystal structure of U_3Si_2, which results in unique diffusion rates in the basal $a-b$ plane and along the c axis. Given the presence of spherical grains, also in this case the equivalent sphere model of Booth [10] was adopted, consequently the intra-granular diffusion problem is

given by:

$$\begin{cases} \dfrac{\partial c_t(r,t)}{\partial t} = \dfrac{1}{r^2}\dfrac{\partial}{\partial r}\left(\underline{\underline{D}}_{\text{eff}}\, r^2 \dfrac{\partial}{\partial r} c_t(r,t)\right) + S & \\ c_t(r,0) = 0 & 0 < r < R \\ c_t(R,t) = 0 & t > 0 \end{cases} \tag{2.1}$$

where D_{eff} is always the effective diffusion coefficient (Equation 1.3) and the boundary conditions are the same adopted in previous Chapter (Equation 1.11). This equation will be implemented in OpenFOAM in order to solve the diffusion problem under constant conditions, i.e. the source term S and the diffusion coefficient D are assumed as constant in time and uniform in space.

2.2 Implementation of the Full Order Model

In this section the high fidelity-full order simulation of the partial differential equations 2.1 is implemented in the OpenFOAM® environment.

The domain and the boundary conditions adopted are identical to those used in the Chapter 1 and are specified in Section 1.2. For the sake of simplicity in the implementation the equations solved in OpenFOAM doesn't consider the quasi-stationary term, i.e. $b/(b+g)$, as was done in Section 1.2 and explained better in Section 1.3. The Xe total diffusivity in the $a-b$ plane ($D_{Xe}^{aa} = D_{Xe}^{bb}$) and along the c axis (D_{Xe}^{cc}) in nearly stoichiometric U_3Si_2 was calculated through the plot 2.1 realized in [19] considering a temperature of 500 K. The formulas used after obtaining the angular coefficient, A, and the intercept, B, from the plot are:

$$D = D_0 \exp\left(-\frac{A}{T}\right) \tag{2.2}$$

where:

$$B = \log D_0 \tag{2.3}$$

In this way the tensor components of the diffusion coefficient are:

$$\begin{bmatrix} D_{Xe}^{aa} = 1.22 \times 10^{-15} & 0 & 0 \\ 0 & D_{Xe}^{bb} = 1.22 \times 10^{-15} & 0 \\ 0 & 0 & D_{Xe}^{cc} = 4.54 \times 10^{-15} \end{bmatrix} \tag{2.4}$$

To simplify implementation, a dimensionless mesh has been adopted consequently the Equation 2.1 have been transformed into a dimensionless form:

$$R^2 \frac{\partial c}{\partial t} = \frac{1}{\rho^2}\frac{\partial}{\partial \rho^2}\left(\underline{\underline{D}}\, \rho^2 \frac{\partial}{\partial \rho} c\right) + R^2 S \tag{2.5}$$

where $\rho = r/R$. Rewritten in generic form results:

$$R^2 \frac{\partial c}{\partial t} = \nabla \cdot \left(\underline{\underline{D}} \nabla c\right) + R^2 S \tag{2.6}$$

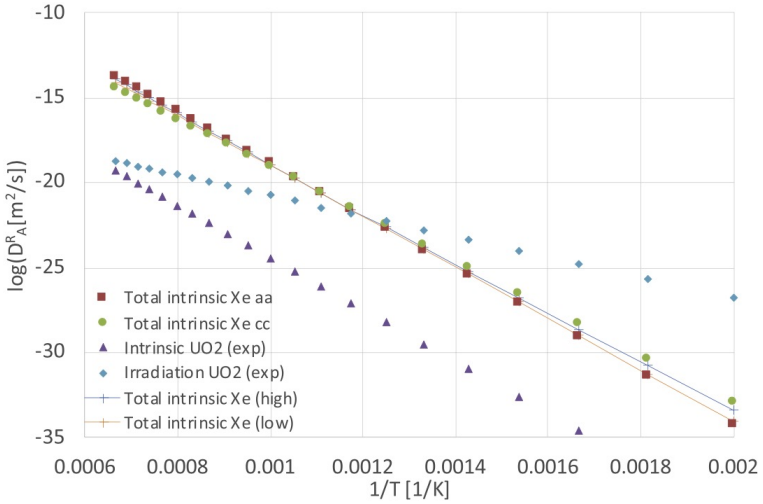

Figure 2.1. The Xe diffusivity tensor components ($D^{aa}_{Xe} = D^{bb}_{Xe}$ and D^{cc}_{Xe}) in nearly stoichiometric U_3Si_2. Model prediction based on experimental data for UO_2 is also showncased [19].

The parameters adopted for the simulation are shown in table 2.1 where is possible to see the units of measurement that have been adopted for the simulation. The simulation was run for 1.5×10^4 s, this time was chosen on the basis of the time taken by the phenomenon to reach equilibrium which is in the order of:

$$\tau = \frac{R^2}{D^{cc}_{Xe}} = 5507s \tag{2.7}$$

The computational time required by a intel Core i5-5300U CPU @ 2.30GHz and 8GB RAM was in the order of 5 minutes. The frequency of snapshot sampling was set to 0.067 Hz, therefore in the 1.5×10^4 s-simulation, 1000 snapshots have been collected. The distribution of concentration field for different time steps resulting from the simulation are showcased in Figure 2.2. In the first instants of the simulation (Figures 2.2a and 2.2b) is possible to see the anisotropic behavior of the diffusion indeed the central region characterized by greater concentration (the red one) assumes a more flattened shape along the z direction compared to the x and y direction, unlike what was obtained in Figure 1.4 related to the case of isotropic diffusion. On the other hand, at equilibrium the diffusion difference smooths out leading to the same situation as in the isotropic case and indeed the concentration assumes a parabolic trend along the spatial coordinates (Figure 2.2d).

The computed quantity of interest is the weighted volume average concentration along time which values are showcased in Figure 2.3.

Table 2.1. List of values and u.o.m adopted in the simulations

Symbol	Definition	Value	u.o.m (original)	u.o.m (simulation)
c	Concentration		mol m^{-3}	-
R	Radius	5×10^{-6}	m	m
T	Temperature	500	K	K
$\dot{F}$	Fission rate	3×10^{19}	fiss m^{-3}s^{-1}	-
y_F	Fission yield	5×10^{-25}	mol fiss^{-1}	s^{-1}
D	Diffusion coefficient	[19]	m^2 s^{-1}	s^{-1}
∇^2	Laplacian term		m^{-2}	-

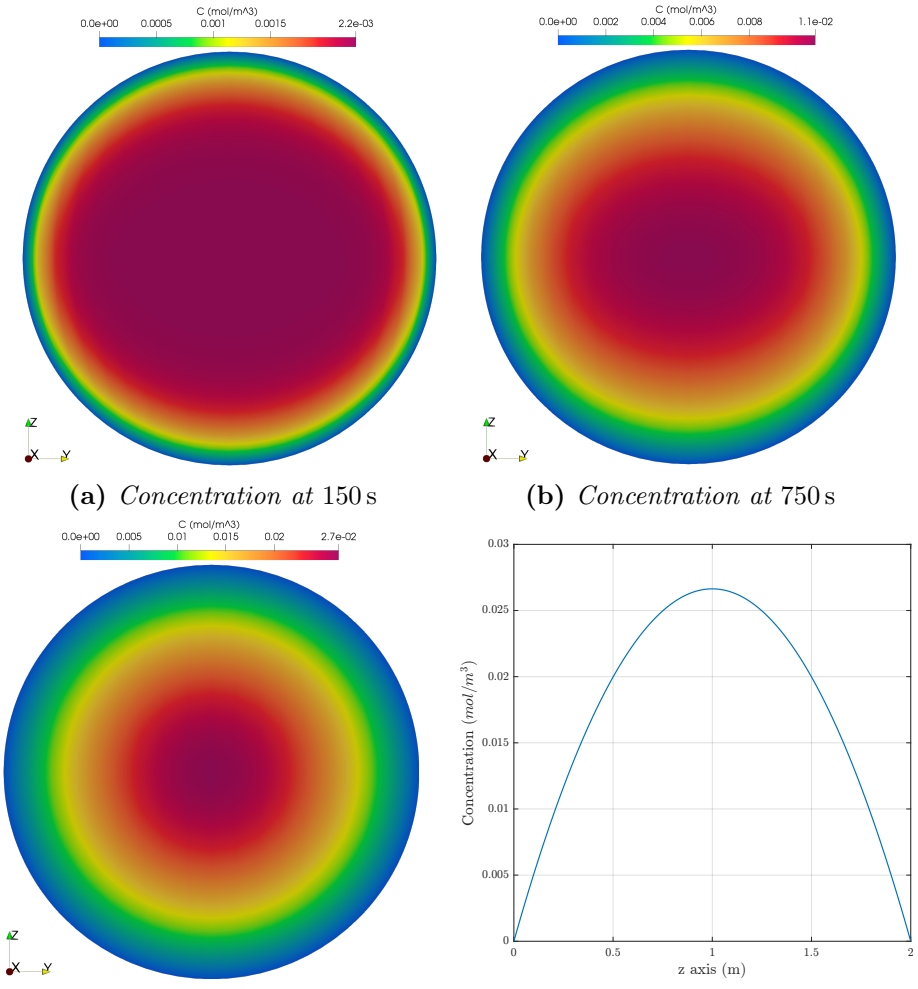

(a) *Concentration at* 150 s **(b)** *Concentration at* 750 s

(c) *Concentration at* 7500 s **(d)** *Concentration trend along the z axis*

Figure 2.2. In (a), (b) and (c) are reported the concentration distributions in correspondence of three time steps resulting from the full order simulation implemented in OpenFOAM. In (d) is reported the concentration trend along the spatial coordinates at equilibrium. In this case we are no longer dealing with an isotropic diffusion, consequently we don't get the same result no matter what plan we adopt to slice the sphere, except at equilibrium where differences smooth out.

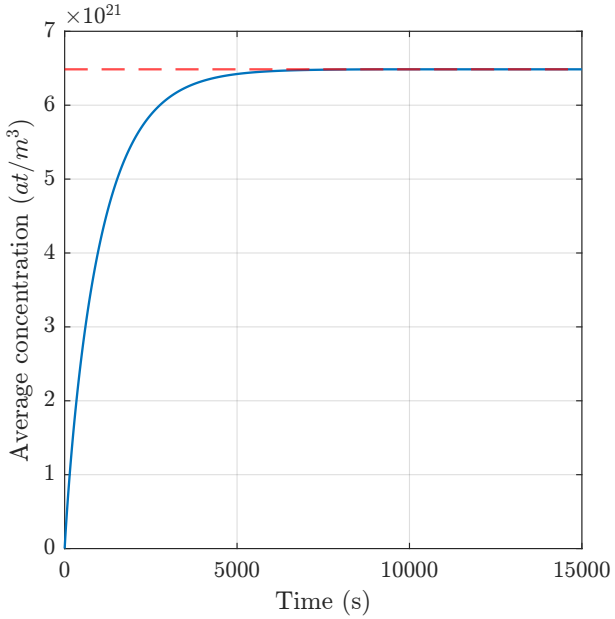

Figure 2.3. Average concentration along time, the red dashed line identify the equilibrium value reach by the OpenFOAM solution.

2.3 POD-FV-ROM of diffusion equation

In this section the POD technique procedure defined in section 1.3 is applied to the problem of fission gas diffusion in uranium silicide fuel spherical grains with the purpose of obtaining a POD-ROM of Equation 1.11 considering the Finite Volume approximation (POD-FV-ROM). Up to the Equation 1.24 it is all identical to what is written in Section 1.3. Before replacing the concentration c with c_r (Equation 1.17) in Equation 2.6 is necessary to rewrite this equation by separating the diffusion coefficient from the matrix containing the anisotropy of the problem:

$$R^2 \frac{\partial c}{\partial t} = \nabla \cdot \left(D_{Xe}^{aa} \begin{bmatrix} 1 & 0 & 0 \\ 0 & 1 & 0 \\ 0 & 0 & \frac{D_{Xe}^{cc}}{D_{Xe}^{aa}} \end{bmatrix} \cdot \nabla c \right) + R^2 S \tag{2.8}$$

where:

$$\underline{\underline{G}} = \begin{bmatrix} 1 & 0 & 0 \\ 0 & 1 & 0 \\ 0 & 0 & \frac{D_{Xe}^{cc}}{D_{Xe}^{aa}} \end{bmatrix} \tag{2.9}$$

This approach will allow to get rid of the anisotropy of the problem in online phase by involving it in the calculation of the matrix (Equation 2.13) of the ODE system so as not to have to face it during the online phase. Now carrying out the replacement mentioned above we obtain:

$$R^2 \sum_{i=1}^{N_c} \phi_i(\mathbf{x}) \frac{\partial a_i(t)}{\partial t} = \nabla \cdot \left[D_{Xe}^{aa} \underline{\underline{G}} \cdot \sum_{i=1}^{N_c} \nabla \left(a_i(t) \phi_i(\mathbf{x}) \right) \right] + R^2 S \tag{2.10}$$

Applying the Galerkin projection over the test functions $\phi_j(\mathbf{x})$:

$$R^2 \frac{da_j(t)}{dt} = D_{Xe}^{aa} \int_\Omega \phi_j(\mathbf{x}) \nabla \cdot \left[\underline{\underline{G}} \cdot \sum_{i=1}^{N_c} \nabla \left(b_i(t) \phi_i(\mathbf{x}) \right) \right] d\Omega + R^2 S \int_\Omega \phi_j(\mathbf{x}) d\Omega \quad j = 1, ..., N_c \tag{2.11}$$

where the term on the left-hand side was written taking into account the orthonormality of basis functions one to each other (Equation 1.19). Rewriting the equation in matrix terms and dividing everything by R^2, the following POD-Galerkin ROM (POD-G-ROM) for Finite Volume discretization (POD-FV-ROM) is obtained:

$$\frac{da_j(t)}{dt} = \frac{D_{Xe}^{aa}}{R^2} \sum_{i=1}^{N_c} a_i(t) E_{ji} + S F_j \quad j = 1, ..., N_c \tag{2.12}$$

where:

$$E_{ji} = \langle \phi_j(\mathbf{x}), \nabla \cdot \left[\underline{\underline{G}} \nabla \phi_i(\mathbf{x}) \right] \rangle_{L^2} \tag{2.13}$$

$$F_j = \langle \phi_j(\mathbf{x}) \rangle_{L^2} \tag{2.14}$$

In the calculation of the matrix E_{ij} I decided to involve only the matrix $\underline{\underline{G}}$ and not all the diffusion coefficient because in this way, as mentioned in the Section 1.3, during the reconstruction phase of the solution it will be possible to modify the diffusion coefficient by also introducing the quasi-stationary term but it will not be possible to modify the anisotropy ratio between the three directions. The original PDE system is thus replaced by an ODE system in which the unknowns are the time-dependent coefficients $a_i(t)$. The dynamical system of the time-dependent coefficients for can be expressed as:

$$\dot{\mathbf{a}} = \frac{D_{Xe}^{aa}}{R^2} \mathbf{a}\mathbf{E} + S\mathbf{F} \tag{2.15}$$

This ODE system is then solved in SCIANTIX by means an implicit Euler scheme in order to derive the time coefficients and finally reconstruct the solution (Section 2.5).

2.4 Implementation of the POD-FV-ROM

In this section the reduction of the model, which consist in going from a set of PDEs to a set of ODEs, is implemented in OpenFOAM. Similarly to the POD-FV-ROM of the previous chapter, the ROM methodology was applied through the same series of steps follow in Section 1.4. The only difference is that the involvement of the matrix $\underline{\underline{G}}$ in the computation of the matrix E_{ij} result in having to implement a Hessian matrix in OpenFOAM. Also in this case have been adopted 2 bases and an accuracy of 1.1 for concentration fields. The outcomes are the two set of orthonormal bases (Figures 2.4a and 2.4b) and the matrices:

$$\mathbf{E} = \begin{bmatrix} -20.167 & -9.5083 \\ -9.6035 & -75.162 \end{bmatrix} \quad \mathbf{F} = \begin{bmatrix} 1.7189 \\ 0.7743 \end{bmatrix} \tag{2.16}$$

As expected, the eigenfunctions trend along the spatial coordinate (Figure 2.4c and 2.4d) correspond to a parabolic and cardinal sine trend. In this case of anisotropic

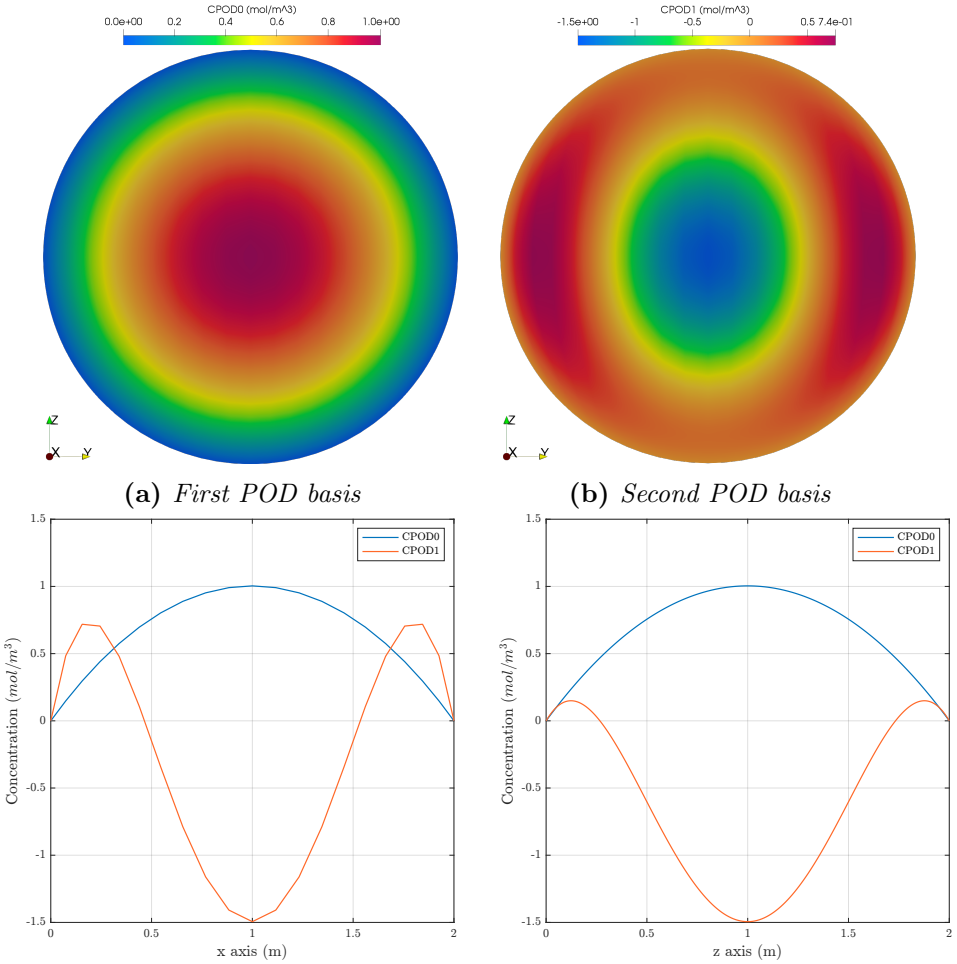

(a) *First POD basis*

(b) *Second POD basis*

(c) *Concentration trend along the x axis for the two POD bases*

(d) *Concentration trend along the z axis for the two POD bases*

Figure 2.4. The POD bases resulting from the POD-FV-ROM implementation in OpenFOAM.

diffusion, the anisotropy is revealed in the second POD basis indeed the trend of the second eigenfunction change from the $x - y$ axis to the z axis.

For the purpose of modelling intra-granular fission gas release, the figure of merit is the average concentration. Therefore are necessary the weighted volume average of the two set of bases:

$$\bar{\phi}_i = \begin{bmatrix} 0.4179 \\ 0.1861 \end{bmatrix} \tag{2.17}$$

In this way, in the implementation of the online phase in SCIANTIX (Section 2.5) will be performed the calculation expressed by Equation 2.19.

2.5 Implementation of the algorithm in SCIANTIX

The ODE system (Equation 2.15) was solved by means the same iterative procedure of the previous chapter based on Backward Euler Scheme implemented in SCIANTIX:

$$\begin{bmatrix} a_1^{i+1} \\ a_2^{i+1} \end{bmatrix} = \left(I - \frac{D_{Xe}^{aa}}{R^2} \Delta t \mathbf{E} \right)^{-1} \begin{bmatrix} a_1^i + S\Delta t F_1 \\ a_2^i + S\Delta t F_2 \end{bmatrix} \tag{2.18}$$

and also the reconstruction of the volume weighted average concentration along time is the same:

$$\bar{c}(\mathbf{x}, t) \approx \sum_{i=1}^{N_c} a_i(t) \bar{\phi}_i(\mathbf{x}) \tag{2.19}$$

2.6 Verification via comparison with High Fidelity

The only verification that has been performed for this anisotropic diffusion case was to compare the solution obtained from the SCIANTIX code with the high-fidelity solution. In Figure 2.5 is possible to see the comparison between this two results and in Figure 2.6 is represented the corresponding relative error along time. The initial relative error stands at 6% and reaches 1.7% at equilibrium. Referring to the uncertainty analysis on the parameters seen in Section 1.6.1 is possible conclude that the reduced order model reproduces with good accuracy the solution relative to the FOM unless a negligible error, comparable to the uncertainty on the parameters.

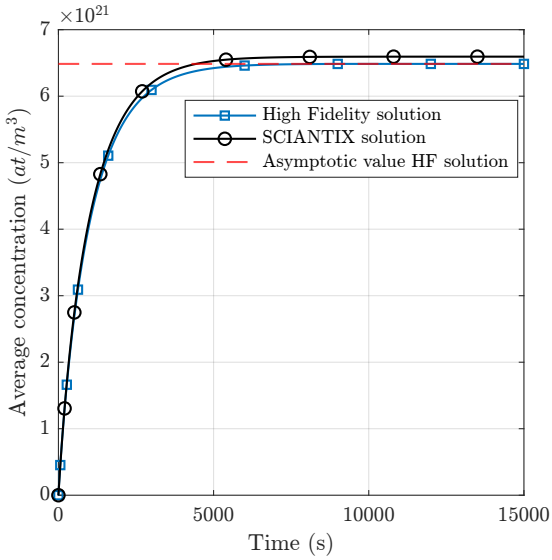

Figure 2.5. Comparison between the SCIANTIX solution and the high fidelity solution in terms of average concentration. The red dashed line identify the asymptotic value of the high fidelity solution.

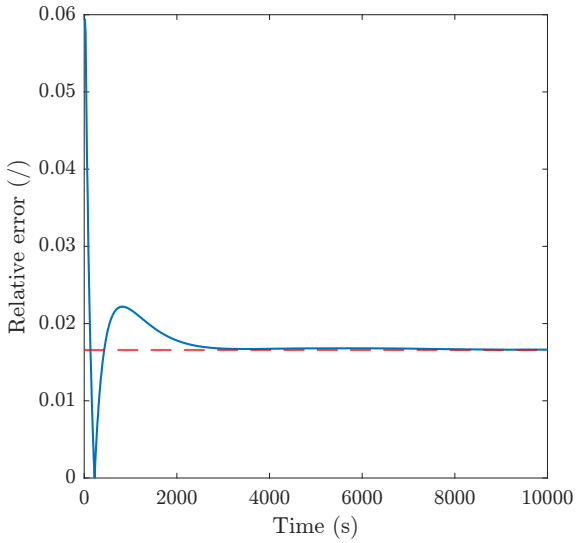

Figure 2.6. The relative error u between the SCIANTIX solution and the high fidelity solution along time. The red dashed line identify the final value.

The implementation of the online phase in OpenFOAM, as explained in Section 1.6.1,

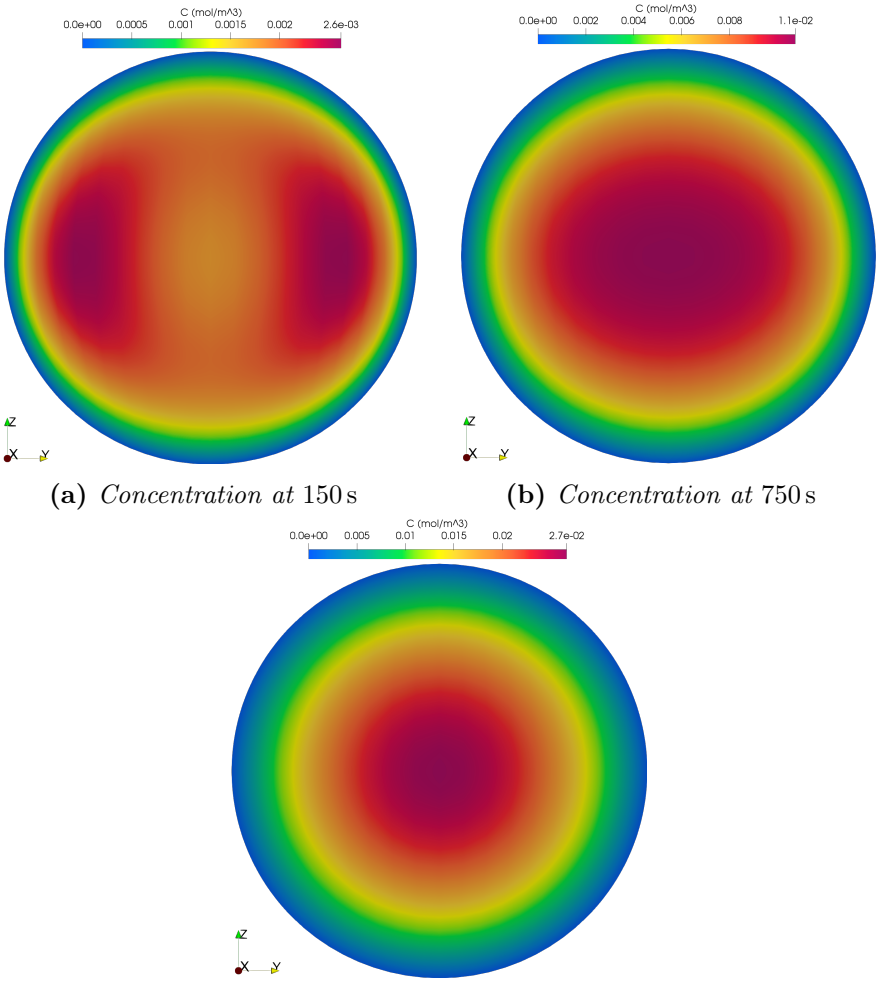

(a) *Concentration at* 150 s **(b)** *Concentration at* 750 s

(c) *Concentration at* 7500 s

Figure 2.7. Reconstruction of the spatial distribution of the concentration field.

made it possible to reconstruct the entire spatial distribution of the concentration field (Figure 2.7). Comparing the distributions in Figure 2.2 and the distributions in the Figure 2.7, can be seen that the error decreases as the time step advances both in terms of the spatially assumed values and in terms of the maximum concentration value reported on the color map, as found in the Section 1.6.1. The trend of the error over time is in complete agreement with the Figure 2.6. As can be seen, the anisotropic behavior of the diffusion is clearly visible in Figure 2.7b therefore the ROM procedure and the strategy adopted have made possible to preserve the main characteristics of the phenomenon.

2.7 Closing remarks

In this Chapter, the POD-FV-ROM technique for the diffusion problem of fission gas in uranium silicide fuel spherical grains was developed. The intent of this chapter was to highlight the strategy that should be adopted in the event that a slightly more complex problem is interfaced with respect to the one seen in previous Chapter in which the additional degree of complexity is the anisotropy of the problem. Not many conclusions can be drawn given the limited verification phase which allows to conclude only that the reduced order model reproduces the high fidelity solution with good accuracy.

In order to learn more about the accuracy of the model one should extend the algorithm verification phase by testing it in non-physical situations through the MMS and comparing it with the state-of-art algorithms. For this last verification, given that FORMAS and ANS-5.4 have been implemented to solve isotropic diffusion problem, will not be possible to use the tensor form but will be necessary to adopt only one of the components of the diffusion tensor. Being forced to adopt only one direction at a time, the result obtained with FORMAS and ANS-5.4 will certainly not be comparable with that obtained with the reduction algorithm but will allow the definition of an upper and lower bound: if the diffusion in the grain were to take place according to the coefficient D_{Xe}^{aa}, whose value is smaller than D_{Xe}^{cc}, there would be more gas in the grain, with respect to the reduction algorithm, and therefore the value correspond to the upper bound, on the contrary with D_{Xe}^{cc} a lower bound would be obtained given the lower concentration of gas in the grain.

The strategy developed in this chapter will be useful in the next one where an anisotropic diffusive problem will still be faced. The anisotropy that will be encountered in the next chapter will no longer be dictated by the crystalline structure of the fuel but by the geometry of the grain which will no longer be spherical but cylindrical. In this way it will be possible to verify further that the strategy developed works correctly even in slightly different situations.

Chapter 3

Reduced order model of fission gas diffusion in MOX fuel cylindrical grains

Abstract

In the previous two chapters, the attention was focused on developing a reduced order model for diffusion problem in a spherical grain. In mixed oxide fuels adopted in fast reactors not only spherical but also cylindrical grains are formed due to the restructuring process. For this type of grains it is no longer possible to adopt the hypothesis of spherical grain and uniform temperature along the grain defined by Booth [10] making the diffusion problem highly non-linear with consequent impossibility of finding the solution within a fuel performance code. In order to introduce a treatment of diffusion in columnar grains suitable for application in fuel performance codes and reduce the computational cost of simulations, in this chapter the aim is to extend what has been done in the previous chapters to cylindrical grains. The added degree of complexity is not only the intrinsic anisotropy of the problem, encountered in the previous chapter, but also the non-linearity.

3.1 Intra-granular fission gas behaviour

MOX fuels are candidate fuels for fast reactors of Generation IV given their: proven burn up >25 at%, good stability and behaviour under irradiation up to very high burn-ups (20 at%), industrial scale fabrication, high thermal creep (this means low mechanical interaction with cladding and so negligible PCMI), low thermal conductivity compensated by high melting temperature (high margin to melt), compatibility with stainless steel cladding and, compared to metal fuel, lower fuel swelling under irradiation (pin design easier) [67]. The temperature conditions reached in fast reactors lead to the need to investigate and model the new, or more accentuated, processes that occur in the fuel compared to the phenomena normally encountered in the fuel for light water thermal reactors [68].

In LWR fuels under nominal conditions the center temperature ($\sim 1000\,^{\circ}\mathrm{C}$) is too low to induce strong change in the oxide fuel microstructure, however the severe

operating conditions in FRs fuel elements cause a recrystallization of the $(U, Pu)\,O_2$ fuel at the beginning of the irradiation, during the first hours and days at full power. This phenomenon of recrystallization is called restructuring and involves changes in the porosity and density of the fuel as well as in the morphology of the grains (we start from a grain size of ≈ 10 μm and with a $95\% - 88\%$ of theoretical density from the sintering process of the fuel) and is governed only by the fuel pellet temperature [69].

Since in fast reactors the alterations of morphology of the fuel are more relevant, they cause restructuring of the $(U, Pu)\,O_2$ fuel to form four distinct microstructural regions at linear heat generation rates of 40 kW m^{-1} and above. The innermost region is a central void that results from the transport of as-fabricated porosity (and some of the fuel-cladding gap) up the temperature gradient to the fuel center. The fuel surrounding this void consists of dense ($>$ 98% Theoretical Density (TD)) grains that are elongated radially (length $>$1mm) and for their shape are called columnar grains. These grains form from lenticular pores that move inwards by fuel vaporizing from the hotter (inner) side of the voids and condensing on the cooler (outer) side, giving a net outward movement of fuel (Figs. 3.1 and 3.2). The fabricated pores are spherical but when dealing with high temperature gradients they move across the temperature gradient taking on a half-moon shape, hence the name of lenticular pores, with a thickness of $\sim 5 \div 10$ μm and a diameter of $50 \div 100$ μm. The velocity of the voids increases exponentially with temperature and approaches 10^{-3} mm s^{-1} at circa 2200 °C, causing columnar grains to form in the first few hours of full power operation of an element, with a limit to such grain growth delineated by an isotherm near 1700 °C. Outward of the columnar grains is a region where temperatures are sufficiently high for grain growth to take place by bulk diffusion and for some biased movement of voids and inclusions also to occur up the temperature gradient by surface diffusion. The enlarged fuel grains in this region, although normally termed "equiaxed", are slightly elongated in the direction of the temperature gradient, with their boundaries invariably decorated with gas bubbles and fission product inclusions. This equiaxed grains reach a value of TD corresponding to 95-97% and ≈ 20 μm of grain size but the porosity does not move enough to guarantee the formation of columnar grains. The driving force behind the growth of the grains is the minimization of surface tension. The 3D geometric shape that minimizes surface tension is the sphere, this is why the equiaxial grains are spherical. The fuel between the equiaxed grain growth region and the cladding retains its original microstructure and density and is simply labeled the unrestructured region. Fuel in this region operates at temperatures below about 1600°C where mobilities are low and where, therefore, the fuel tends to retain most of its original characteristics. However, radiation does enhance bulk diffusion and creep rates in this region so that limited hot pressing and oxygen redistribution may take place [70]. In summary, moving from the outside to the inside of the fuel pellet, we have (Fig. 3.3):

- Unrestructured zone (T<1600 °C): an external as-fabricated zone with unchanged density ($95\% - 88\%$ of theoretical density);
- Equiaxed grains zone (1600 °C<T<1800 °C): an intermediate zone with equiaxed grains (spherical grain) with higher density and grain size of around ≈ 20 μm;
- Columnar grain zone (T>1800 °C): an internal zone with columnar grains

oriented in the radial direction with almost theoretical density, length of approximately 1mm and radius of $10 \div 20\mu$m;

- Central void.

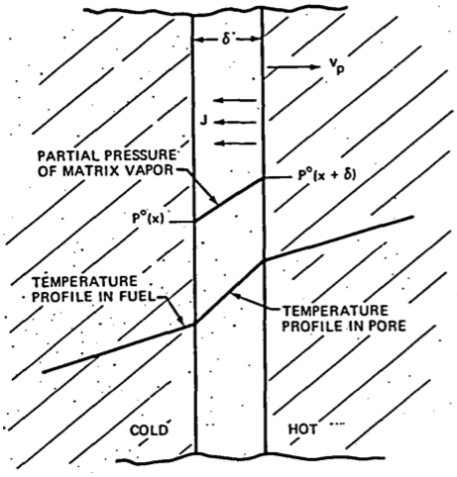

Figure 3.1. A Lenticular pore in solid fuel is characterized by a temperature gradient consequently the pressure of the fuel vapor on the hot face is much greater than the vapor pressure on the cold face. This difference in vapor pressure induces an *evaporation-condensation* mechanism: the matter that evaporates from the hot face and condenses on the cold face travels down the thermal gradient (and so towards the outside of the pellet), inducing a reverse shift of the pores lenticulars that go up the thermal gradient towards the center of the pellet. Moving towards the center of the pellet, the lenticular pores destroy the microstructure of the initial fuel and leave the columnar grains behind them [27].

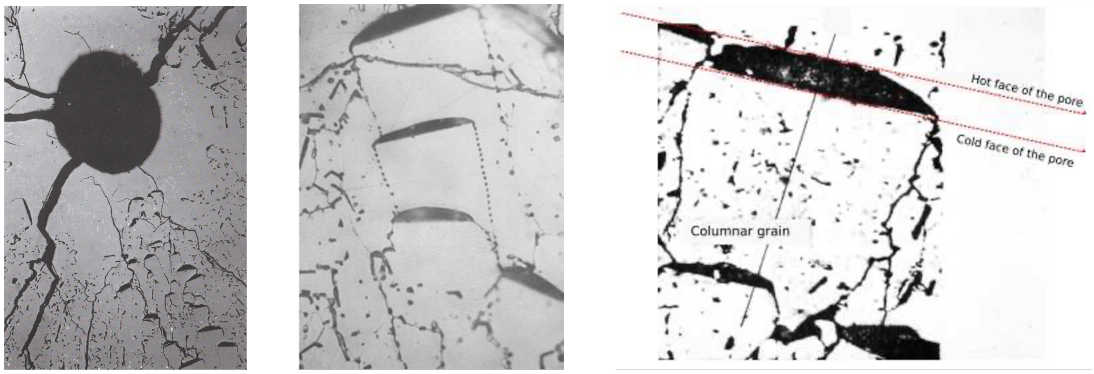

Figure 3.2. Close-up of lenticular pores move towards central void via evaporation-condensation mechanism.

In chapter 1 and 2 we have seen that the classical description of fission gas behaviour diffusion adopted in fuel performance codes relies on the model by Booth [10]. The assumption of spherical grains in Equation 1.10, hinders a priori the application of this diffusion description to columnar grains. It is common in fuel performance codes, however, to model diffusion in the columnar grain zone as if the grain were spherical, eventually considering a specific spherical radius representative of cylindrical geometry.

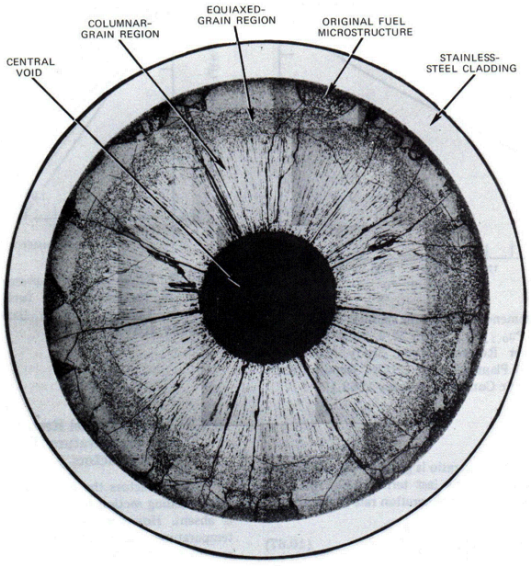

Figure 3.3. Cross section of an irradiated mixed oxide fuel rod from a FR. Is possibile to se the the different regions formed as a result of the restructuring process [27].

On the one hand, this modelling approach is partially justified by the high fission gas release expected (not to mention the large uncertainty pertaining to the diffusion coefficient), which makes the modelling simplification less impactful. On the other hand, treating columnar grains according to Equation 1.10 implies two degrees of simplification which should be taken into consideration:

- The dynamics of diffusion are different in a sphere and in a cylinder and cannot be set equal by the selection only of a representative spherical grain radius;
- Given the temperature dependence of the diffusion coefficient and the temperature profile in the columnar zone, the use of a single value of the diffusion coefficient outside of the Laplacian is inaccurate.

To demonstrate the different diffusion dynamics in a sphere and in a cylinder, we can consider the eigenfunctions of the radial component of the Laplacian in spherical and cylindrical coordinates, i.e., cardinal sines and the J_0 Bessel function, respectively. The corresponding eigenvalues are for the sphere

$$\lambda_n^2 = n^2\pi^2\frac{D_{\text{eff}}}{R_s^2} \tag{3.1}$$

And for cylinder

$$\alpha_n^2 = z_n^2\frac{D_{\text{eff}}}{R_c^2} \tag{3.2}$$

Where, the index n stands for the mode, i.e., the eigenfunction, $R_s(m)$ is the spherical grain radius and $R_c(m)$ is the radius of the columnar grain, and z_n are the zeros of the J_0 Bessel function. By equating the eigenvalues in Equations 3.1 and 3.2 the relation between R_s and R_c depends on n

$$n^2\pi^2\frac{D_{\text{eff}}}{R_s^2} = z_n^2\frac{D_{\text{eff}}}{R_c^2} \tag{3.3}$$

from which

$$R_c^2 = \frac{z_n^2}{n^2\pi^2} R_s^2 \tag{3.4}$$

and hence the use of a spherical Laplacian with a representative grain radius fails as a surrogate of the dynamics of diffusion in a cylindrical grain. In order to properly consider the temperature profile along the columnar grain, we should write the diffusion problem as:

$$\frac{\partial}{\partial t} c_t(r,z,t) = \frac{1}{r}\frac{\partial}{\partial r}\left(D_{\text{eff}}\left(T(z)\right) r \frac{\partial}{\partial r} c_t(r,z,t)\right) + \frac{\partial}{\partial z}\left(D_{\text{eff}}\left(T(z)\right) \frac{\partial}{\partial z} c_t(r,z,t)\right) + S \tag{3.5}$$

where z (m) is the coordinate along the axis of the cylindrical grain (i.e., along the radius of the pellet), r (m) is the coordinate along the radius of the cylindrical grain, T (K) is temperature and now the effective diffusion coefficient D_{eff} is temperature dependent. For this reason, the Equation 3.5 is highly non-linear and its solution within a fuel performance code is impractical. Even if the conclusion in Equation 3.4 is achieved neglecting the diffusion along the columnar grain axis, it should be noted that neglecting the diffusion of gas in this direction is a non-conservative hypothesis. The diffusion coefficient is higher in the inner part of the pellet (higher temperature) and decreases moving outside along the columnar grain axis, hence the gas concentration diffuses (towards the lateral surface of the grain) more in the inner part than in the outer part. This creates a concentration gradient along the z axis of the grain (opposite to the temperature gradient) and consequently a flux of gas moving towards the inner part of the grain. This transport of gas implies a higher release since it is directed towards the part of the columnar grain with higher diffusivity. The physical problem of gas diffusion through the columnar grains is mathematically described by a system of coupled PDEs, one for the temperature and the other one for the gas concentration. These PDEs in cylindrical coordinate are:

$$\begin{cases} \dfrac{\partial}{\partial t} T(z,t) = \dfrac{1}{r}\dfrac{\partial}{\partial r}\alpha\left(T(z,t) r \dfrac{\partial}{\partial r} T(z,t)\right) + \dfrac{\partial}{\partial z}\alpha\left(T(z,t)\dfrac{\partial}{\partial z} T(z,t)\right) + Q \\ \dfrac{\partial}{\partial t} c_t(r,z,t) = \dfrac{1}{r}\dfrac{\partial}{\partial r}\left(D_{\text{eff}}\left(T(z)\right) r \dfrac{\partial}{\partial r} c_t(r,z,t)\right) + \dfrac{\partial}{\partial z}\left(D_{\text{eff}}\left(T(z)\right) \dfrac{\partial}{\partial z} c_t(r,z,t)\right) + S \end{cases} \tag{3.6}$$

where α ($\text{m}^2\ \text{s}^{-1}$) is the thermal diffusivity which is in turn given by the thermal conductivity, k, divided by the density, ρ, and the specific heat, c_p, and Q ($\text{K}\ \text{s}^{-1}$) is the heat generation rate which is in turn given by the fission rate $\dot{F}$ ($\text{fiss}\ \text{s}^{-1}$) multiplied by fission heat q ($\text{K}\ \text{fiss}^{-1}$). The fission heat q is given by the ratio between the power density, the density and the specific heat ($q'''/\rho\ c_p$).

For concentration problem was assumed grain boundaries as perfect sinks which results in a boundary condition of Dirichlet type and null initial condition, as in chapter 1 and chapter 2. Consequently $c_t(r,z,t)$ satisfy the following well-posed

problem:

$$\begin{cases} \dfrac{\partial}{\partial t}c_t(r,z,t) = \dfrac{1}{r}\dfrac{\partial}{\partial r}\left(D_{\text{eff}}\left(T(z)\right) r \dfrac{\partial}{\partial r}c_t(r,z,t)\right) + \\ \qquad\qquad + \dfrac{\partial}{\partial z}\left(D_{\text{eff}}\left(T(z)\right)\dfrac{\partial}{\partial z}c_t(r,z,t)\right) + S \\ c_t(r,z,0) = 0 \qquad\qquad 0 < r < R, 0 < z < L \\ c_t(r,z,t) = 0 \qquad\qquad \text{on } \partial\Omega, t > 0 \end{cases} \tag{3.7}$$

where R is the radius of the cylindrical grain and L is the length of the cylindrical grain. For what concern temperature problem was set an initial condition of 2000 K, a Dirichlet BC of 2000 K on one of the cylinder bases, γ_1, and a null Neumann BC on the other basis, γ_2, and on the lateral surface, γ_3 (Figure 3.4). Consequently $T(z,t)$ satisfy the following well-posed problem:

$$\begin{cases} \dfrac{\partial}{\partial t}T(z,t) = \dfrac{1}{r}\dfrac{\partial}{\partial r}\alpha\left(T(z,t) r \dfrac{\partial}{\partial r}T(z,t)\right) + \\ \qquad\qquad + \dfrac{\partial}{\partial z}\alpha\left(T(z,t)\dfrac{\partial}{\partial z}T(z,t)\right) + Q \\ T(z,0) = 2000K \qquad\qquad 0 < z < L \\ T(z,t) = 2000K \qquad\qquad \text{on } \gamma_1, t > 0 \\ \left(\dfrac{\partial}{\partial r}T(z,t) + \dfrac{\partial}{\partial z}T(z,t)\right)\cdot \mathbf{n} = 0 \qquad\qquad \text{on } \gamma_2, \gamma_3, t > 0 \end{cases} \tag{3.8}$$

The null Neumann boundary condition applied to temperature means, from the physical point of view, null heat flux in correspondence of γ_2 and γ_3.

These equations will be implemented in OpenFOAM in order to solve the diffusion problem under constant conditions, i.e. the source term S and the heat generation rate Q are assumed as constant in time and uniform in space.

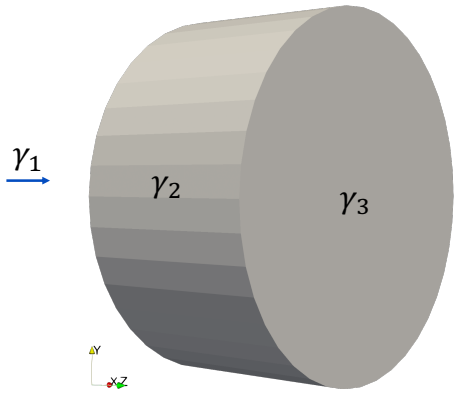

Figure 3.4. The cylindrical dimensionless mesh used in OpenFOAM.

3.2 Implementation of the Full Order Model

In this section the high fidelity-full order simulation of the partial differential equations 3.6 is implemented in OpenFOAM® environment.

For the sake of simplicity in the implementation the equations solved in OpenFOAM doesn't consider the quasi-stationary term, i.e. $b/(b+g)$, as was done in Section 1.2 and explained in Section 1.3. The anisotropy of the problem has been exploited through the tensor representation of the Turnbull diffusion coefficient. Indeed, the terms of the diagonal matrix used in Equation 3.9 are divided by three different quantities in the code implemented in OpenFOAM. In particular, D_x and D_y have been divided by the squared length of the radius and D_z has been divided by the squared length of the height of the cylinder (Equations 3.10 and 3.11). The value of R and L are reported in Table 3.1.

$$\begin{bmatrix} D_x & 0 & 0 \\ 0 & D_y & 0 \\ 0 & 0 & D_z \end{bmatrix} \tag{3.9}$$

where

$$D_x = D_y = \frac{1}{R^2}\left(7.6 \times 10^{-10} e^{-35217/T} + 5.64 \times 10^{-25}\sqrt{\dot{F}} e^{-13840/T} + 2 \times 10^{-40}\dot{F}\right) \tag{3.10}$$

$$D_z = \frac{1}{L^2}\left(7.6 \times 10^{-10} e^{-35217/T} + 5.64 \times 10^{-25}\sqrt{\dot{F}} e^{-13840/T} + 2 \times 10^{-40}\dot{F}\right) \tag{3.11}$$

Since the cylindrical geometry is quite complex and given the temperature and radial dependencies, the two equations have been transformed into a dimensionless form:

$$\begin{cases} L^2\dfrac{\partial}{\partial t}T - L^2\dfrac{1}{\rho}\dfrac{\partial}{\partial\rho}\alpha\left(T(\xi)\right)\rho\dfrac{\partial}{\partial\rho}T - R^2\dfrac{\partial}{\partial\xi}\alpha\left(T(\xi)\right)\dfrac{\partial}{\partial\xi}T = L^2 Q \\ L^2\dfrac{\partial}{\partial t}c - L^2\dfrac{1}{\rho}\dfrac{\partial}{\partial\rho}\underline{\underline{D}}\left(T(\xi)\right)\rho\dfrac{\partial}{\partial\rho}c - R^2\dfrac{\partial}{\partial\xi}\underline{\underline{D}}\left(T(\xi)\right)\dfrac{\partial}{\partial\xi}c = L^2 S \end{cases} \tag{3.12}$$

where $\rho = r/R$ and $\xi = z/L$. Rewritten in generic form result[1]:

$$\begin{cases} L^2\dfrac{\partial T(\mathbf{x},t)}{\partial t} = \alpha\nabla^2 T(\mathbf{x},t) + L^2 Q \\ L^2\dfrac{\partial c}{\partial t} = L^2\nabla\cdot(\underline{\underline{D}}\nabla c) + L^2 S \end{cases} \tag{3.13}$$

This adimensionalization allows:

- The use of an dimensionless mesh make the code easier to use since it is not necessary to change the mesh as the geometry do;
- The inclusion of the anisotropy of the problem into the diffusion coefficient, i.e. in the algebraic model.

[1]To solve this diffusion problem has been added the temperature equation to the solver previously implemented in Section 1.2. In the header file *createFields.H* each field was defined as explained in Section 1.2.

Table 3.1. List of values and u.o.m adopted in the simulations

Symbol	Definition	Value	u.o.m (original)	u.o.m (simulation)
T	Temperature		K	K
c	Concentration		mol m^{-3}	-
R	Radius	1×10^{-5}	m	m
L	Length	1×10^{-3}	m	m
D	Diffusion coefficient	Turnbull	m^2 s^{-1}	s^{-1}
α	Thermal diffusivity	5×10^{-7}	m^2 s^{-1}	m^2 s^{-1}
$\dot{F}$	Fission rate	3×10^{19}	fiss $m^{-3}s^{-1}$	-
y_F	Fission yield	5×10^{-25}	mol $fiss^{-1}$	s^{-1}
q	Fission heat	7.27×10^{-18}	K $fiss^{-1}$	K s^{-1}
∇^2	Laplacian term		m^{-2}	-

Table 3.2. Parameters necessary to derive α and q.

Symbol	Definition	Value	u.o.m
ρ	Density	11 040	kg m^{-3}
c_p	Specific heat	400	J kg^{-1} K^{-1}
q'''	Power density	3.21×10^{-11}	W m^{-3}
k	Thermal conductivity	2.5	W m^{-1} K^{-1}

In this way it is possible to bring considerable advantages during the implementation. More precisely, dimensionless mesh means that the length of the radius and of the height of the cylinder have the same unitary value[2]. The non-dimensional 3D cylindrical mesh was implemented on GMSH, an open source 3D finite element mesh generator[3]. On the boundaries were set the boundary conditions defined in 3.8 and 3.7. The parameters adopted for the simulation are shown in Table 3.1.

The simulation was run for 1×10^7 s. this time was chosen on the basis of the time taken by the phenomenon to reach equilibrium which is in the order of:

$$\tau = \frac{R^2}{D} = 2.3 \times 10^6 \,\mathrm{s} \tag{3.14}$$

The computational time required by a intel Core i5-5300U CPU @ 2.30GHz and 8GB RAM was in the order of 5 minutes. The frequency of snapshot sampling was set to $0.333\,33 \times 10^{-4}$ Hz, therefore in the 1×10^7 s-simulation, 333 snapshots have been collected.

Since the z-direction of the columnar grains is oriented along the radius of the pellet, it is the direction of greatest interest to be analyzed because it allows to understand the redistribution of the fuel during the restructuring process. Consequently the results of the simulation for the temperature and concentration field were obtained

[2]Consequently in the *blockMeshDict* file, where the mesh parameters are defined, the conversion for the meters has been deleted and the value of the radius, together with the height of the cylinder have been set to one.

[3]the discretization of the mesh is characterized by different mesh blocks, defined in the `blocks` list present in the file *blockMeshDict*, so as to obtain a very fine mesh

by slicing the cylinder with a plane perpendicular to the x axis in order to highlight the behavior of the two fields along the z-direction (Figures 3.5 and 3.6). The gas concentration exhibits the longitudinal distribution effect, as mentioned in Section 3.1, with the maximum of the gas concentration in the outer part of the columnar grain (outer with the respect to the fuel pellet radius). Indeed the gas concentration diffuses more in the inner part, where the temperature value is lower, than in the outer part, where the temperature value is higher. This behavior is caused by the concentration gradient which originates along the z axis of the grain and which is responsible for the transfer of gas towards the inner, and hotter, part of the grain. This effect can be only obtained by solving the coupled partial differential equations considering the diffusion both along the grain axis and along the radial direction which is what is exactly done with OpenFOAM.

As expected the concentration field assumes a parabolic trend along the radial

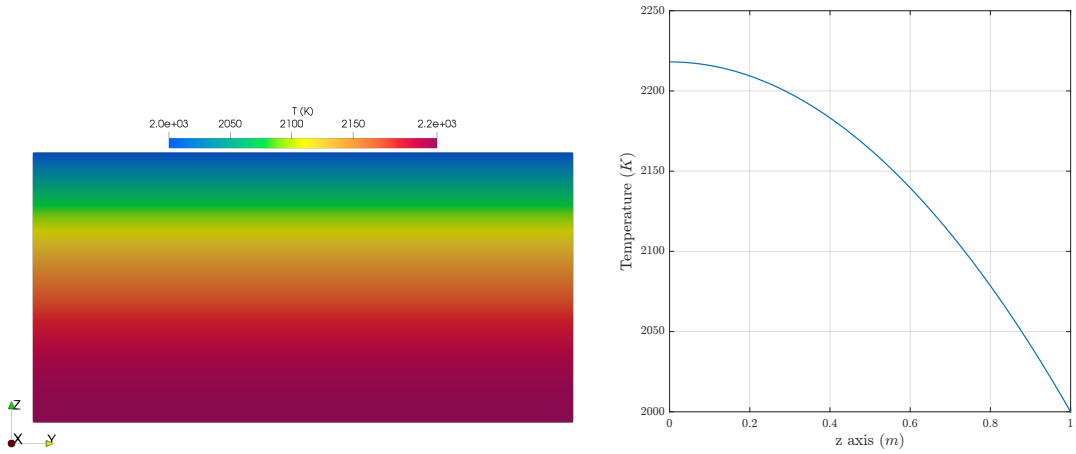

(a) *Temperature at* 1×10^7 s **(b)** *Temperature trend along the z axis*

Figure 3.5. In (a) is reported the temperature distribution resulting from the full order simulation implemented in OpenFOAM which is reached instantaneously. In (b) is reported the temperature trend along the z axis.

coordinate (Figure 3.6e) whereas along the longitudinal coordinate (Figure 3.6f) the trend depends on the longitudinal temperature trend (Figure 3.5b).

As in previous Chapters, the computed quantity of interest is the weighted volume average concentration along time which values are showcased in Figure 3.7.

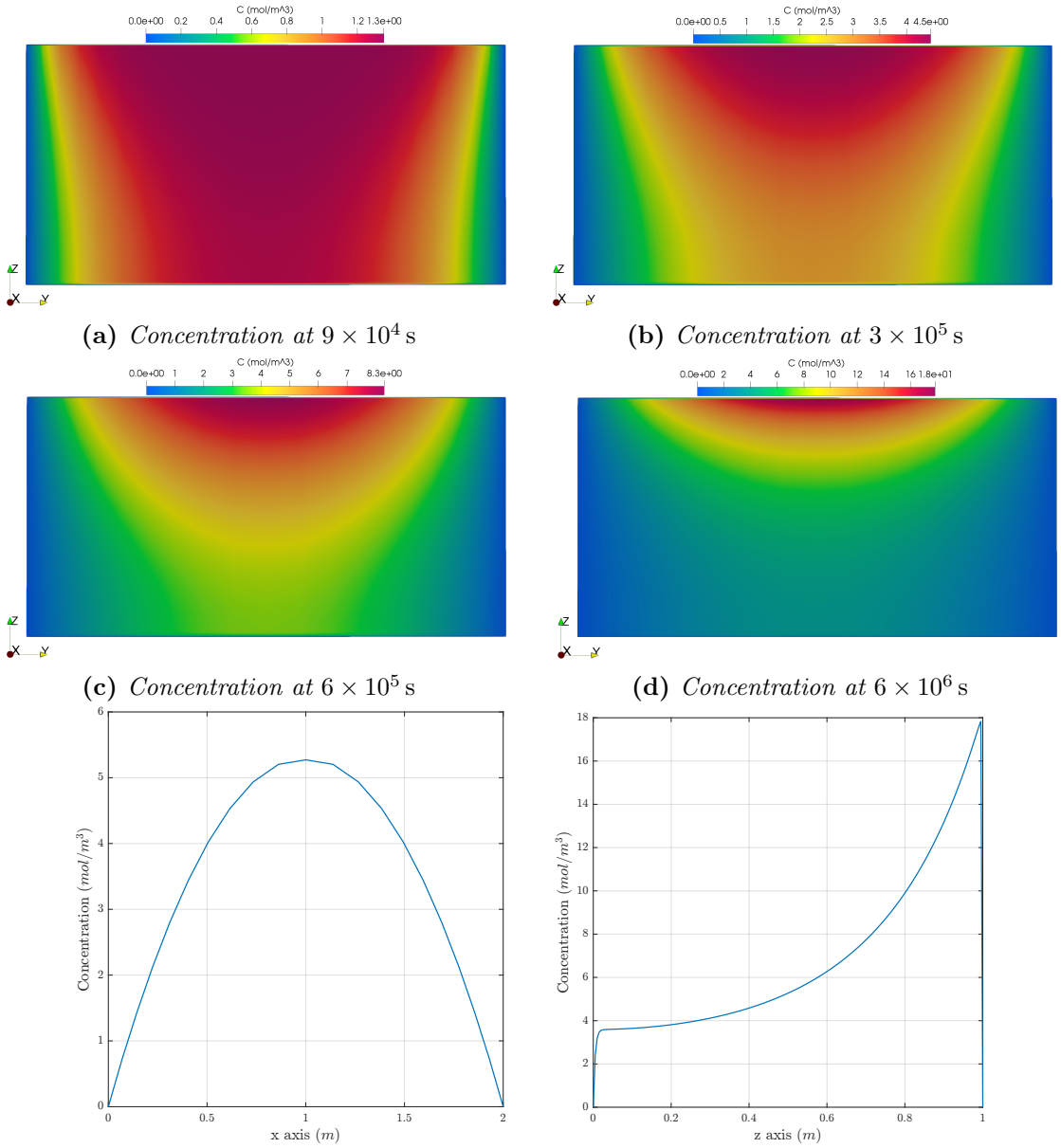

(a) *Concentration at* 9×10^4 s **(b)** *Concentration at* 3×10^5 s

(c) *Concentration at* 6×10^5 s **(d)** *Concentration at* 6×10^6 s

(e) *Concentration trend along the* x *axis* **(f)** *Concentration trend along the* z *axis*

Figure 3.6. In (a), (b), (c), (d) are reported the concentration distributions in correspondence of four time steps resulting from the full order simulation implemented in OpenFOAM. In (e) and (f) are reported the concentration trend respectively along the x and z axis.

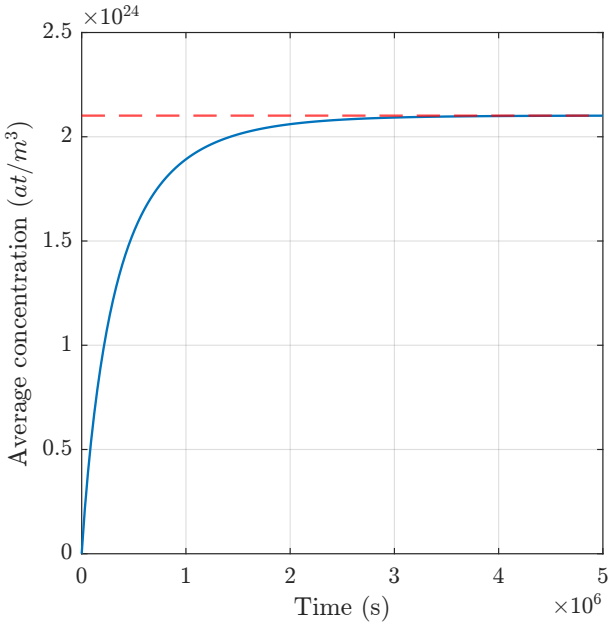

Figure 3.7. Average concentration along time, the red dashed line identify the equilibrium value reach by the OpenFOAM solution.

3.3 POD-FV-ROM of diffusion equation

In this section the POD technique procedure defined in sections 1.3 and 2.3 is applied directly to the problem of fission gas diffusion in columnar grains with the purpose of obtaining a POD-ROM of Equations 3.6 considering the Finite Volume approximation (POD-FV-ROM). Having to deal with a system of coupled PDEs, the first step is to express not only the concentration field but also the temperature field as linear combination of spatial modes, $\varphi_i(\mathbf{x})$ and $\phi_i(\mathbf{x})$, multiplied by temporal coefficients, $a_i(t)$ and $b_i(t)$:

$$T(\mathbf{x},t) \approx T_r(\mathbf{x},t) = \sum_{i=1}^{N_T} a_i(t)\varphi_i(\mathbf{x}) \tag{3.15}$$

$$c(\mathbf{x},t) \approx c_r(\mathbf{x},t) = \sum_{i=1}^{N_c} b_i(t)\phi_i(\mathbf{x}) \tag{3.16}$$

where N_T and N_c are the number of bases adopted respectively for temperature and concentration field. It is not possible to expand in series of orthogonal modes also the diffusion coefficient because it's equation is not affine consequently another strategy has been adopted which, as will be seen later, consists in its linearization.

In order to expand in series of orthogonal modes temperature and concentration two set of basis functions, $\{\varphi_i(\mathbf{x})\}_{i=1}^{N_T}$ and $\{\phi_i(\mathbf{x})\}_{i=1}^{N_c}$, are used for temperature and concentration. consequently the subspaces are two, given by the span of the sets of basis functions introduced for temperature and concentration

$$X_T^{POD} = \text{span}\{\varphi_1, \varphi_2, ..., \varphi_{N_c}\} \tag{3.17}$$

$$X_c^{POD} = \text{span}\{\phi_1, \phi_2, ..., \phi_{N_c}\} \tag{3.18}$$

Being the member of each set of basis functions orthogonal one to each other, they can be normalized in order to obtain

$$\langle \varphi_i(\mathbf{x}), \varphi_j(\mathbf{x}) \rangle_{L^2} = \delta_{ij} \tag{3.19}$$

$$\langle \phi_i(\mathbf{x}), \phi_j(\mathbf{x}) \rangle_{L^2} = \delta_{ij} \tag{3.20}$$

The snapshots of each field are then collected for N_s time instants

$$T_n = T(\mathbf{x}, t_n) = 1, ..., N_s \tag{3.21}$$

$$c_n = c(\mathbf{x}, t_n) = 1, ..., N_s \tag{3.22}$$

Minimizing the L^2 norm of the difference between the snapshots and their projection in the subspace, the basis sets can be defined.

$$X_T^{POD} = \arg\min \frac{1}{N_s} \sum_{n=1}^{N_s} \left\| T_n - \sum_{i=1}^{N_T} \langle T_n, \varphi_i(\mathbf{x}) \rangle \varphi_i(\mathbf{x}) \right\|_{L^2}^2 \tag{3.23}$$

$$X_c^{POD} = \arg\min \frac{1}{N_s} \sum_{n=1}^{N_s} \left\| c_n - \sum_{i=1}^{N_c} \langle c_n, \phi_i(\mathbf{x}) \rangle \phi_i(\mathbf{x}) \right\|_{L^2}^2 \tag{3.24}$$

Such sets are computed through the same procedure based on the correlation matrices of Section 1.3 which consist in considered the following eigenvalue-eigenvector problem:

$$E\boldsymbol{\xi}_i = \lambda_i \boldsymbol{\xi}_i \quad i = 1, ..., N_s \tag{3.25}$$

$$K\boldsymbol{\chi}_j = k_j \boldsymbol{\chi}_j \quad j = 1, ..., N_s \tag{3.26}$$

where λ_i and k_j are the eigenvelues, $\boldsymbol{\xi}_j$ and $\boldsymbol{\chi}_j$ are the eigenvectors and $E \in \mathbb{R}^{N_s \times N_s}$ and $K \in \mathbb{R}^{N_s \times N_s}$ are the correlation matrices whose components are calculated as follows:

$$[E]_{jk} = \frac{1}{N_T} \langle T_j(\mathbf{x}), T_k(\mathbf{x}) \rangle_{L^2} \tag{3.27}$$

$$[K]_{ml} = \frac{1}{N_c} \langle c_m(\mathbf{x}), c_l(\mathbf{x}) \rangle_{L^2} \tag{3.28}$$

where $T_j(\mathbf{x}) = T(t_j, \mathbf{x})$ and $T_k(\mathbf{x}) = T(t_k, \mathbf{x})$ are the j-th and k-th temperature snapshots while $c_m(\mathbf{x}) = c(t_m, \mathbf{x})$ and $c_l(\mathbf{x}) = c(t_l, \mathbf{x})$ are the m-th and l-th concentration snapshots. The $\left(\lambda_j, \boldsymbol{\xi}_j\right)$ and $\left(k_j, \boldsymbol{\chi}_j\right)$ eigenvalue–eigenvector pairs are used to build the basis modes as:

$$\varphi_i(\mathbf{x}) = \frac{1}{\sqrt{\lambda_i}} \sum_{n=1}^{N_s} \xi_{i,n} T_n(\mathbf{x}) \quad i = 1, ..., N_T \tag{3.29}$$

$$\phi_i(\mathbf{x}) = \frac{1}{\sqrt{k_i}} \sum_{n=1}^{N_s} \chi_{i,n} c_n(\mathbf{x}) \quad i = 1, ..., N_c \tag{3.30}$$

Let us first consider the equation of temperature and then that of concentration

Temperature

Replacing the temperature T with T_r (Equation 3.15) in the first Equation of the system 3.13 we obtain:

$$L^2 \sum_{n=1}^{N_T} \varphi_i(\mathbf{x}) \frac{\partial a_i(t)}{\partial t} = \alpha \sum_{n=1}^{N_T} a_i(t) \nabla^2 \varphi_i(\mathbf{x}) + L^2 Q \tag{3.31}$$

Applying the Galerkin projection over the test functions $\varphi_j(\mathbf{x})$

$$\begin{aligned} L^2 \sum_{i=1}^{N_T} \frac{\partial a_j(t)}{\partial t} \int_\Omega \varphi_j(\mathbf{x}) \cdot \varphi_i(\mathbf{x}) d\Omega = \alpha \sum_{n=1}^{N_T} a_i(t) \int_\Omega \varphi_j(\mathbf{x}) \cdot \nabla^2 \varphi_i(\mathbf{x}) d\Omega + \\ + L^2 Q \int_\Omega \varphi_j(\mathbf{x}) d\Omega \quad j = 1, ..., N_T \end{aligned} \tag{3.32}$$

where Ω is the spatial domain. Being the members of each set of basis functions orthonormal one to each other (Eq. 3.20), the integration on the left hand side brings to a unitary term:

$$L^2 \frac{da_j(t)}{dt} = \alpha \sum_{n=1}^{N_T} a_i(t) \int_\Omega \varphi_j(\mathbf{x}) \cdot \nabla^2 \varphi_i(\mathbf{x}) d\Omega + L^2 Q \int_\Omega \varphi_j(\mathbf{x}) d\Omega \quad j = 1, ..., N_T \tag{3.33}$$

Rewriting the equation in matrix terms and dividing everything by L^2, the following POD-Galerkin ROM (POD-G-ROM) for Finite Volume discretization (POD-FV-ROM) is obtained

$$\frac{da_j(t)}{dt} = \frac{\alpha}{L^2} \sum_{n=1}^{N_T} H_{ji} a_i(t) + Q L_j \quad j = 1, ..., N_T \tag{3.34}$$

where:

$$H_{ji} = \langle \varphi_j(\mathbf{x}), \nabla^2 \varphi_i(\mathbf{x}) \rangle_{L^2} \tag{3.35}$$

$$L_j = \langle \varphi_j(\mathbf{x}) \rangle_{L^2} \tag{3.36}$$

The ODE system can be written as Equations 1.31 and 2.15

$$\dot{\mathbf{a}} = \frac{\alpha}{L^2} \mathbf{a}\mathbf{H} + Q\mathbf{L} \tag{3.37}$$

The boundary conditions might as well be enforced explicitly through the use of the Penalty Method, originally developed for Dirichlet BCs in [71]. In this case it is not necessary to extend the penalty method to Neumann BCs being this condition null, a discussion on the application of the penalty method to Neumann BCs can be found in [72]. Given γ_1 the portion of the domain on which the Dirichlet BC is applied to the temperature:

$$T(\mathbf{x} \in \gamma_1, t) = T_{BC} \tag{3.38}$$

Let Γ_1 the function that is null everywhere except on γ_1 (Equation 3.40) and let τ_T the Penalty factor, one can then enforce the boundary condition T_{BC} in the PDE as follows:

$$L^2 \frac{\partial T(\mathbf{x}, t)}{\partial t} = \alpha \nabla^2 T(\mathbf{x}, t) + L^2 Q + \tau_T \Gamma_1 (T - T_{BC}) \tag{3.39}$$

with

$$\Gamma_1 = \begin{cases} \neq 0 & \delta\Omega \\ = 0 & \forall\Omega \end{cases} \tag{3.40}$$

Consequently, the field is substituted by his approximated expansion and the Galerkin projections is performed, leading to the new integral:

$$-\tau_T \int_{\gamma_1} \varphi_j(\mathbf{x}) \left(T_{BC} - \sum_{i=1}^{N_T} a_i(t)\varphi_i(\mathbf{x}) \right) d\gamma_1 \tag{3.41}$$

which from a volume integral reduces to a surface integral due to the Γ_1 characteristic (Equation 3.40). Finally, the POD-Galerkin ROM (POD-G-ROM) for Finite Volume discretization (POD-FV-ROM) is:

$$\frac{da_j(t)}{dt} = \frac{\alpha}{L^2} \sum_{n=1}^{N_T} H_{ji} a_i(t) + QL_j + \frac{\tau_T}{L^2} \sum_{i=1}^{N_T} J_{ji} a_i(t) - \frac{\tau_T T_{BC}}{L^2} K_j \quad j = 1, ..., N_T \tag{3.42}$$

where:

$$J_{ji} = \langle \varphi_j(\mathbf{x}), \varphi_i(\mathbf{x}) \rangle_{L^2,\Gamma_1} \tag{3.43}$$

$$K_j = \langle \varphi_j(\mathbf{x}) \rangle_{L^2,\Gamma_1} \tag{3.44}$$

The ODE system can be rewritten as:

$$\dot{\mathbf{a}} = \frac{\alpha}{L^2}\mathbf{aH} + Q\mathbf{L} + \tau_T \left[\frac{1}{L^2}\mathbf{Ja} - \frac{T_{BC}}{L^2}\mathbf{K} \right] \tag{3.45}$$

Concentration

Before replacing the concentration c with c_r (Equation 3.16) in the second equation of the system 3.13 is necessary to rewrite this equation by separating the Turnbull's diffusion coefficient from the matrix containing the anisotropy of the problem

$$L^2 \frac{\partial c}{\partial t} = \nabla \cdot \left(D \frac{L^2}{R^2} \begin{bmatrix} 1 & 0 & 0 \\ 0 & 1 & 0 \\ 0 & 0 & \frac{R^2}{L^2} \end{bmatrix} \cdot \nabla c \right) + L^2 S \tag{3.46}$$

where

$$\underline{\underline{\mathrm{G}}} = \begin{bmatrix} 1 & 0 & 0 \\ 0 & 1 & 0 \\ 0 & 0 & \frac{R^2}{L^2} \end{bmatrix} \tag{3.47}$$

This approach will make things easier when implementing POD-FV-ROM on OpenFOAM. Now carrying out the replacement mentioned above we obtain

$$L^2 \sum_{i=1}^{N_C} \phi_i(\mathbf{x}) \frac{\partial b_i(t)}{\partial t} = \nabla \cdot \left(D \frac{L^2}{R^2} \underline{\underline{\mathrm{G}}} \cdot \sum_{i=1}^{N_C} \nabla \left(b_i(t)\phi_i(\mathbf{x}) \right) \right) + L^2 S \tag{3.48}$$

The dependence on temperature by the diffusion coefficient has been modeled by means of the linear relation:

$$D = D^0 + \alpha^D (T - T^0) \tag{3.49}$$

where D^0, T^0 and α^D are constant values. α^D is equal to the partial derivative of diffusion coefficient with respect to temperature obtained in correspondence of T^0. In this way we obtain

$$L^2 \sum_{i=1}^{N_C} \phi_i(\mathbf{x}) \frac{\partial b_i(t)}{\partial t} = \nabla \cdot \left(\left[D^0 + \alpha^D (T - T^0) \right] \frac{L^2}{R^2} \underline{\underline{\mathrm{G}}} \cdot \sum_{i=1}^{N_C} \nabla \left(b_i(t) \phi_i(\mathbf{x}) \right) \right) + L^2 S \tag{3.50}$$

Replacing the temperature T with T_r (Equation 3.15)

$$\begin{aligned} L^2 \sum_{i=1}^{N_C} \phi_i(\mathbf{x}) \frac{\partial b_i(t)}{\partial t} = \frac{L^2}{R^2} \left(D^0 - \alpha^D T^0 \right) \nabla \cdot \left[\underline{\underline{\mathrm{G}}} \cdot \sum_{i=1}^{N_C} \nabla \left(b_i(t) \phi_i(\mathbf{x}) \right) \right] + \\ + \frac{L^2}{R^2} \alpha^D \nabla \cdot \left[\underline{\underline{\mathrm{G}}} \cdot \sum_{k=1}^{N_T} a_k(t) \varphi_k(\mathbf{x}) \cdot \sum_{i=1}^{N_C} \nabla \left(b_i(t) \phi_i(\mathbf{x}) \right) \right] + L^2 S \end{aligned} \tag{3.51}$$

where the indexes i and j are related to concentration modes while the index k is related to temperature modes. Applying the Galerkin projection over the test functions $\phi_j(\mathbf{x})$

$$\begin{aligned} L^2 \frac{db_j(t)}{dt} = \frac{L^2}{R^2} \left(D^0 - \alpha^D T^0 \right) \int_\Omega \phi_j(\mathbf{x}) \nabla \cdot \left[\sum_{i=1}^{N_C} \underline{\underline{\mathrm{G}}} \cdot \nabla \left(b_i(t) \phi_i(\mathbf{x}) \right) \right] d\Omega + \\ + \frac{L^2}{R^2} \alpha^D \int_\Omega \phi_j(\mathbf{x}) \nabla \cdot \left[\sum_{k=1}^{N_T} a_k(t) \varphi_k(\mathbf{x}) \cdot \sum_{i=1}^{N_C} \underline{\underline{\mathrm{G}}} \cdot \nabla \left(b_i(t) \phi_i(\mathbf{x}) \right) \right] d\Omega + \\ + L^2 S \int_\Omega \phi_j(\mathbf{x}) d\Omega \quad j = 1, ..., N_c \end{aligned} \tag{3.52}$$

where the term on the left-hand side was written taking into account the orthonormality of basis functions one to each other (Equation 3.20). The second term on the right-hand side becomes

$$\begin{aligned} \frac{L^2}{R^2} \alpha^D \sum_{k=1}^{N_T} \sum_{i=1}^{N_C} a_k(t) b_i(t) \int_\Omega \phi_j(\mathbf{x}) \varphi_k(\mathbf{x}) \nabla \cdot \left[\underline{\underline{\mathrm{G}}} \nabla \phi_i(\mathbf{x}) \right] d\Omega + \\ + \frac{L^2}{R^2} \alpha^D \sum_{k=1}^{N_T} \sum_{i=1}^{N_C} a_k(t) b_i(t) \int_\Omega \phi_j(\mathbf{x}) \nabla \varphi_k(\mathbf{x}) \cdot \left[\underline{\underline{\mathrm{G}}} \nabla \phi_i(\mathbf{x}) \right] d\Omega \end{aligned} \tag{3.53}$$

The whole equation turns out

$$\begin{aligned} L^2\frac{db_j(t)}{dt} = \frac{L^2}{R^2}\left(D^0-\alpha^D T^0\right)\sum_{i=1}^{N_C} b_i(t)\int_\Omega \phi_j(\mathbf{x})\nabla\cdot\left[\underline{\underline{\mathrm{G}}}\nabla\phi_i(\mathbf{x})\right]d\Omega + \\ \frac{L^2}{R^2}\alpha^D\sum_{k=1}^{N_T}\sum_{i=1}^{N_C} a_k(t)b_i(t)\int_\Omega \phi_j(\mathbf{x})\varphi_k(\mathbf{x})\nabla\cdot\left[\underline{\underline{\mathrm{G}}}\nabla\phi_i(\mathbf{x})\right]d\Omega + \\ +\frac{L^2}{R^2}\alpha^D\sum_{k=1}^{N_T}\sum_{i=1}^{N_C} a_k(t)b_i(t)\int_\Omega \phi_j(\mathbf{x})\nabla\varphi_k(\mathbf{x})\cdot\left[\underline{\underline{\mathrm{G}}}\nabla\phi_i(\mathbf{x})\right]d\Omega + \\ +L^2 S\int_\Omega \phi_j(\mathbf{x})d\Omega \quad j=1,...,N_c \end{aligned} \tag{3.54}$$

Rewriting the equation in matrix terms and dividing everything by L^2, the following POD-FV-ROM is obtained

$$\begin{aligned} \frac{db_j(t)}{dt} = \frac{1}{R^2}\left(D^0-\alpha^D T^0\right)\sum_{i=1}^{N_C} b_i(t)X_{ij} + \frac{1}{R^2}\alpha^D\sum_{k=1}^{N_T}\sum_{i=1}^{N_C} a_k(t)b_i(t)M_{jki} + \\ +\frac{1}{R^2}\alpha^D\underline{\underline{\mathrm{G}}}\sum_{k=1}^{N_T}\sum_{i=1}^{N_C} a_k(t)b_i(t)N_{jki} + SP_j \quad j=1,...,N_c \end{aligned} \tag{3.55}$$

Where:

$$X_{ji} = \langle\phi_j(\mathbf{x}), \nabla\cdot\left[\underline{\underline{\mathrm{G}}}\nabla\phi_i(\mathbf{x})\right]\rangle_{L^2} \tag{3.56}$$

$$M_{jki} = \langle\phi_j(\mathbf{x}), \left(\varphi_k(\mathbf{x}), \nabla\cdot\left[\underline{\underline{\mathrm{G}}}\nabla\phi_i(\mathbf{x})\right]\right)\rangle_{L^2} \tag{3.57}$$

$$N_{jki} = \langle\phi_j(\mathbf{x}), \left[\nabla\varphi_k(\mathbf{x}), \underline{\underline{\mathrm{G}}}\nabla\phi_i(\mathbf{x})\right]\rangle_{L^2} \tag{3.58}$$

$$P_j = \langle\phi_j(\mathbf{x})\rangle_{L^2} \tag{3.59}$$

The ODE system can be written as:

$$\dot{\mathbf{b}} = \frac{1}{R^2}\left(D^0-\alpha^D T^0\right)\mathbf{bX} + \frac{1}{R^2}\alpha^D\mathbf{a}^T\mathbf{bM} + \frac{1}{R^2}\alpha^D\mathbf{a}^T\mathbf{bN} + S\mathbf{P} \tag{3.60}$$

where the T at apex indicates the transposition of the vector. The ODE systems 3.37 and 3.60 are then solved in SCIANTIX by means an implicit Euler scheme in order to derive the time coefficients and finally reconstruct the solutions (Section 3.5).

3.4 Implementation of the POD-FV-ROM

In this section the reduction of the model is implemented in OpenFOAM. The procedure follows the same steps defined in Section 2.4 with the difference that now we are dealing with a non-linear problem. In this case, to derive the matrices of the ODE system of concentration field (Equation 3.60) is first necessary to obtain the set of orthonormal modes related to the temperature field. Also in this case have been adopted 2 bases and an accuracy of 1.1 for both temperature and concentration fields. Therefore now the outcomes are the four set of orthonormal bases (Figures 3.8a, 3.8b, 3.8c and 3.8d) and the matrices:

$$\begin{aligned} \mathbf{H} &= \begin{bmatrix} -0.2031 & -1.0326 \times 10^{-8} \\ 5.1876 \times 10^{-6} & -4.9786 \times 10^{-12} \end{bmatrix} \quad \mathbf{L} = \begin{bmatrix} 1.7680 \\ 9.0465 \times 10^{-8} \end{bmatrix} \\ \mathbf{J} &= \begin{bmatrix} 0.8683 & 5.7155 \times 10^{-8} \\ 5.7155 \times 10^{-8} & 3.7623 \times 10^{-15} \end{bmatrix} \quad \mathbf{K} = \begin{bmatrix} 1.6482 \\ 1.0850 \times 10^{-7} \end{bmatrix} \end{aligned} \tag{3.61}$$

$$\begin{aligned} \mathbf{M_1} &= \begin{bmatrix} -3.3168 & -0.3985 \\ -1.7249 \times 10^{-7} & -1.8323 \times 10^{-8} \end{bmatrix} \quad \mathbf{X} = \begin{bmatrix} -6.0588 & -0.5544 \\ -0.5544 & -7.1076 \end{bmatrix} \\ \mathbf{M_2} &= \begin{bmatrix} -0.3986 & -3.9379 \\ -1.8324 \times 10^{-8} & -2.0344 \times 10^{-7} \end{bmatrix} \quad \mathbf{P} = \begin{bmatrix} 1.3560 \\ 0.7647 \end{bmatrix} \end{aligned} \tag{3.62}$$

Is important to underline that the different colors in Figure 3.8b are all refer to values close to zero. Since the matrix $\mathbf{M}$ is three-dimensional, in the implementation in OpenFOAM it has been separated into two two-dimensional matrices[4].

As expected, the eigenfunctions trend along the radial coordinate correspond to a bessel (Figure 3.8e) whereas along the longitudinal coordinate (Figure 3.8f) the trend depends on temperature trend as specified in Section 3.2.

Being the figure of merit the average concentration, are necessary the weighted volume average of the two set of bases:

$$\bar{\phi}_i = \begin{bmatrix} 0.4334 \\ 0.2444 \end{bmatrix} \tag{3.63}$$

in this way, in the implementation of the online phase in SCIANTIX (Section 1.5) will be performed the calculation expressed by Equation 3.66.

[4]Matrix $\mathbf{N}$ is not shown because I was unable to implement its calculation in OpenFOAM.

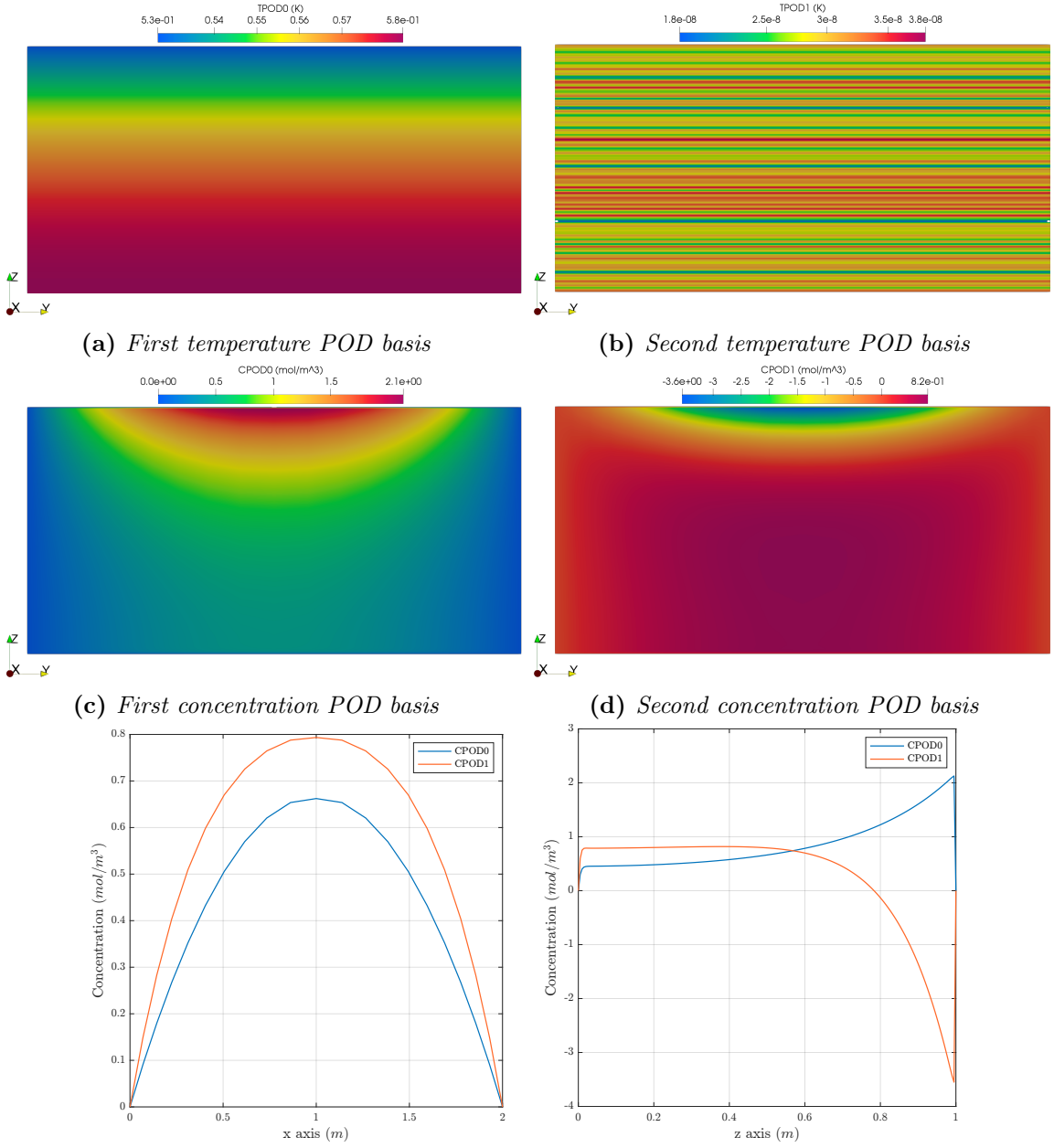

(a) *First temperature POD basis*

(b) *Second temperature POD basis*

(c) *First concentration POD basis*

(d) *Second concentration POD basis*

(e) *Trend of the two concentration POD bases along the x axis*

(f) *Trend of the two concentration POD bases along the z axis*

Figure 3.8. The POD bases resulting from the POD-FV-ROM implementation in OpenFOAM.

3.5 Implementation of the algorithm in SCIANTIX

The ODE systems (Equations 3.45 and 3.60) were solved by means the same iterative procedure of the previous Chapters based on Backward Euler Scheme implemented in SCIANTIX:

$$\begin{bmatrix} a_1^{i+1} \\ a_2^{i+1} \end{bmatrix} = \left(I - \frac{\alpha}{L^2}\Delta t\mathbf{H} - \frac{\tau_T}{L^2}\Delta t\mathbf{J}\right)^{-1} \begin{bmatrix} a_1^i + Q\Delta t L_1 - \frac{\tau_T T_{BC}}{L^2}\Delta t K_1 \\ a_2^i + Q\Delta t L_2 - \frac{\tau_T T_{BC}}{L^2}\Delta t K_2 \end{bmatrix} \tag{3.64}$$

$$\begin{aligned} \begin{bmatrix} b_1^{i+1} \\ b_2^{i+1} \end{bmatrix} = \Bigg(I - \frac{1}{R^2}\Delta t\left(D^0 - \alpha^D T^0\right)\underline{\underline{\mathrm{G}}}\mathbf{X} - \frac{1}{R^2}\alpha^D\underline{\underline{\mathrm{G}}}\Delta t \begin{bmatrix} a_1^i \\ a_2^i \end{bmatrix}^T \mathbf{M} + \\ - \frac{1}{R^2}\alpha^D\underline{\underline{\mathrm{G}}}\Delta t \begin{bmatrix} a_1^i \\ a_2^i \end{bmatrix}^T \mathbf{N}\Bigg)^{-1} \begin{bmatrix} b_1^i + S\Delta t P_1 \\ b_2^i + S\Delta t P_2 \end{bmatrix} \end{aligned} \tag{3.65}$$

The only difference is that now we have four coupled equations: two for temperature field and two for concentration field.

The reconstruction of the volume weighted average concentration along time, similarly to other chapters, is:

$$\bar{c}(\mathbf{x}, t) \approx \sum_{i=1}^{N_c} b_i(t)\bar{\phi}_i(\mathbf{x}) \tag{3.66}$$

3.6 Verification via comparison with High Fidelity

The verification phase that has been performed for this case is also limited to compare the solution obtained from the SCIANTIX code with the high-fidelity solution. The result related to the simulation performed in SCIANTIX was obtained using a null penalty factor, τ_T. In Figure 3.9 is possible to see the comparison between this two results and in Figure 3.10 is represented the corresponding relative error along time. The maximum relative error stands at 13.10%. Remember that the result reported here is partly incomplete due to the failure in the implementation of the matrix $\mathbf{N}$, therefore a small part of this error is due to this, small because the calculation of that matrix (Equation 3.58) involves two gradients which contribute little in the overall calculation. Referring to the uncertainty on the parameters seen in Section 1.6.1 is possible conclude that the reduced order model reproduces with good accuracy the solution relative to the FOM unless a negligible error and comparable to the uncertainty on the parameters.

The implementation of the online phase in OpenFOAM, as explained in Section 1.6.1, made it possible to reconstruct the entire spatial distribution of the concentration field (Figure 3.11). Comparing the distributions in Figure 3.6 and the distributions in the Figure 3.11, can be seen that the error decreases as the time step advances both in terms of the spatially assumed values and in terms of the maximum concentration value reported on the color map, as found in the Section 1.6.1. The trend of the error over time is in complete agreement with the Figure 3.10 indeed the error turns out to be minimal in correspondence of the Figure 3.11c and no longer in correspondence with the last time step as in previous Chapters.

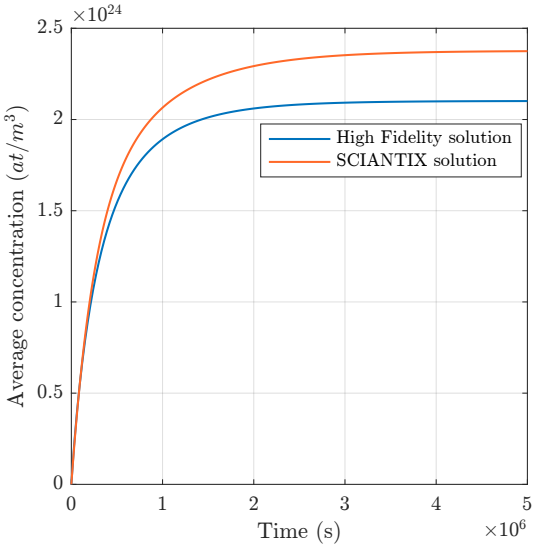

Figure 3.9. Comparison between the SCIANTIX solution, the high fidelity solution and the analytical solution at equilibrium in terms of average concentration.

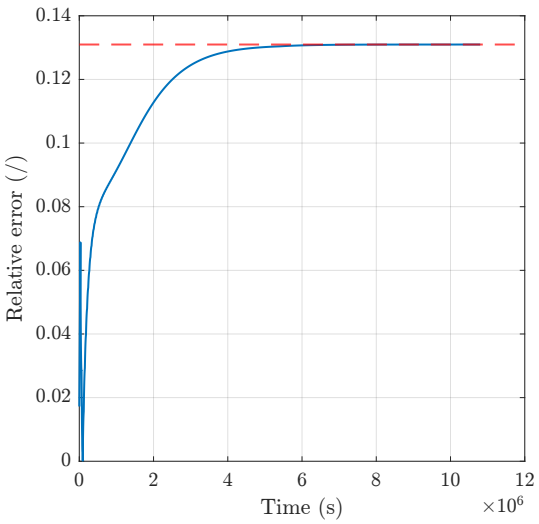

Figure 3.10. The relative error u between the SCIANTIX solution and the high fidelity solution along time. The red dashed line identify the final value.

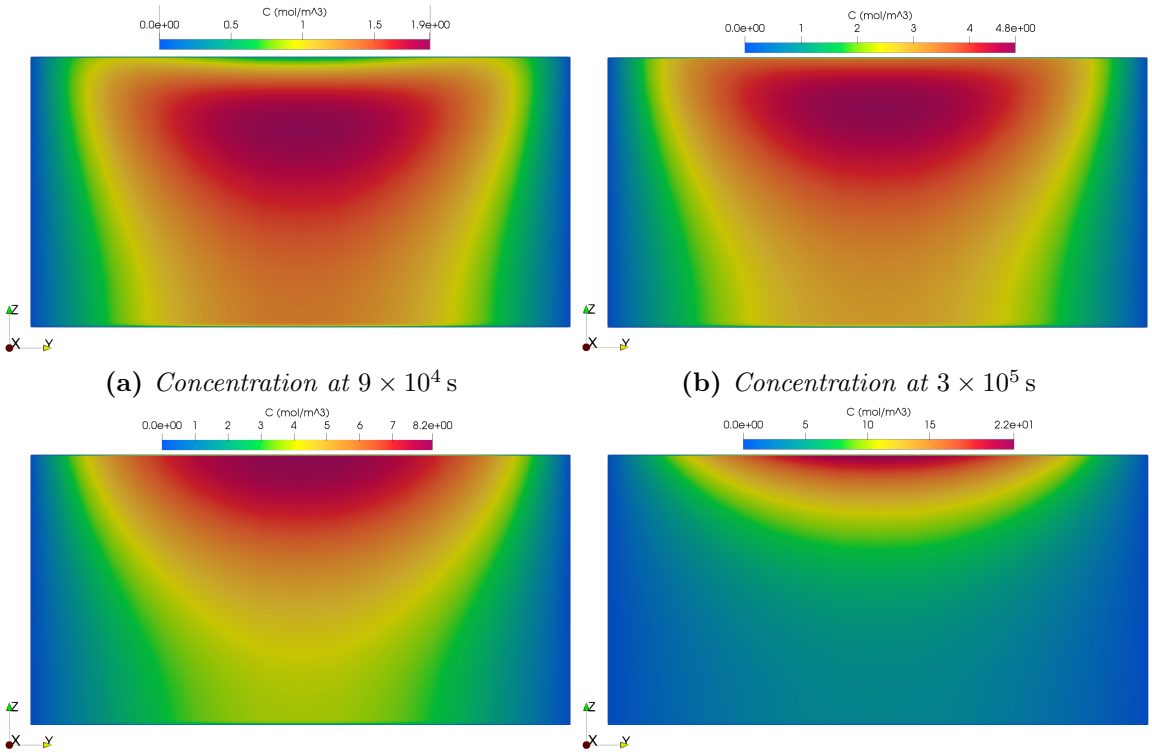

(a) *Concentration at* 9×10^4 s

(b) *Concentration at* 3×10^5 s

(c) *Concentration at* 6×10^5 s

(d) *Concentration at* 6×10^6 s

Figure 3.11. Reconstruction of the spatial distribution of the concentration field.

3.7 Closing remarks

In this Chapter, the POD-FV-ROM technique for the diffusion problem of fission gas in MOX fuel cylindrical grains was developed. The intent of this chapter was to highlight the strategy to be adopted in the event that a diffusion problem with two coupled equations were to be faced. This problem, in addition to being non-linear, has an anisotropic diffusion behavior dictated by the geometry of the grains and this has allowed to apply, and verify, the strategy proposed in the previous Chapter. Even in this case, not many conclusions can be drawn other than the good accuracy of the reduced order model with respect to the high fidelity solution.

The reduction algorithm implemented in this chapter cannot be compared with the state-of-art algorithms seen so far (FORMAS and ANS-5.4) because they solve the problem of diffusion in spherical and non in cylindrical coordinates. In this case, the in-house developed *SpectralDiffusionCylinder* solver will be adopted for the comparison, whose main features are similar to ANS-5.4 except that it deals with solving the problem in cylindrical coordinates. This solver consists in applying a spectral approach in space, projecting the equation on the eigenfunctions of the laplacian operator, i.e. Bessel, and using the first order Backward Euler scheme in time with the purpose to obtain the average spatial solution in cylindrical coordinates.

Among other things missing to complete the verification phase, would be necessary to enrich the investigation by carrying out a sensitivity analysis on the penalty factor, τ_T, in order to identify its optimal value.

The problem of diffusion of fission gas in columnar grains is, nowadays, still considered in fuel performance codes only under very strong hypotheses, aimed at simplifying the treatment. This way of proceeding constitutes a conservative approach that, despite being reliable in terms of safety issues, represents a limitation from the economic and technological point of view. Having implemented a model that does not compromise will allow to deal more accurately with the physics of the problem.

Conclusions

In this Master Thesis, a reduced order modeling approach for fission gas behaviour has been developed. In particular, the focus was on the diffusion of fission gases in the grains of different nuclear fuels and operating under different conditions. This work is aimed at tackling the need of nuclear engineering field to have a fast-running simulation tool. The global goal has been to demonstrate that reduced order modelling is suited to be applied in more complex industrial problems in order to introduce competitive computational performance.

The goal has been pursued with a three-step procedure in which the ROM technique was progressively enriched. In the first part of the research work, the analysis focused on implementation of the POD-FV-ROM technique for the diffusion problem of fission gas in oxide fuel spherical grains. As a start, the FOM and the strategies adopted to simplify his implementation was outlined. Then, the procedure through which the equation of the full order model is reduced was illustrated. Finally, the resolution of the ODE system, by means a first order Backward Euler Scheme in time, and the reconstruction of the solution were performed in SCIANTIX.

The technique outlined in this part was verified in multiple ways. First, the reduction algorithm result was compared with the analytical and high-fidelity solutions, in terms of average concentration. Second, the algorithm behaviour in non-physical situations was tested through MMS. Finally, the algorithm was compared with the state-of-art algorithms already implemented in SCIANTIX through random numerical experiments with the intent to test its behavior in any condition.

In light of this verification, the ROM technique described in this first part has a good accuracy in predicting the result and is suitable in many situations, even non-physical ones. The computational expenses required to perform the reduced order simulations have been drastically limited with respect to the full order simulations. As a matter of fact, once the *Offline* stages have been concluded, the *Online* phase, i.e. the ODE system solving, demands a simulation whose duration is in the order of the seconds. Nonetheless, as testified by the limited errors such computational economy does not impact on the accuracy of the results.

Moreover, the algorithm was applied in the TRANSURANUS fuel performance code in order to test his correct functioning even in a case of integral irradiation. The results obtained in this framework represent proof that reduced order models are indeed useful and constitute a good way to proceed for the solution of models intended to be integrated into more complex systems. Moreover, this represents the first case of applying a reduce order algorithm in a FPC. It is important to underline that this algorithm represents a "demonstrator" in the framework of fission gas that works if applied in the TRANSURANUS performance code but clearly there would

be to do a full code validation on the entire validation database to see that the new models introduced allow to have a better adherence to the experimental data.

Future developments foresee: (i) the optimization of the algorithm in terms of accuracy and computational time, which basically this means into an increase in the number of bases to see how the accuracy and calculation times scale and then, through a sensitivity analysis, determine the number of optimal bases and (ii) make corrections to the algorithm in order to extend the range of intra-granular fission gas release covered, which basically this means correct the algorithm in correspondence with the low fission gas release region where it is inaccurate, $f < 0.02$.

In the second part of the research work, the POD-FV-ROM technique previously implemented was enhanced by including the anisotropic diffusion behavior in the discussion. This case finds application in U_3Si_2 fuel in which an anisotropic diffusion occurs due to its tetragonal crystal structure. After having discussed the strategy adopted to include the anisotropic behaviour in the reduce equation, the same steps of the first part up to the comparison with the high fidelity solution were followed. The strategy developed in this second part was useful in the third part of the work where an anisotropic diffusive problem was still faced.

In the third part of the research work, the non linearity was included in the analysis implementing the POD-FV-ROM technique for the diffusion problem of fission gas in MOX fuel cylindrical grains. In this case, the anisotropy was no longer dictated by the crystalline structure of the fuel but by the grain geometry and the non linearity was due to the temperature gradient along the grain. The discussion of the strategy adopted was followed by the same steps taken in the second part.

The results obtained in the last two parts give good hope that the strategies adopted will prove to be effective but before drawing any definitive conclusions is necessary to continue with the investigations. Having introduced anisotropy and the non linearity in the model will allow to extend the discussion to a greater number of fuels and to interface with more complex problems.

It is important to remember that the diffusive problem solved in each part of this thesis work was addressed by considering constant conditions, i.e. the source term S, the heat generation rate Q and the diffusion coefficient D was assumed as constant in time and uniform in space. Therefore, it will be necessary to extend the treatment by solving the diffusion equation under time-varying conditions so that it can be applied to realistic problems.

In conclusion, the present work may represent a starting point for future developments of ROM techniques in the framework of fission gas behaviour. What could be done to further enrich the discussion is, for example, consider that: (i) for some systems it may be useful to solve not a single diffusion equation but to take into account the two coupled equations relating to the gas in the bubbles and the gas in solution, (ii) there could be a diffusion term on the bubbles, i.e. a mobility of the intra-granular bubbles, which comes into play beyond 1800 °C and (iii) an advective term could be introduced in order to more accurately describe the transport of fission gases in the fuel matrix. Despite the many other features that could be considered, the models implemented up to now with this thesis work still allow to deal with a good number of nuclear systems.

The development of the ROM has focused on the diffusion of fission gases but in a FPC there are many other physics, for example the gap conductance, on which such

an approach could work. Consequently, this thesis can be considered more generally a "demonstrator" of using a ROM approach to sub-modules in an FPC.

Bibliography

[1] J. Rest, "An improved model for fission product behavior in nuclear fuel under normal and accident conditions," *Journal of Nuclear Materials*, vol. 120(2–3), p. 195–212, 1984.

[2] P. Lösönen, "Modelling intragranular fission gas release in irradiation of sintered lwr uo2 fuel," *Journal of Nuclear Materials*, vol. 304(1), p. 29–49, 2002.

[3] K. Lassmann, "Transuranus: a fuel rod analysis code ready for use," *Journal of Nuclear Materials*, vol. 188, p. 295–302, 1992.

[4] A. Denis and R. Piotrkowski, "Simulation of isothermal fission gas release," *Journal of Nuclear Materials*, vol. 229, p. 149–154, 1996.

[5] OECD-NEA, "State-of-the-art report on multi-scale modelling of nuclear fuels." *Organisation for Economic Co-Operation and Development NEA-NSC-R-*, p. 380, 2015.

[6] T. Lassila, A. Manzoni, A. Quarteroni, and G. Rozza, "Model order reduction in fluid dynamics: Challenges and perspectives." *Reduced Order Methods for Modeling and Computational Reduction, (Springer International Publishing)*, p. 235–273, 2014.

[7] A. Manzoni, A. Quarteroni, and G. Rozza, "Computational reduction for parametrized pdes: Strategies and applications." *Milan Journal of Mathematics*, vol. 80, p. 283–309, 2012.

[8] L. Sirovich, "Turbulence and the dynamics of coherent structures. i. coherent structures. part i-iii," *Quarterly of Applied Mathematics*, vol. 45, p. 561–571, 1987.

[9] S. Lorenzi, A. Cammi, L. Luzzi, and G. Rozza, "Pod-galerkin method for finite volume approximation of navier–stokes and rans equations." *Computer Methods in Applied Mechanics and Engineering*, vol. 311, p. 151–179, 2016.

[10] A. Booth, "A method of calculating fission gas diffusion from uo_2 fuel and its application to the x-2-f loop test." *Atomic energy of Canada Limited*, 1957.

[11] M. Beauvy, G. Berthoud, and M. Defranceschi, *A Nuclear Energy Division Monograph: Nuclear fuels*, J.-F. Parisot, Ed. Philippe Pradel, 2009.

[12] M. Speight, "A calculation on the migration of fission gas in material exhibiting

precipitation and re-solution of gas atoms under irradiation." *Nuclear Science and Engineering 37, 180–185.*, vol. 37, pp. 180–185, 1969.

[13] J. A. Turnbull, C. A. Friskney, J. R. Findlay, F. A. Johnson, and A. J. Walter, "The diffusion coefficients of gaseous and volatile species during the irradiation of uranium dioxide," *Journal of Nuclear Materials*, vol. 107, pp. 168–184, 1982.

[14] FOAMextend. (2018) Foamextend version 4.1.

[15] G. Pastore, L. Swiler, J. Hales, S. Novascone, D. Perez, B. Spencer, L. Luzzi, P. Van Uffelen, and R. Williamson, "Uncertainty and sensitivity analysis of fission gas behavior in engineering-scale fuel modeling," *Journal of Nuclear Materials*, vol. 456, p. 398–408, 2015.

[16] B. Shapiro, "Creating compact models of complex electronic systems: An overview and suggested use of existing model reduction and experimental system identification tools." *IEEE Transactions on Components and Packaging Technologies*, vol. 26, p. 165–172, 2003.

[17] M. Romano, "On the intra-granular behaviour of a cocktail of helium and fission gas in oxide nuclear fuel," Master's thesis, Politecnico di Milano, 4 2021.

[18] G. Pastore, D. Pizzocri, C. Rabiti, T. Barani, P. Van Uffelen, and L. Luzzi, "An effective numerical algorithm for intra-granular fission gas release during non-equilibrium trapping and resolution," *Journal of Nuclear Materials*, vol. 509, p. 687–699, 2018.

[19] D. A. Andersson, X. Y. Liu, B. Beeler, S. C. Middleburgh, A. Claisse, and C. R. Stanek, "Density functional theory calculations of self- and xe diffusion in u_3si_2," *Journal of Nuclear Materials*, vol. 515, p. 312–325, 2019.

[20] A. Quarteroni, G. Rozza, and A. Manzoni, "Certified reduced basis approximation for parametrized partial differential equations and applications," *Journal of Mathematics in Industry*, vol. 1, p. 1–49, 2011.

[21] J. Fourier, "Mémoire sur la propagation de la chaleur dans les corps solides. in oeuvres de fourier," *Cambridge University Press*, p. 213–222, 2014.

[22] J. Lumley, "The structure of inhomogeneous turbulent flows." *In Proceedings of the International Colloquium, (Publishing house Nakua)*, vol. 80, p. 166–167, 1967.

[23] A. Noor and J. Peterst, "Reduced basis technique for nonlinear analysis of structures," *AIAA Journal*, vol. 18, p. 455–462, 1980.

[24] A. Quarteroni and G. Rozza, "Numerical solution of parametrized navier-stokes equations by reduced basis methods." *Numerical Methods for Partial Differential Equations*, p. 923–948, 2007.

[25] B. Haasdonk and M. Ohlberger, "Reduced basis method for finite volume approximations of parametrized linear evolution equations." *Mathematical Modelling and Numerical Analysis*, vol. 42, p. 277–302, 2008.

[26] P. Holmes, J. Lumley, and G. Berkooz, *Turbulence, Coherent Structures, Dynamical Systems and Symmetry*. Cambridge University Press, 1996.

[27] D. R. Olander, *Fundamental Aspects of Nuclear Reactor Fuel Elements*. Berkeley, CA, USA: Technical Information Center – Energy Research and Development Administration, University of California, 1976.

[28] H. Matzke, "Gas release mechanisms in UO_2 – a critical review," *Radiation Effects*, vol. 53, pp. 219–242, 1980.

[29] R. J. White and M. O. Tucker, "A new fission-gas release model," *Journal of Nuclear Materials*, vol. 118, no. 1, pp. 1–38, 1983.

[30] R. J. White, "The development of grain-face porosity in irradiated oxide fuel," *Journal of Nuclear Materials*, vol. 325, pp. 61–77, 2004.

[31] G. Pastore, L. Luzzi, V. Di Marcello, and P. Van Uffelen, "Physics-based modelling of fission gas swelling and release in UO_2 applied to integral fuel rod analysis," *Nuclear Engineering and Design*, vol. 256, pp. 75–86, 2013.

[32] C. Friskney and M. Speight, "A calculation on the in-pile diffusional release of fission products forming a general decay chain." *Journal of Nuclear Materials*, vol. 62, p. 89–94, 1976.

[33] C. Wise, "Recoil release of fission products from nuclear fuel." *Journal of Nuclear Materials*, vol. 136, p. 30–47, 1987.

[34] B. Lewis, "Fission product release from nuclear fuel by recoil and knockout." *Journal of Nuclear Materials*, vol. 148, p. 28–42, 1987.

[35] S. D. Beck, "The diffusion of radioactive fission products from porous fuel elements," april 1960.

[36] D. Pizzocri, T. Barani, and L. Luzzi, "Sciantix: A new open source multi-scale code for fission gas behaviour modelling designed for nuclear fuel performance codes." *Journal of Nuclear Materials*, vol. 532, 2020.

[37] C. Baker, "The migration of intragranular fission gas bubbles in irradiated uranium dioxide," *Atomics International*, vol. 71(1), no. NAA-SR-10621, p. 117–123, 1977.

[38] P. Lösönen, "On the behaviour of intragranular fission gas in UO_2 fuel," *Journal of Nuclear Materials*, vol. 280, pp. 56–72, 2000.

[39] J. Turnbull and C. Beyer, "Background and derivation of ans-5 . 4 standard fission product release model." *United States Nuclear Regulatory Commision*, vol. 11, 2009.

[40] H. Matzke, "Lattice disorder and metal self-diffusion in non-stoichiometric uo2 and (u,pu)o2," *J. Phys. Colloques*, vol. 34, pp. C9–317 – C9–325, 1973.

[41] K. Lassmann and H. Benk, "Numerical algorithms for intragranular fission gas release," *Journal of Nuclear Materials*, vol. 280, pp. 127–135, 2000.

[42] D. Pizzocri, C. Rabiti, L. Luzzi, T. Barani, P. Van Uffelen, and G. Pastore, "Polypole-1: An accuraete numerical algorithm for intra-granular fission gas release," *Journal of Nuclear Materials*, vol. 478, pp. 333–342, 2016.

[43] OpenFOAM®-foundation. (2017) Openfoam version 8.0. [Online]. Available: https://openfoam.org

[44] S. Volkwein, "Model reduction using proper orthogonal decomposition." *Lecture Notes*, vol. 118, pp. 1–29, 2013.

[45] S. Lorenzi, "Improvement of the control-oriented modelling of the gen-iv lead-cooled fast reactor: development of reduced order methods," Ph.D. dissertation, Politecnico di Milano, 2015.

[46] G. Berkooz, P. Holmes, and J. Lumley, "The proper orthogonal decomposition in the analysis of turbulent flows." *Annual Review of Fluid Mechanics*, vol. 25, p. 539–575, 1993.

[47] K. Salari and P. Knupp, "Code verification by the method of manufactured solutions," *Journal of Fluids Engineering*, vol. 124, p. 4, 2000.

[48] K. Forsberg and A. Massih, "Diffusion theory of fission gas migration in irradiated nuclear fuel uo2," *Journal of Nuclear Materials*, vol. 135, p. 140–148, 1985.

[49] P. Hermansonn and A. R. Massih, "An effective method for calculation of diffusive flow in spherical grains," *Journal of Nuclear Materials*, vol. 304, pp. 204–211, 2002.

[50] W. N. Rausch and F. E. Panisko, "Ans-5.4: a computer subroutine for predicting fission gas release," 8 1979. [Online]. Available: https://www.osti.gov/biblio/5495268

[51] J. Cheon, Y. Koo, B. Lee, J. Oh, and D. Sohn, "A two-zone method with an enhanced accuracy for a numerical solution of the diffusion equation," *Journal of Nuclear Materials*, vol. 359, pp. 139—-149, 2006.

[52] P. Lösönen, "Methods for calculating diffusional gas release from spherical grains." *Nuclear Engineering and Design*, vol. 196, pp. 161—-173, 2000.

[53] S. Boneva, R. Calabrese, G. Chassie, D. Chulkin, and A. Denis, "The third risø fission gas project: Bump test ge7 (zx115)," 1990.

[54] I. A. E. Agency, "Improvement of computer codes used for fuel behaviour simulations (fumex-iii)," International Atomic Energy Agency, Tech. Rep. IAEA-TECDOC-1697, 2013.

[55] E. Sartori, J. Killeen, and J. Turnbull. (2010) International fuel performance experiments (ifpe) database.

[56] D. G. Cacuci, *Handbook of Nuclear Engineering, Vol. 1: Nuclear Engineering Fundamentals*. Boston, MA Springer US 2010, 2010.

[57] S. J. Zinkle, K. A. Terrani, J. C. Gehin, L. J. Ott, and L. L. Snead, "Accident tolerant fuels for lwrs: A perspective," *Journal of Nuclear Materials*, vol. 448(1–3), p. 374–379, 2014.

[58] S. Bragg-Sittona, B. Merrill, M. Teaguea, L. Ott, K. Rob, M. Farmer, M. Billone, R. Montgomery, C. Stanek, M. Todosow, and N. Brown, "Advanced fuels campaign light water reactor accident tolerant fuel performance metrics," U.S. Department of Energy: Advanced Fuels Campaign, Tech. Rep. INL/EXT-13-29957, 2 2014.

[59] H. G. Kim, J. H. Yang, W. J. Kim, and Y. H. Koo, "Development status of accident-tolerant fuel for light water reactors in korea," *Nuclear Engineering and Technology*, vol. 48(1), p. 1–15, 2016.

[60] N. E. Agency, "State-of-the-art report on light water reactor accident-tolerant fuels," no. OECD/NEA, No.7317, 11 2018.

[61] J. T. White, A. T. Nelson, J. T. Dunwoody, D. D. Byler, D. J. Safarik, and K. J. Mcclellan, "Thermophysical properties of u_3si_2 to 1773 k," *Journal of Nuclear Materials*, vol. 464, p. 275–280, 2016.

[62] K. A. Terrani, S. J. Zinkle, and L. L. Snead, "Advanced oxidation-resistant iron-based alloys for lwr fuel cladding," *Journal of Nuclear Materials*, vol. 448(1–3), p. 420–435, 2016.

[63] J. L. Snelgrove, R. F. Doraagala, G. L. Hofraan, and T. C. Wiencek, "The use of u_3si_2 dispersed in aluminum in plate-type fuel elements for research and test reactors," no. ANL/RERTR/TM-11, 11 2018.

[64] *Capsule Irradiation Tests of U-Si and U-Me (Fe,Ni,Mn) Alloys for Use in Research Reactors*, 10 1993.

[65] A. Leenaers, S. Van Den Berghe, E. Koonen, P. Jacquet, C. Jarousse, B. Guigon, and L. Sannen, "Microstructure of u3si2 fuel plates submitted to a high heat flux," *Journal of Nuclear Materials*, vol. 327(2–3), p. 121–129, 2004.

[66] H. Shimizu, "The properties and irradiation behavior of u_3si_2," *Atomics International*, no. NAA-SR-10621, p. 1–44, 1965.

[67] R. Konings, T. Allen, R. Stoller, and S. Yamanaka, *Comprehensive nuclear materials*. Elsevier Ltd, 2012.

[68] N. E. Todreas and M. Kazimi, *Nuclear Systems Volume I*. CRC Press, 2012.

[69] C. Lemaignan, *Nuclear Materials and Irradiation Effects*, D. G. Cacuci, Ed. Boston, MA: Springer US, 2010.

[70] B. R. T. Frost, *Materials Science and Technology: Nuclear Materials vol 10 : A Comprehensive Treatment*. R. W. Cahn, P. Huusen, and E. J. Kramer, Weinheim, 1996.

[71] S. Sirisup and G. E. Karniadakis, "Stability and accuracy of periodic flow solutions

obtained by a pod-penalty method," *Physica D: Nonlinear Phenomena*, vol. 202(3-4), p. 218–237, 2005.

[72] L. Vergari, A. Cammi, and S. Lorenzi, "Reduced order modeling approach for parametrized thermal-hydraulics problems: inclusion of the energy equation in the pod-fv-rom method." *Progress in Nuclear Energy*, vol. 118, 2020.